Doctoral theses at NTNU, 2020:301

Luigi Mario Viespoli

Mechanical characterization of lead alloys for subsea high voltage power cable applications

Doctoral thesis

Luigi Mario Viespoli

ISBN 978-82-326-4950-1 (printed ver.)
ISBN 978-82-326-4951-8 (electronic ver.)
ISSN 1503-8181

NTNU
Norwegian University of Science and Technology

NTNU
Norwegian University of Science and Technology
Thesis for the Degree of
Philosophiae Doctor
Faculty of Engineering
Department of Mechanical and Industrial Engineering

Doctoral theses at NTNU, 2020:301

NTNU
Norwegian University of Science and Technology

Luigi Mario Viespoli

Mechanical characterization of lead alloys for subsea high voltage power cable applications

Thesis for the Degree of Philosophiae Doctor

Trondheim, October 2020

Norwegian University of Science and Technology
Faculty of Engineering
Department of Mechanical and Industrial Engineering

NTNU
Norwegian University of
Science and Technology

NTNU
Norwegian University of Science and Technology

Thesis for the Degree of Philosophiae Doctor

Faculty of Engineering
Department of Mechanical and Industrial Engineering

ISBN 978-82-326-4950-1 (printed ver.)
ISBN 978-82-326-4951-8 (electronic ver.)
ISSN 1503-8181

Doctoral theses at NTNU, 2020:301

Printed by NTNU Grafisk senter

Preface

This thesis is submitted in partial fulfilment to the requirements for the philosophiae doctor degree. The work was performed in the period from November 2017 to May 2020 under the supervision of prof. Filippo Berto at the Department of Mechanical and Industrial Engineering of the Norwegian University for Science and Technology.

BLANK

Abstract

Subsea power cables are an important component in electrical grids, connecting both offshore facilities to the mainland and interconnecting countries through sea stretches, for lengths up to hundreds of kilometres. Such cables ideally consist of three components: the conductor, copper or aluminium, the insulation, mass impregnated oil-paper or cross-linked polyethylene and the armouring, to withstand axial and radial loads. Cables for the use with voltages in excess of 52 kV require a sheathing layer of a stable, watertight material, to prevent electrical failure of the powerline due to water penetration through the polymer layers. The materials universally adopted for this purpose are lead alloys, due to their great chemical stability, ductility and ability to be continuously extruded for great lengths.

The low melting point of lead, together with low self-diffusion activation energy and vacancy formation enthalpy make so that these alloys are affected by time dependent deformation, or creep, even at room temperature. It would certainly be of great advantage for the industry and the environment to gain a deeper understanding of the damage mechanics of these alloys, in particular the interaction between creep and fatigue phenomena, in order to acquire the necessary tools for a conscious estimate of their structural integrity, in contrast to what has been done traditionally. That is relying on experience and previous designs rather than scientific knowledge, thus leading to potentially overconservative designs naturally affected by excessive use of a potentially hazardous material with a consequent economic and environmental negative impact.

The purpose of this thesis is to investigate the mechanical properties of a lead alloy commercially used for producing submarine power cable sheathing with a goal focused approach based on the special necessities of this industry. The work performed, here summarized in the form of the papers appended, consists in the study of the tensile properties at different strain rate with the influence of microstructure, the fatigue performance of full-scale cables and small scale specimens cut out from the component together with in situ observations of the monotonic and cyclic deformation behaviour, focused on the qualitative observation of the mechanisms causing deformation and damage. Due to the high ductility of the material tested, numerous practical challenges have arisen and the digital image correlation has been a fundamental tool for computing the strain experienced by the material. The results have been used for the calibration of material models able to account for the time dependent deformation behaviour and used for the full scale modelling of the component with the goal of connecting some of the design parameters with the stress state of the sheathing and, consequentially, with the full scale fatigue performance.

Contents

List of Figures

List of Tables

Chapter 1: Introduction

1.1 Motivation and background

Object of the research is to understand the behaviour of lead alloys adopted as typical subsea power-cable sheathing. The construction of a power cable, described in major detail in the following paragraph, consists of the conductors and different layers of polymer, lead and, depending on the model, a dedicated armour pressing on the lead sheathing. The adoption of a sheathing for the conductors is necessary for protection against the permeability of water in the polymeric components of the assembly. The choice of lead is due to different factors, mainly among which the low cost, the high ductility for the extrusion process and the high stability in presence of water. The penetration of seawater through the layers of polymer, which is subjected to a degree of water absorption, makes necessary the presence of the sheathing to prevent cable failure. The use of lead alloys for this purpose is not a recent technology, it has been successfully adopted for decades. The main issue with the design of the cable, in terms on sheathing thickness, is that this has been determined empirically by previous experience and not by the understanding of the material behaviour and damage of the alloys adopted. Observation of cables recently substituted have shown how the design has been effective, since very few failures have been detected even after a very long operational time (decades). To date, most of the research done on creep fatigue for ductile alloys is focused on the old lead solders joints and the more recent lead-free solders for electronics applications. On the specific issue of power cable sheathing lead the literature is instead not satisfactory and there are consistent gaps in the current knowledge [1,2].
The question addressed by the research here presented is whether the established design is in fact too conservative. If the answer is positive, the design of the cables could be modified, with a great environmental advantage due to the possibility of reducing the metal amount.
The problem related to the plasticity and fatigue behaviour of the sheathing should be dealt with as a creep fatigue interaction problem. Most of the work done on this subject comes from the power and the microelectronics industries, with the goal of understanding which can be the best approach for the specific problem.
Lead alloys used in subsea cable sheathing are usually associated with a low melting point Tm, i.e. about 590 K and therefore a high relative operation temperature, around 0.5 Tm [3], even at room temperature. At this temperature, time dependent phenomena including creep, relaxation and recrystallization are highly significant with respect to the mechanical properties of the material. The time dependent mechanisms which imply a strain rate dependency on the monotonic tensile properties must therefore be accounted for in order to accurately predict the mechanical behaviour of components manufactured from lead alloys, such as power cable sheathing or battery grids. Thus, the aim of the

project is to provide a material model of the alloy adopted able to reproduce its mechanical response to deformations imposed at room temperature and suitable for integration in finite element component modelling. In order to collect the necessary data, a series of tests on tensile specimens will be executed. The tensile specimens realized from lead sheathings of different thicknesses and tested at room temperature at different strain rates. To enhance the precision of the numerical models, their correctness will be verified with respect to the results from relaxation tests. During the testing the material has shown primary and secondary creep behaviour, with the latter reached for the slower strain rate tests. The behaviour expected is characterized by an influence of the strain rate both on the stress level and on the apparent elastic modulus. These responses are due to the influence of the active creep mechanisms also at low stress levels; in particular the apparent variation of the elastic modulus both in function of temperature and strain rate has been already reported in the literature both for lead and lead-free solders [4, 5, 6]. Since all the tests will be performed at room temperature, no temperature dependence is accounted for. Moreover, the thickness of the specimen is expected to influence the tensile and fatigue performance of the material. In the case of pure polycrystalline metal lattices, the size of the grain has an influence on the creep response, with an increase of strain rate for a given stress in the presence of smaller grains, due to a greater contribution of boundary sliding [7]. A similar influence has been detected and reported on the yield stress [8].

1.2 Subsea power cables

Subsea power cables are used to transport transfer electrical energy between electrical grids or structures separated by sea. The necessity for the realization of an electrical energy transport infrastructure can arise for several conditions. Connections between autonomous grids of different countries are diffused worldwide. To provide an example of the order of magnitude cost and capacity of such infrastructure, the NorNed high-voltage direct current submarine power cable connects southern Norway to northern Netherlands and is, with its 580 km of length, one of the longest currently in operation [9,10]. The project is able to transfer a maximum power of 700 MW at a voltage of ±450 kV (symmetrical monopole), a 95% efficiency and had a cost of €600 million. Similarly, the connection of a island to the main national grid can be beneficial especially in case the necessities of the islands in terms of power are not sufficient for the realization of a power plant of satisfactory efficiency or in case this would simply result anti economical. Offshore wind farms are located at a few hundred meters from the mainland with which they require a connection. Recently a few projects of floating wind turbines have been completed of are under construction, needing a dynamic cable at least in the first trait. An introduction to static and dynamic cables, as well as to the main components, will be provided in the following paragraphs. In analogy with small islands, also offshore platforms for the extraction of fossil combustibles use energy, but the generation of it directly of the platform would require the use of a low efficiency generator adding weight and influencing the layout of the structure.

It is beneficial to briefly introduce some distinction in the design of subsea power cables due to voltage, insulation material and current for some of the most common design solutions [11].

Polymeric materials are characterized by a certain capacity to absorb water (hygroscopy), which reduces their insulation properties. Cables working at high voltage (major than 36 kV) need a watertight, chemically stable barrier to prevent failure of the entire powerline due to water penetration and consequent dielectric perforation. Such barrier, or sheathing, is expected to endure a design operational life of circa 50 years. Lead (in alloyed form), due to elevated plasticity, the ability to easily follow the global deformations of the component and the easiness of extrusion, has for long been the material universally adopted for the production of the sheathing layer of dry design submarine power cables.

Depending on the application, a cable can be installed in a static or dynamic configuration. The load history for a static configuration includes the deformations due to the drum winding, installation and then the thermal expansion cycles due to operational life. A dynamic cable has a much more complex history which provides additional challenges to the realization of dry dynamic designs.

The construction of most cable dry designs consists of two categories: mass impregnated high voltage direct current (MI HVDC) and cross-linked polyethylene alternating current (XLPE AC). Direct current transmission is characterized by higher efficiency. The

structure of a cable with its insulation and sheathing is analogous to that of a capacitor, which dampens part of the energy in case of use of alternating current.

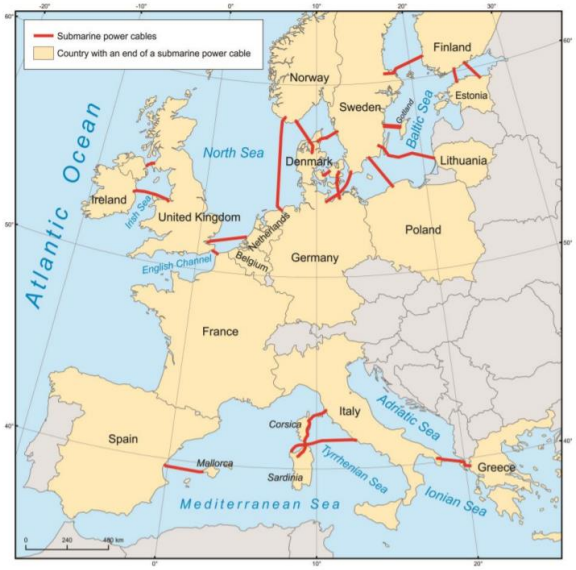

Figure 1.2.1. European submarine cable connections. [12]

a) b)

Figure 1.2.2. Examples of typical cable designs: mass impregnated insulation (a), Cross-linked polyethylene insulation (b). [13]

1.3 Creep and plastic deformation

The purpose of this paragraph is to introduce some useful concepts on the inelastic deformation of metals, with a brief description of the main mechanisms involved, namely: dislocation glide, twinning, diffusion, dislocation climb, grain boundary sliding. Each of these mechanisms can contribute to the deformation, but, in most cases, at least one will be dominant depending on the conditions of stress and temperature [14].

Dislocation glide

This is the dominant mechanism for plastic deformation at room temperature, characterized by a migration of dislocations on their slip plane, the most favourable, according to the stress state, of the crystallographic planes at maximum atomic density. It is a highly localized phenomenon, in the sense that, even for high plastic strains, only a small fraction of the potentially favourable slip planes will be active and participating to the deformation. The plastic deformation due to glide of dislocations is initiated when the shear stress resolved on the most favourable potential slip plane reaches a determinate value. The casual orientation of grains in polycrystalline metals makes so that not all grains experience yielding at once and the cohesion of grain boundaries requires multiple slip systems to be activated contemporarily. The fact that not all grains will be in the favourable direction and that the grain boundaries hinder the movement of dislocations will cause a higher resistance to plastic deformation in metals with finer grain structure, a tendency represented by the Hall Petch formula [15].

$$\sigma_Y = k_1 + k_2/\sqrt{d}$$

Where k_is are material constants and d is the average grain diameter.
Metallic alloys generally have a dislocation density in the order of magnitude of 10^6 mm^{-2}. When a sufficient stress is applied and dislocation begin to glide new dislocation sources are generated on one hand, but the fraction dislocations which is mobile is reduced on the other. The result of this reduction of mobile dislocation as a consequence of plastic strain is the phenomena macroscopically observed as strain hardening. Two of the most common methods used for increasing the resistance of metals to plastic deformation are the introduction of alloying elements forming hard precipitates of being dissolved in the matrix as substitutional atoms. Both strategies act on the movement freedom of dislocations. Temperature and strain rate influence the dislocation glide. Thermal activation can help dislocations to overcome obstacles and continue their motion, while a slower deformation rate will favour deformation allowing the necessary time for gliding. It must be stressed that this is a highly localized phenomenon which heavily distorts areas of the lattice creating residual second order stresses. These stresses influence the behaviour in case of alternating loads, with plastic deformation starting at

an inferior level of stress in case of reversal, a characteristic commonly known as Bauschinger effect [16].

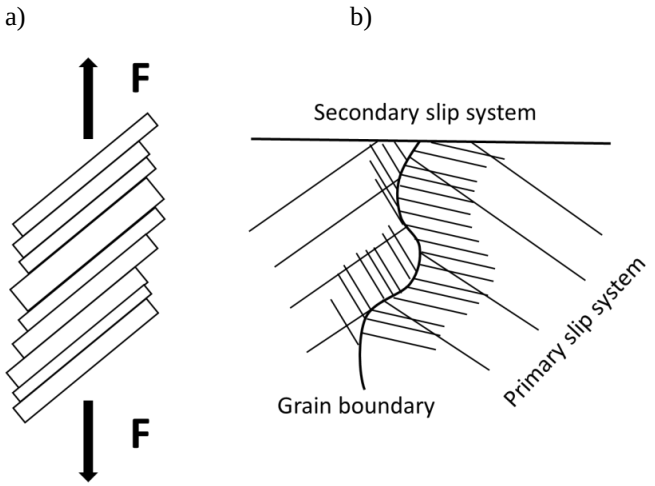

Figure 1.3.1. Single grain plastic deformation (a), multiple slip systems activated at the grain boundary in polycrystalline metal (b).

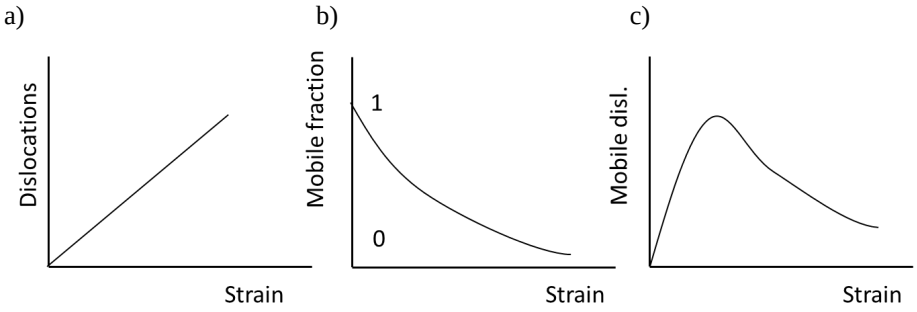

Figure 1.3.2. Strain hardening: total number of dislocations (a), fraction of mobile dislocations (b), number of mobile dislocations (c).

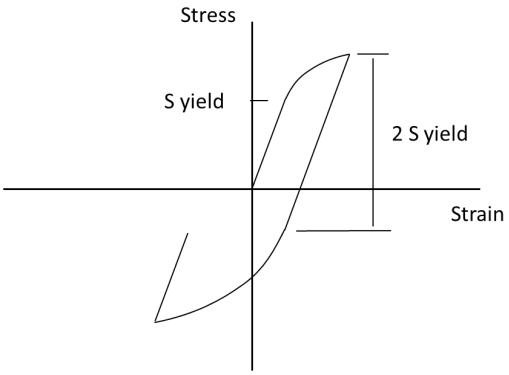

Figure 1.3.3. Bauschinger effect.

Twinning

Twinning is characterized by a sudden rotation of a portion of the lattice mirrored to the twin plane [17]. This process requires an energy superior to dislocation glide and, as a consequence, has less relevance in materials with numerous slip planes, FCC and BCC, while it is more frequently found in hexagonal lattices. In contrast with dislocation glide, which requires time to happen, twinning is a fast evolution of the matrix's layout and, consequently, becomes the active mechanism when other processes are blocked, especially at low temperatures and high strain rates. It generally leads to modest global strains and, in analogy with dislocation glide, regards certain crystallographic planes and interests a limited part of the grain.

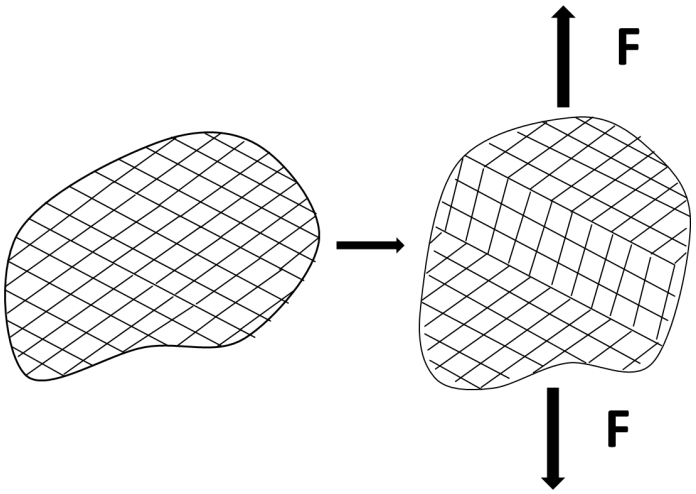

Figure 1.3.4. Grain elongation due to twinning.

Stress directed diffusion

This is the first of the deformation mechanisms directly related to creep which are described in the introduction of the thesis. The amount of vacancies in the metal lattice depends by the material and by the temperature at which this is. Being N the number of atoms in the region, R the universal gas constant, T the temperature and ΔU the activation energy, their number is approximated by the formula:

$$n = N\, e^{-\Delta U/RT}$$

The vacancies travel randomly in the lattice and, if the atoms substituting the vacancies belong to the matrix, the process is called self-diffusion and, in absence of stress, has no preferential direction. When stress is present the development and migration of vacancies is influenced by it: the vacancies develop at the grain boundaries orthogonal to the first principal stress and migrate to the parallel boundaries. This is the dominant phenomenon in high temperature and low stress creep, known as Nabarro-Herring creep. At lower temperatures the diffusion happens through the grain boundary, a process called Coble creep [18].

a) b)

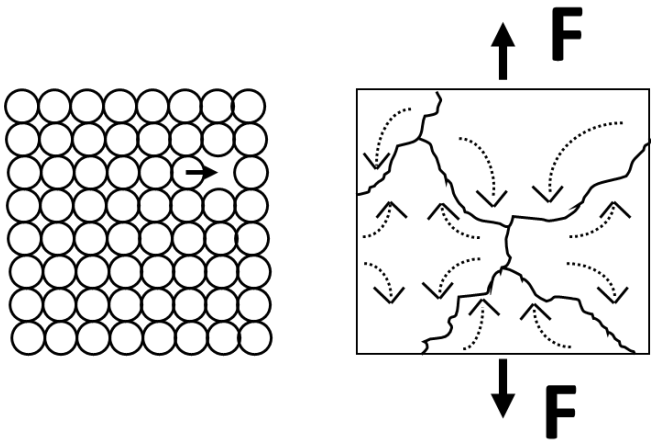

Figure 1.3.5. Atom migrating to vacancy (a), stress directed diffusion grain elongation (b).

Dislocations climb

The movement of dislocation is involved, and is indeed one of the most relevant mechanisms, in time dependent plasticity as well. Compared to diffusion, this happens at lower temperatures and higher stresses. Recalling the concepts introduced in the dislocation glide section, during plastic deformation lines of dislocations pile up at

obstacles, as for example a precipitate and is possible that the applied stress and the thermal activation are not sufficient to overcome the obstacle. With higher temperatures, in the range of over half the melting temperature, the amount of vacancies increases dramatically. Such vacancies can help the dislocation line to rise by several layers in the matrix climbing over the obstacle and continuing its motion. This is clearly a combined process, in which the vacancy driven climb provides a sufficient number of mobile dislocations which continue the glide, resulting in a macroscopic creep deformation [19].

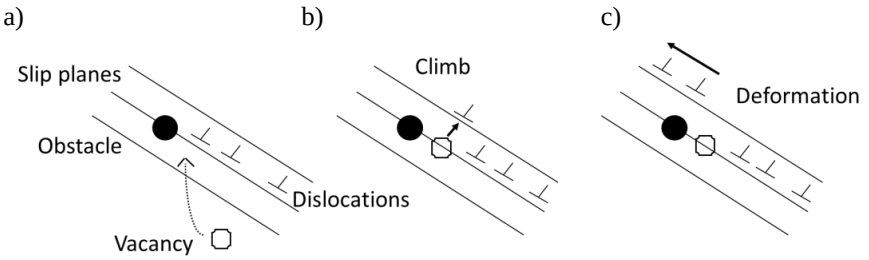

Figure 1.3.6. Dislocation pile-up at obstacle (a), dislocation climb due to vacancy (b), deformation resumes (c).

Grain boundary sliding

The sliding of grain boundaries happens as a direct consequence of the other mechanisms deforming the grain and of the forces of cohesion among the grains. Considering stress directed diffusion, the grains are elongated by the motion of vacancies from the boundary regions orthogonal to the maximum principal stress towards the adjacent boundaries, thus causing the elongation of the grains. It is intuitive that real boundaries are not perfectly planar: a series of voids nucleate at the interface between voids and, since overlapping of material is not possible, atoms move to these voids by diffusion. The process is not capable to regenerate every interface interrupted by a crack and consequently the boundary results damaged. The coalescence of these defects leads to catastrophic failure by intergranular fracture, generally for limited strains. A lower ratio of boundary surface over volume, that is a bigger average grain size, reduces the probability of defect nucleation and is preferable for applications of which the stress and temperature levels induce such process in the material.

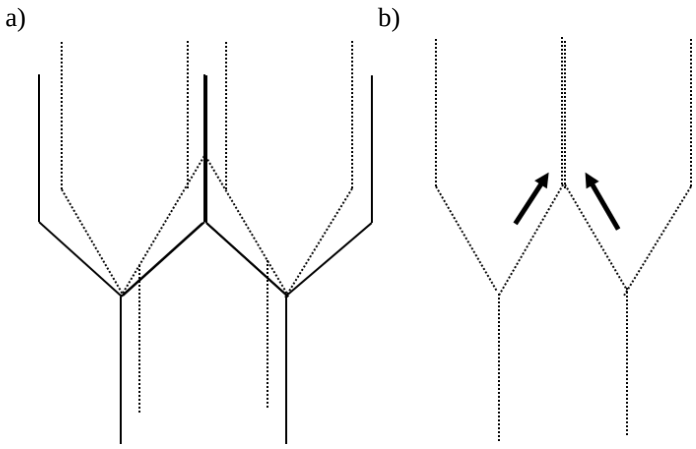

Figure 1.3.7. Stress directed diffusion grain elongation and idealized boundary decohesion (a), grain boundary sliding to prevent grain decohesion (b).

1.4 Creep fatigue

When a metal is subjected to repeated loading at relatively elevated temperature, the damaging processes of fatigue and creep combine. This broad topic is intuitively of great interest, but also of great complexity, and has been studied with attention by several industries, in particular by the energy, aerospace and microelectronics communities.

The activation of both fatigue and creep related damage mechanisms can greatly reduce the service life of a component by accelerating the processes of crack nucleation and propagation [20]. As a general rule, fatigue cracks generate at intrusion/extrusion sites on the maximum shear plane of the surface and then propagate as transgranular fracture in the maximum stress plane driven by the crack tip opening at every cycle. The phenomenon is enhanced by the increased thermal activation. Creep fracture typically happens as a nucleation and coalescence of voids at the grain boundaries, generating intergranular cracks. In case of alloys with second phases at the grain boundary, this second phase has a lower melting temperature and is then susceptible to the temperature increase.

The strain rate impacts the proportion between creep and fatigue damage. A slower deformation causes less cycles in a given time, but allows for thermally activated phenomena to alter and damage the component, while a high frequency of deformation causes fatigue-dominated damage. Under the right, intermediate conditions, both mechanisms are present and one augments the effects of the other, leading to a n anticipated failure. The shape of the load path, with the multiple combination of load,

dwell time and relaxation, has a determinant influence on the amount of creep damage caused in the material.

The interaction between the fatigue-dominated transgranular crack and the creep-dominated intergranular crack can be summarized in three different categories: competitive, additive and interactive. For competitive interaction is intended the mechanisms act independently and uninfluenced by one another, until the reaching of the critical value for one of the two leads to failure. In the additive interaction fatigue and creep contribute in equal measure to the reduction of the resisting section of the component. The interaction is defined combined when the transgranular and intergranular crack influence and end enhance each other's effect, leading to accelerated failure. It is possible to define a damage parameter both for creep and fatigue as a number, function of creep time or number of cycles respectively, which reaches a unit value in case of failure purely caused by one of the two processes. The total damage parameter, given by the sum of the two, assumes a value superior, equal and inferior to the unit for the competitive, additive and combined interaction respectively. A conservative modification of the damage parameter is to add a third damage term which accounts for the combination of the mechanisms.

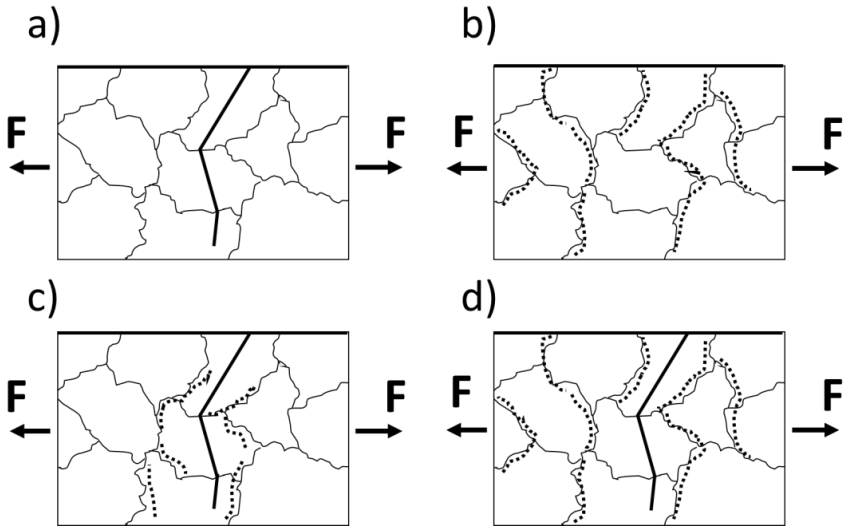

Figure 1.4.1. Fatigue dominated damage (a), creep dominated damage (b), interaction between fatigue and creep damage (c), competition of fatigue and creep damage (d).

1.5 Lead and cable sheathing

Commercial alloys for cable sheathing

The alloys used for the extrusion of cable sheathing include a variety of elements the proportions of which often been determined by trial and error [21]. The addition of Ca, Te, As, Sn, Sb, Cd, Bi, Cu result in the strengthening of the material through solid solution or precipitation hardening. Some of these elements, Cd, Sn, Sb, due to a non-negligible solid solubility in lead, can provide both types of strengthening, while Bi has limited influence on strength despite its good solubility. The other elements listed have low solubility and their impact on strength is mostly due to a reduction of grain boundary mobility. Second phase precipitates are generally not present in a proportion sufficient to guarantee any significant influence on the mechanical properties, but impact ductility and fatigue resistance. In order to avoid sheathing fatigue failures and consequent dielectric breakdown it is important to select alloys which can be continuously extruded for great length to form homogeneous sheathing free from imperfections and inclusions. Due to the wide variety of mineral sources, independent producers, technological parameters and applications, several alloys have been developed. The European Union has answered the necessity for standardization with the CEN/TC 306 Lead and Lead Alloys standard [22]. The denomination, composition and preferential applications for some of the most common commercial alloys are reported in table 1.5.1.

Notes on the manufacturing process

It is important to keep the composition of the lead used for the extrusion as uniform as possible, result which is achieved by producing the alloy in batches of 60-300 tons. The lead for the bath must be 99.99 % pure and then no recycled material is accepted. For the same necessity of purity, the other elements composing the alloy are generally not added as master alloys, but in elemental form. According to the elements to be added the bath is kept at a temperature 430-490 ºC and they are mixed by submerged injection or by a vortex mixer. The use of master alloys is acceptable for those elements, Sn, Sb, Cd, which have a non-negligible solubility in lead. The alloy is then cast in 25-40 kg ingots, with the heavier ones preferred for the favourable surface to volume ratio, which reduces the amount of oxide introduced in the sheathing. It is clear that heavier ingots would be preferred, but logistical difficulties related to handling and transportation reduce the capability to do so. The ingots are directionally water-cooled from the bottom at a rate of 20 ºC/min and then air cooled after reaching 150 ºC. Due to the necessity of keeping the properties of the extruded material, as distribution and microstructure, as uniform as possible for considerable length of cable, the use of screw Hansson-Robertson continuous lead extruders is preferred to ram extruders. The uniformity of the extruded material makes so that a smaller amount of alloying elements is required, resulting in lower costs

and better performance due to the reduction of undesired precipitates. The extruder receives molten alloy at a rate of 25-120 kg/min from a melting pot where 10 to 60 tons of bath are stored at around 370 ºC. Given the lower density of oxide compared to lead (9.5 vs 11.3 kg/dm^3 circa), a bigger melting pot is preferred because it allows the necessary time for reaching the surface. A series of filters is also used to reduce the risk of potentially dangerous inclusions in the sheathing. The temperature in the extruder is maintained, by balancing flow of lead alloy and water or steam in the outer jacket, in the range 200 to 300 ºC. The presence of a molten region in the extruder, elongated by a higher screw rotational velocity, reduces the friction with beneficial effects on the duration of the equipment and economy of production. Generally, the process is adjusted to obtain a sheathing of 2-4 mm of thickness at a rate of 20 to 30 kg/min. The extrusion temperature must be kept at an adequate level to guarantee a solid welding in the extrusion direction, to prevent cracking in the longitudinal direction as well.

Commercial designation	Composition	CEN 306 designation	Applications
B	0.8-0.95% Sb	PB001K	Solid and telecommunication cables. Severe vibrations.
½ B	0.55 Sb	PB002K	Solid and telecommunication cables. Severe vibrations.
C	0.35-0.45% Sn – 0.12-0.18% Cd	PB011K	Power transmission in ships.
½ C	0.18-0.22% Sb – 0.06-0.09% Cd	PB012K	Oil filled and submarine cables. Severe vibrations. Most reinforced types.
E	0.35-0.45% Sn – 0.15-0.25% Sb	PB021K	Solid and telecommunication cables, reinforced gas or oil filled power cables. Moderate vibrations.
Pb-Cu	0.04-0.05% Cu	PB061K	Gas or oil filled power cables.
Pb-Cu-Te	0.03-0.04% Cu – 0.03-0.04% Te	PB041K	Oil filled. Elevated vibrations.
F3	0.15% As – 0.15% Sn – 0.1% Bi	PB031K	Submarine. Power cables with high creep, bending, vibration resistance.
Pb-Ca-Sn	0.033% Ca – 0.38% Sn	PB051K	Long high voltage AC and DC cables.

Table 1.5.1. List of some popular commercial alloys [22].

1.6 Research plan

Objectives

The objective to reach is a full characterization of the alloy used for the sheathing in order to understand whether it is possible to modify the design or the process using less material. This requires a number of sub-steps in the research, as follows:

- Characterization of the tensile behavior at different strain rates with room temperature creep;
- Fatigue curves for different strain rates;
- Metallographic investigation;
- Full scale fatigue testing;
- Calibrating a material model to describe the tensile behavior of the alloy;
- In situ observation of the dominant mechanisms of deformation and damage;
- Full scale modelling focused on stress state evolution during the cycle.

Scope (limitations and coverage)

The scope of the research here presented includes understanding and describing the mechanical properties of the alloy adopted, especially those related to creep, fatigue and size effect. Issues which are not addressed are the developing of new alloys or new technological processes for the production of the cables. In order to provide the characterization of the material it is necessary to adopt different testing techniques, especially in the microstructural and mechanical testing. The project necessities the developing of a know-how related to the testing of a such soft alloys. The difficulties originated by the extreme ductility of lead make challenging the performing of tensile and fatigue testing, because of the deformation in clamping and the easiness of displacement out of plane in compressive phases. Part of these issues, in particular the unreliability of the strains computed by the displacement of the clamps, are overcome by the adoption of the digital image correlation as a procedure to evaluate the real strain pattern on the specimen's surface. Another issue caused by the ductility and the easy of recrystallization is the difficulty to perform metallographic investigation, because of which it is very difficult to polish the alloy's surface and thus capturing the real aspect of the grains. It is then necessary to develop a procedure to perform the polishing and etching in a way suitable for the alloy treated. The research is completed by the numerical implementation of a suitable material model for the reproduction of the material behavior in FEM environment. The model is expected to describe the strain rate sensitivity and the relaxation under constant strain/creep under constant stress.

Research method

The research is divided into two main branches: the mechanical characterization and the material investigation. Part of the goal is to determine the correlation between the microstructural properties and the stress-strain response, relaxation and fatigue life. The mechanical testing requires the use of electrically or hydraulically operated fatigue testing machines to collect the necessary data. The specimens will be produced from the actual sheathing by disassembly of the cable and cut to non-standard geometries adequately studied to reduce the instability which inherently affects the material. After generation of a random speckle pattern on the surface of the specimen, 2D DIC is performed to get the real strain pattern. The post-processing and analysis of the results is used to investigate the deformation mechanisms which characterize the alloy and as a base for the calibration of the material models adopted. Softwares of choice for the numerical modelling are Abaqus, Isight. The tests planned for the characterization of the alloy are: tensile at different strain rates, step tests, relaxation, fatigue. For the metallographic investigation, it was necessary to develop a procedure to polish the specimen without modifying the microstructure, non-trivial due to the extreme sensitivity to mechanical and thermal inputs. The procedure will be not described in detail due to secrecy limitations.

Ethical issues

Issues related to the project are mainly the careful handling of the material, which might be poisonous and polluting and to the not disclosing sensible details related to the manufacturing of the final product.

Provided results

The results provided regard the knowledge of the characteristics of the lead alloy used for sub-sea high voltage cable sheathing and the acquisition of the necessary know how for performing investigations on this class of materials. This has been done in different steps: the creation of a database of results obtained from different kind of tests the scope of which is the ability to fully predict the behaviour of the material when subjected to a mechanical input; the correlation of the microstructure of the alloy to the history of the specimen analysed and to its mechanical properties; the modelling of the stress/strain static and cyclic response of the material and the combination of creep and fatigue damage. These results are useful and find direct application for the manufacturers of power cables filling part of the gap nowadays present in the literature and allowing to a more aware design and life prediction for the sheathing, a failure of which in marine environment causes the failure of the entire cable.

1.7 List of publications

Paper I

Tensile characterization of a lead alloy: creep induced strain rate sensitivity

Luigi M. Viespoli[1], Audun Johanson[2], Antonio Alvaro[3], Bård Nyhus[3], Alberto Sommacal, Filippo Berto[1]

[1]*Department of Mechanical and Industrial Engineering, Norwegian University of Science and Technology (NTNU), Norway*
[2]*Nexans Norway, Innspurten 9, 0663 Oslo, Norway*
[3]*Sintef Industry, Richard Birkelands vei 2B, 7031, Trondheim, NORWAY*

Abstract: The aim of this work is to investigate and define the tensile properties of cable sheathing lead alloy. In particular its strain rate sensitivity due to the pronounced creep already present at room temperature, in relation to the material work hardening and processing is object of study. Therefore, a series of specimens have been manufactured using cable sheathing of three different extrusion thicknesses and tested in displacement control at different strain rates. The practical difficulties generated by the highly plastic behavior have been overcome by the use of Digital Image Correlation (DIC) technique as a tool for measuring the strain field on the specimen surface. The creep behavior has been described, modeled and calibrated using Isight and finally implemented in the FEA code Abaqus. Two different numerical models have been used for modelling the time dependent deformation, a power law and the Anand model. The first predict correctly the response of the alloy in the primary creep region while the second shows better results for secondary creep.
Keywords: creep, plasticity, digital image correlation, finite element analysis, lead, microstructure

Materials Science and Engineering: A
Volume 744, 28 January 2019, Pages 365-375

L.M.V. contributed to the postprocessing of test results and metallographic investigation, numerical analysis, literature review and drafting of the manuscript.

Paper II

Room temperature creep mechanism of a Pb-Sn-Sb lead alloy

Luigi Mario Viespoli[a*], Audun Johanson[b], Antonio Alvaro[c], Bård Nyhus[c], Filippo Berto[a]

[a]*Department of Mechanical and Industrial Engineering, Norwegian University of Science and Technology (NTNU), Norway*
[b]*Nexans Norway, Innspurten 9, 0663 Oslo, Norway*
[c]*Sintef Industry, Richard Birkelands vei 2B, 7031, Trondheim, NorwayAbstract*

Abstract: Lead alloys are the most common materials adopted for the production of subsea power cable sheathing. The sheathing is a layer of stable and watertight metal, which serves to prevent the electrical failure of the cable. During the predicted operational life of the cables of several decades, these experience strains due to the installation process, the oceanic currents and the thermal expansion of the cable. The low melting temperature of such alloys, around 600 K, imply that creep deformation will occur when subjected to loading even at room temperature. The goal of the present study is to investigate the tensile behavior of the Pb-Sb-Sn alloy of interest in order to predict the correlation between strain rate and stress level. A mechanical characterization was performed through tensile testing at different strain rates of specimens cut from power cable sheathing. Due to the extreme ductility of the material, the use of digital image correlation was necessary to compute an acceptable approximation of the in-plane strain field on the surface of the specimens. The results were implemented in finite element method environment using Abaqus and Isight to calibrate a creep model able to reproduce at best the behavior of the material. Such model was also positively tested in the case of a relaxation test. In addition, a tensile test of several steps at different loads was executed with the aim of extrapolating and interpreting the steady state creep exponents at different creep regimes and the indications that these can provide on the deformation mechanisms of the alloy.
Keywords: lead; creep; plasticity mechanisms; modelling; digital image correlation

Procedia Structural Integrity
Volume 18, 2019, Pages 86-92

L.M.V. contributed to the planning of the tests, postprocessing and analysis of the results and drafting of the manuscript.

Paper III

Subsea power cable sheathing: an investigation of lead fatigue performance

Luigi Mario Viespoli[1], Audun Johanson[2], Antonio Alvaro[1,3], Bård Nyhus[3], Filippo Berto[1]

[1]*Department of Mechanical and Industrial Engineering, Norwegian University of Science and Technology (NTNU), Norway*
[2]*Nexans Norway, Innspurten 9, 0663 Oslo, Norway*
[3]*Sintef Industry, Richard Birkelands vei 2B, 7034, Trondheim, NORWAY*

Abstract: The protection of subsea power cables against electrical failure is achieved by the use of a watertight layer. Due to its properties of chemical stability and ductility, lead has been the material of choice for this purpose for several decades. Due to the low melting temperatures of lead alloys, their behaviour is strongly influenced by time-dependent phenomena, such as creep and recrystallization, which become more prominent for lower strain rate deformations. In order to understand the performance of the alloys of interest under cyclic loading experienced during and after installation in combination with the different variables influencing its behaviour, extensive testing is necessary. This manuscript presents the results of fatigue tests at two different strain rates for an alloy of industrial interest. The tests are monitored with the aid of digital image correlation, which greatly reduces the uncertainty on the quantification of the real strain field. The post-mortem fracture surfaces are investigated through scanning electron microscopy and metallurgical characterization to help understanding the differences in the failure modes active in the different stress/strain regimes.

Submitted to: 1st Virtual European Conference on Fracture - VECF1

L.M.V. contributed to the planning of the fatigue tests and their interpretation, the scanning electron microscope fracture investigation and the drafting of the manuscript.

Paper IV

Tensile and fatigue behavior of a Pb-Sn-Sb alloy investigated via small-scale in-situ mechanical testing in SEM

Di Wan[1], Luigi Mario Viespoli[1], Audun Johanson[2], Anette Brocks Hagen[3], Filippo Berto[1], Antonio Alvaro[3]

[1]*Department of Mechanical and Industrial Engineering (MTP), Norwegian University of Science and Technology (NTNU), Richard Birkelands vei 2B, 7491 Trondheim, Norway*
[2]*Nexans Norway, Innspurten 9, 0663 Oslo, Norway*
[3]*Department of Materials Integrity and Welding, SINTEF Industry, 7456 Trondheim, Norway*

Abstract Pb-Sn-Sb alloys (E-alloy) are commonly used in subsea power cable sheathing. Due to the relatively low melting temperature, i.e. around 600 K, this type of alloy can experience some microstructure evolution such as recovery, relaxation, recrystallization and creep deformation even at room temperature, in contrast to other conventional materials that involve these mechanisms only at high temperatures. To better understand the deformation mechanisms of Pb-Sn-Sb alloys, small-scale in-situ mechanical testing inside a scanning electron microscope (SEM) has been conducted under both monotonic loading and cyclic loading conditions. Thanks to the in-situ imaging technique, the deformation behavior as well as the damage mechanisms were revealed with high resolution. The possible deformation mechanisms, including the creep behavior, has been discussed and the results can provide necessary input to damage calculations and modelling work of the studied alloy system used for cable sheathing.

Submitted to: 1st Virtual European Conference on Fracture - VECF1

L.M.V. contributed to the experimental activity in terms of planning, execution and discussion of the results together with revision of the draft.

Paper V

Small- and Full-Scale Fatigue Testing of Lead Cable Sheathing

Audun Johanson[1], Luigi Mario Viespoli[2], Antonio Alvaro[3], Filippo Berto[2]

[1]*Nexans Norway,*
[2]*Dept. Of Mechanical and Industrial Engineering, Norwegian University of Science and Technology (NTNU), Norway*
[3]*Dept. of Materials and Nanotechnology, SINTEF Industry, Norway*

Abstract: The fatigue behavior of a PbSnSb alloy used in subsea power cable sheathing was studied using small- and full-scale experiments. The aim of the work was to understand the transferability between the scales and suitable testing methods. Creep phenomena are addressed by considering the cyclic strain rate as well as the small-scale loading mode. The fatigue test results show significant difference between different loading modes and scales. It is also evident that fatigue- creep interaction is highly important.
Keywords: Lead Sheath; Fatigue; Creep; Subsea Power Cables.

ISOPE - International Offshore and Polar Engineering Conference. Proceedings
ISSN 1098-6189, Page(s) 1922 – 1927, 2019

L.M.V. participated to the activity of analysis and interpretation of the results and review of the draft.

Paper VI

Strain controlled medium cycle fatigue of a notched Pb-Sn-Cd lead alloy

Luigi M. Viespoli[1], Audun Johanson[2], Antonio Alvaro[3], Bård Nyhus[3], Filippo Berto[1]

[1]*Department of Mechanical and Industrial Engineering, Norwegian University of Science and Technology (NTNU), Norway*
[2]*Nexans Norway, Innspurten 9, 0663 Oslo, Norway*
[3]*Sintef Industry, Richard Birkelands vei 2B, 7031, Trondheim, NORWAY*

Abstract: During the extrusion process of subsea power cable sheathing layer it is possible that metallic and/or non-metallic debris present in the processing environment enter the metal lattice originating discontinuities that might have a detrimental effect on the fatigue life and the overall integrity of the sheathing. In order to understand the influence of these production defects on the reliability of installed power-lines, a series of specimens directly retrieved from the extruded sheathing were fatigue tested at different strain rates and range both in presence and absence of a non-passing through notch simulating the geometrical discontinuity induced by a particle. In order to collect the necessary information for the understanding of the failure mechanism, Digital Image Correlation and Scanning Electron Microscopy were used to understand the influence of the testing condition on the material resistance and failure mode.
Keywords: Lead, creep-fatigue interaction, digital image correlation, notch sensitivity

Engineering Failure Analysis
Volume 104, October 2019, Pages 96-104

L.M.V. contributed to the planning of the most recent set of tests, their postprocessing and interpretation, the activity of scanning electron microscopy of the fractures and the drafting of the manuscript.

Paper VII

Experimental and numerical investigation of strain distribution of notched lead fatigue test specimen

Audun Johanson[1,*], Luigi Mario Viespoli[2], Bård Nyhus[3], Antonio Alvaro[3] and Filippo Berto[2]

[1]*Nexans Norway, Innspurten 9, 0663 Oslo, Norway*
[2]*Department of Mechanical and Industrial Engineering, Norwegian University of Science and Technology (NTNU), Norway*
[3]*Sintef Materials and Chemistry, Richard Birkelands vei 2B, 7031, Trondheim, NORWAY*

Abstract. The work here presented focuses on the test methodology related to effect of stress concentrators in strain controlled structures. Cable sheathing as used in subsea power cables are investigated by cyclic fatigue testing, Digital Image Correlation (DIC) and 3D Finite Element Analysis. Focus is put on the strain distribution in conventional specimen geometries and under the presence of artificial notches. It is evident that standardized fatigue testing provides limited input to the final fatigue life of strain controlled power cable sheathing- taken into account both intended and unintended stress concentrators. The limitations can be explained by measured strain distribution inherent in most fatigue test specimens. The use of DIC and 3D FEM provides valuable insight into both the theoretical and practical stress and strain distribution. This can help in understanding and overcoming geometrical test constraints, when compared to the actual component loading mode.

MATEC Web of Conferences. 2018, 165:05003 1-6

L.M.V. participated to the analysis of experimental results, numerical analysis and drafting of the manuscript.

Paper VIII

Tape winding angle influence on subsea cable sheathing fatigue performance

Luigi Mario Viespoli[1*], Luigi Panza[1-2], Audun Johanson[3], Antonio Alvaro[1-4], Aurelio Somà[2], Filippo Berto[1]

[1]*Department of Mechanical and Industrial Engineering, Norwegian University of Science and Technology (NTNU), Richard Birkelands vei 2B, 2034, Trondheim, Norway*
[2]*Dipartimento di Ingegneria Meccanica e Aerospaziale, Politecnico di Torino, Italy*
[3]*Nexans Norway, Innspurten 9, 0663 Oslo, Norway*
[4]*Sintef Industry, Richard Birkelands vei 2B, 7031, Trondheim, NORWAY*

Abstract: A fundamental component of subsea power cables is the thin galvanized steel tape winded around the dielectric and sheathing layer to prevent permanent deformation due to thermal cycling. The pressure state induced by the resistance offered by such tapes against radial reformation reduces the triaxiality ratio of the stress state of the lead sheathing layer. It is known that a reduced triaxiality has a beneficial effect on ductility and fatigue life of metals. In the present work a series of finite element simulations are performed in presence of galvanized steel tapes at three different winding angles and without such reinforcement at all, obtaining a qualitative indication of its effect on the stress state induced in the sheathing layer. Loading conditions as internal pressure due to thermal dielectric expansion and cable bending are modelled. The numerical qualitative results are discussed in light of a series of full-scale fatigue tests performed on subsea power cables with and without the support of steel tapes.
Keywords: subsea power cable, viscous deformation, fatigue, triaxiality factor, lead alloy

Submitted to: Engineering Structures

L.M.V. contributed with planning and interpreting the results of the numerical analysis and drafting the manuscript.

1.8 Thesis outline

Chapter I
The first chapter constitutes an introduction to the thesis. It is conceptually divided in three sections: in the first the background and motivation for the study are provided, in the second part there is a synthesis of concepts regarding the component, materials and mechanical behaviours of interest which will be useful for the comprehension of the thesis and in the third section the methods used for the research are explained.

Chapter II
The second chapter provides, through a journal and a conference paper, the necessary information on the microstructure, tensile and secondary creep behaviour and modelling of the alloy of interest.

Chapter III
The third chapter is composed of three conference papers focused on the fatigue testing of the material in three different conditions. The first observes the performance of the material under different strain rate displacement-controlled fatigue conditions. The second in focused on the observation of the tensile and cyclic deformation behaviour through in situ observation with scanning electron microscopy. The third collects a series of results of full-scale tests which will be object of further discussion in Chapter V.

Chapter IV
The fourth chapter is constituted of a journal paper and the relative journal extension on the fatigue properties of a lead alloy in presence of a geometrical discontinuity. The scope of the chapter is the assessment of the influence of manufacturing defects on the structural integrity of the sheathing.

Chapter V
The fifth chapter investigates the impact of the cable's layout, in particular of the steel tape armouring winded around the sheathing on the stress state of this component under different loads. The analysis if performed through finite element modelling and the results discussed in light of the data provided in Chapter III.

Chapter VI
The sixth chapter summarizes the main conclusions of the thesis.

Appendix
The appendix contains two additional works by the author on the topic of high temperature fatigue and creep of two different kind of metallic alloys.

1.9 Bibliography Chapter 1

[1] Program on Technology Innovation: Grain Growth in Lead Alloy Sheathing and Its Influence on the Life of Lead-Sheathed Power Cables. EPRI, Palo Alto, CA: 2007. 1015214.
[2] ANELLI, P.; DONAZZI, F.; LAWSON, W. G. The fatigue life of lead alloy E as a sheathing material fur submarine power cables. IEEE transactions on power delivery, 1988, 3.1: 69-75.
[3] M.E. Kassner, Fundamentals of Creep in Materials (Third Edition), Butterworth-Heinemann, 2015, ISBN 9780080994277.
[4] H. L. J. Pang, Y. P. Wang, X. Q. Shi and Z. P. Wang, Sensitivity study of temperature and strain rate dependent properties on solder joint fatigue life, Proceedings of 2nd Electronics Packaging Technology Conference (Cat. No.98EX235), 1998, pp. 184-189.
[5] Pradeep Lall, Di Zhang, Vikas Yadav, David Locker, High Strain-Rate Constitutive Behavior of SACI05 and SAC305 Leadfree Solder, 1EEE , 2015.
[6] M. Motalab, Z. Cai, J. C. Suhling and P. Lall, "Determination of Anand constants for SAC solders using stress-strain or creep data," 13th InterSociety Conference on Thermal and Thermomechanical Phenomena in Electronic Systems, San Diego, CA, 2012, pp. 910.
[7] Farghalli A. Mohamed, Terence G. Langdon, The transition from dislocation climb to viscous glide in creep of solid solution alloys, Acta Metallurgica, Volume 22, Issue 6, 1974, Pages 779-788, ISSN 0001-6160.
[8] Kassner, M. E. (2000). Five-power-law creep in single phase metals and alloys. Oxford: Pergamon.
[9] J.E. Skog et al. The NorNed HVDC cable link B1 Colloquium, Bergen, June 2009
[10] J.E. Skog et al. The NorNed cable link. A power transmission highway between Norway and the
Netherlands, Stavanger 2006.
[11] Worzyk, Thomas. Submarine Power Cables: Design, Installation, Repair, Environmental Aspects. Springer-Verlag Berlin Heidelberg. 2009.
[12] Ardelean, M., Minnebo, P.; 2015; HVDC Submarine Power Cables in the World; EUR 27527 EN; doi: 10.2790/95735
[13] Ana Aguado-Cornago. European Energy Studies, Volume VII: The European Supergrid. Claeys & Casteels Publishers BV. 2015.
[14] Thomas Courtney. Mechanical Behavior of Materials. McGraw-Hill International Editions.
[15] Smith, William F.; Hashemi, Javad (2006), Foundations of Materials Science and Engineering (4th ed.), McGraw-Hill.
[16] Dieter, George E. (1988). Mechanical Metallurgy. McGraw Hill Book Company.
[17] S. Mahajan, Deformation Twinning, Encyclopedia of Materials: Science and Technology, Elsevier, 2002.

[18] Jun-Shan Zhang. High Temperature Deformation and Fracture of Materials. Woodhead Publishing in Materials. 2007.
[19] M.E. Kassner. Fundamentals of Creep in Metals and Alloys. Butterwotrh-Heinemann. 2015.
[20] Holdsworth S. Creep-Fatigue Failure Diagnosis. Materials (Basel). 2015.
[21] S. Sahay, S. Guruswamy, and F. E. Goodwin, Proc. IEEE Electr. Insul. Magazine II: 12 (1995).
[22] CEN/TC 306 - LEAD AND LEAD ALLOYS.

Chapter 2: Tensile properties

This chapter provides, through a journal and a conference paper, the necessary information on the microstructure, tensile and secondary creep behaviour and modelling of the alloy of interest.

2.1 Paper I

Tensile characterization of a lead alloy: creep induced strain rate sensitivity

Luigi M. Viespoli[1], Audun Johanson[2], Antonio Alvaro[3], Bård Nyhus[3], Alberto Sommacal, Filippo Berto[1]

[1]*Department of Mechanical and Industrial Engineering, Norwegian University of Science and Technology (NTNU), Norway*
[2]*Nexans Norway, Innspurten 9, 0663 Oslo, Norway*
[3]*Sintef Industry, Richard Birkelands vei 2B, 7031, Trondheim, NORWAY*

luigimv@stud.ntnu.no
Richard Birkelands vei 2B, Trondheim, Norway

Abstract: The aim of this work is to investigate and define the tensile properties of cable sheathing lead alloy. In particular its strain rate sensitivity due to the pronounced creep already present at room temperature, in relation to the material work hardening and processing is object of study. Therefore, a series of specimens have been manufactured using cable sheathing of three different extrusion thicknesses and tested in displacement control at different strain rates. The practical difficulties generated by the highly plastic behavior have been overcome by the use of Digital Image Correlation (DIC) technique as a tool for measuring the strain field on the specimen surface. The creep behavior has been described, modeled and calibrated using Isight and finally implemented in the FEA code Abaqus. Two different numerical models have been used for modelling the time dependent deformation, a power law and the Anand model. The first predict correctly the response of the alloy in the primary creep region while the second shows better results for secondary creep.
Keywords: creep, plasticity, digital image correlation, finite element analysis, lead, microstructure

2.1.1 Introduction

Lead alloys used in subsea cable sheathing are usually associated with a low melting point Tm, i.e. about 590 K, and therefore a high relative operation temperature, around 0.5 Tm [1], even at room temperature. At this temperature, time dependents phenomena including creep, relaxation and recrystallization have a significant influence on the mechanical properties of the material. The time dependent mechanisms, which imply a strain rate dependency on the monotonic tensile properties, must therefore be accounted for in order

to accurately predict the mechanical behavior of components manufactured from lead alloys, such as power cable sheathing or battery grids. These responses are due to the influence of the active creep mechanisms also at low stress levels; particularly the apparent variation of the elastic modulus both in function of temperature and strain rate has been studied both for lead and lead-free solders [2, 3, 4]. In the case of pure polycrystalline metal lattices, the size of the grain has an influence on the creep response, with an increase of strain rate for a given stress in the presence of smaller grains, due to a greater contribution of boundary sliding [5]. A similar influence has been detected and reported on the yield stress [6]. On the specific topic of the characterization of the mechanical properties of lead alloys used for the production of subsea cable sheathing, some studies have been conducted. Feltham [7] investigated the mechanisms of creep deformation for lead alloys focusing on the influence of the grain size and intragranular substructure. Its conclusion is that the dislocation movement activation energy is a function of the volume self-diffusion, of the stress and, through a parameter q, of the Burgers' vector and of the average distance between dislocations. q is found independent of the applied stress and satisfactory results were obtained in the assumption of an exponential correlation of q with the temperature.Sahota et al. [8] performed compressive tests on work hardened commercially pure and on three different lead alloys, investigating the influence of alloying elements such as copper, antimony and tellurium on the secondary creep strain rate.Harvard [9] tested several different lead alloys with the aim of categorizing them for the proper use in the different power cables.Dollins and Betzer [10] synthetized the results of an extensive testing campaign of lead alloys for cable sheathing focusing also on the influence of the production process on the long term creep behavior.Anelli et al. [11] conducted fatigue testing on lead alloy E, slightly supersaturated Pb-Sb alloy. Their tests at different strain amplitude and rate have found a limited influence of temperature and grain size on the fatigue life of a properly manufactured cable.

2.1.2 Material and metallurgical investigation

Lead alloy of composition according to Table 1 was extruded into a pipe of 82 mm outer diameter (OD) and 1.1, 1.8 and 3.3 mm thickness during the cable production process. The choice of the alloy object of the study is driven by the necessity of working on a real sub-sea power cable sheathing material. Due to the slow operational cycles undergone by the cables generated by oceanic currents, tides and thermal expansion, it is important to understand the influence of the strain rate on the stress level induced in the cable. The cables have been cut, the pipes unfolded, then the specimens have been machined to a flat dog-bone geometry, figure 5. During the flattening procedure, the same train rate has been applied according to the different thickness.

Pb [wt%]	Sb [wt %]	Sn [wt %]
99.3	**0.2**	**0.5**

Table 2.1.1. Test material composition.

For the understanding and characterization of the alloy's properties, it is important to understand the microstructure of the sheathing and its influence on the stress-strain response. With careful procedure, due to the extreme thermal and mechanical sensitivity of the alloy, a series of samples for metallographic investigation have been prepared. They have been cut from the non-tested sheathing in as-manufactured condition. The planes along which the investigation has been performed are indicated as A and B in figure 1. The grain size has been measured with the average grain intercept technique and the results are summarized in table 2. Figure 4 shows the result of the investigation in the two planes for the three specimens at a magnification of 200x.

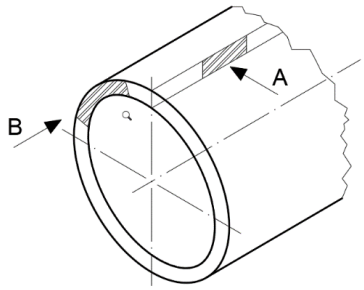

Figure 2.1.1. Scheme of the planes adopted for the metallography.

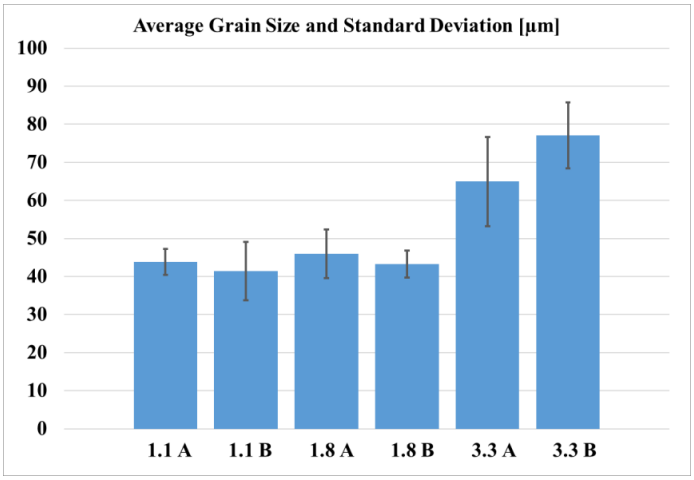

Figure 2.1.2. Average Grain Intercept synthetic results according to thickness and grinding plane, see figure 3, 50x.

Extrusion thickness [mm]	Plane orientation (see figure 1)	Line	Line length [µm]	Grain boundaries count	Average grain size on line [µm]
1.1	A	1	2428	51	47.6
		2	2423	52	46.6
		3	2421	63	38.4
		4	1026	24	42.8
		5	1026	22	46.7
		6	1024	25	41.0
	B	1	2452	43	57.0
		2	2448	56	43.7
		3	2432	60	40.5
		4	1094	29	37.7
		5	1055	31	34.0
		6	1037	29	35.7
1.8	A	1	2438	47	51.9
		2	2458	44	55.9
		3	2446	56	43.7
		4	1821	50	36.4
		5	1821	40	45.5
		6	1825	43	42.4
	B	1	2438	55	44.3
		2	2436	54	45.1
		3	2444	53	46.1
		4	1813	42	43.2
		5	1809	40	45.2
		6	1821	51	35.7
3.3	A	1	2440	41	59.5
		2	2438	41	59.4
		3	2444	27	90.5
		4	3259	51	63.9
		5	3255	59	55.2
		6	3244	53	61.2
	B	1	2470	28	88.2
		2	2421	37	65.4
		3	2398	30	79.9
		4	3303	38	86.9
		5	3277	48	68.2
		6	3259	44	74.1

Table 2.1.2. Average Grain Intercept extended results, see figure 3, 50x

	A (Tangential view/longitudinal cut)	B (Longitudinal view/transversal cut)
3.3 mm	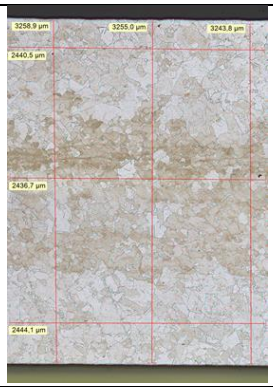	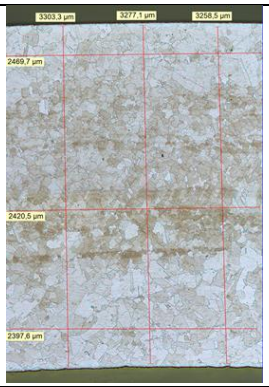
1.8 mm	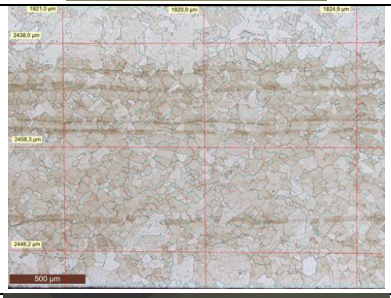	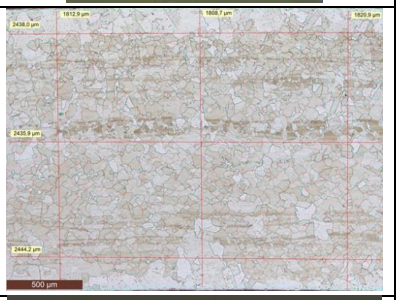
1.1 mm	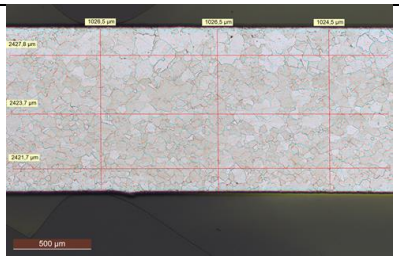	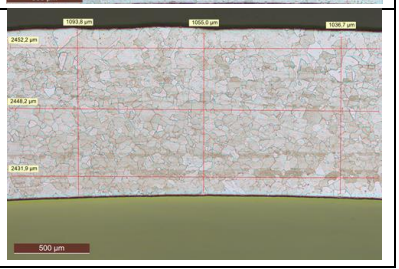

Figure 2.1.3. Synthesis of the Average Grain Intercept measurements reported in table 2 according to figure 1 grinding plane, 50x.

	A (Tangential view/longitudinal cut)	B (Longitudinal view/transversal cut)
3.3 mm	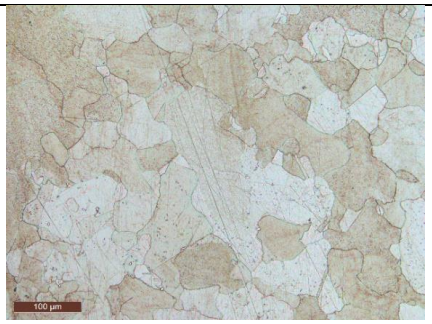	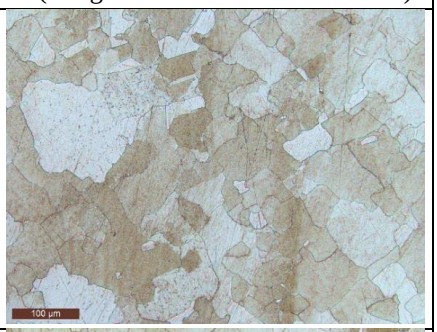
1.8 mm	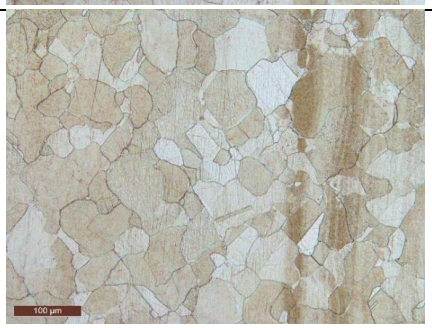	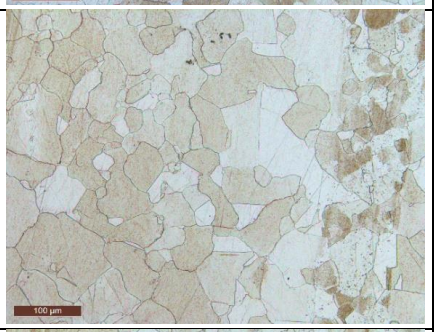
1.1 mm	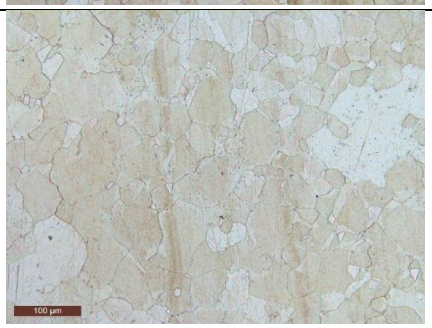	

Figure 2.1.4. Detail of the grain structure according to figure 1 grinding plane, 200x.

According to the results of the AGI, in table 2, the average grain size for the 1.1 and 1.8 mm extrusion thickness is very similar, around 43 µm, while the 3.3 mm extrusion thickness leads to a bigger grain size, around 70 µm. This has a major influence in the creep behavior and material's mechanical response, as shown in the following paragraph. During the polishing process it is possible that small localized plastic deformations are induced in the material, like surface scratching. This originates small grains, which are not indicative of the true structure of the sheathing. These grains have been discarded from the statistical computation. Differentiating the results of the AGI on the A plane, no

systematic difference of the grain size in the longitudinal and radial direction is seen for the 1.1 and 1.8 mm thick specimens, while a slight difference, with the grains on average 17.7% longer in the longitudinal direction, is present for the 3.3 mm thick samples. This indicates that the recrystallization of the sheathing at room temperature after the manufacturing removes the grain elongation induced by the extrusion.

2.1.3 Tensile testing procedure

The aim of the paper is to provide a material model of the alloy adopted able to reproduce its mechanical response to deformations imposed at room temperature and suitable for integration in finite element component modelling. In order to collect the necessary data, a series of tests on tensile specimens has been executed. The tensile specimens have been cut from lead sheathings of three different thicknesses and tested at room temperature at different strain rates. To enhance the precision of the numerical models, their correctness has then been verified with respect to the results from a relaxation test. During the testing the material has shown primary and secondary creep behavior, with the latter reached for the slower strain rate tests. The behavior observed is characterized by an influence of the strain rate both on the stress level and on the apparent elastic modulus. Since all the test have been performed at room temperature, no temperature dependence is accounted for. Moreover, the thicker specimens, 3.3 mm, have shown a higher stress response compared to the 1.8 and 1.1 mm thick ones. The results presented consist in a series of static tests performed at different strain rates on specimens of different thicknesses, whose design and dimensions are reported in Figure 5a. The nominal strain rate imposed to the specimens during the test, ranging from 1E-7 1/s to 1E-3 1/s, is computed over the free length, that is, the constant width section of the specimen. The tests have been recorded via a Prosilica GC 2450 digital camera and the frames used have been then used for DIC analysis of the field of deformation in the plane using the eCorr DIC post-processer. The strain adopted as reference, to approximate the material behavior, is the infinitesimal strain in the longitudinal direction, computed on a vector in the central section of the specimen, as indicated by a white line in fig. 5b.

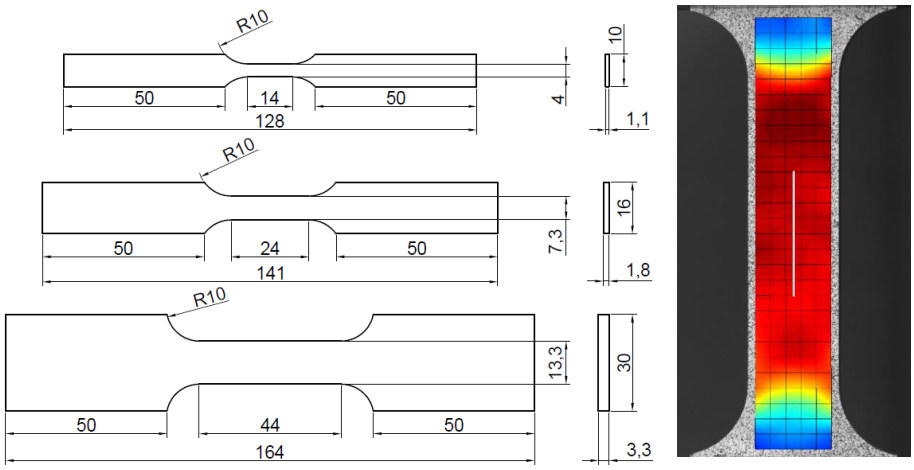

Figure 2.1.5. a) Specimens geometries and dimensions. b) An example of the DIC mesh and longitudinal strain field: the white line represents the vector adopted for the quantification of the strain.

The extremely low stresses at which the alloy shows plastic behavior, united with the presence of room temperature viscous flowing, originate practical difficulties in performing the tensile testing. In particular, the border effects due to the deformation of the specimen under the pressure of the clamping system, makes impossible to accurately estimate the strain imposed to the material simply by utilizing the clamp stroke. Therefore, the adoption of the DIC technique has permitted to investigate the behavior of the material, numerically reconstructing the in-plane strain field on the specimen's surface.

2.1.4 Tensile testing results

The results, summarized in figures 6 and 7, indicate that two major factors influence the tensile response of the material: the thickness and the strain rate. As the strain rate is reduced, so it is the load necessary in order to reach a given strain level indicating a pronounced viscous behavior of lead alloy, even at room temperature. The first sensible influence can be as the strain rate is lowered from 1E-3 to 1E-4 1/s of strain rate and the loss in maximum stress is enhanced as the testing strain rate is further lowered. The second variable that clearly affect the material tensile properties is the sample thickness: contrarily to what is common seen for metals, the thicker is specimens, the higher is the resistance in terms of nominal stress.

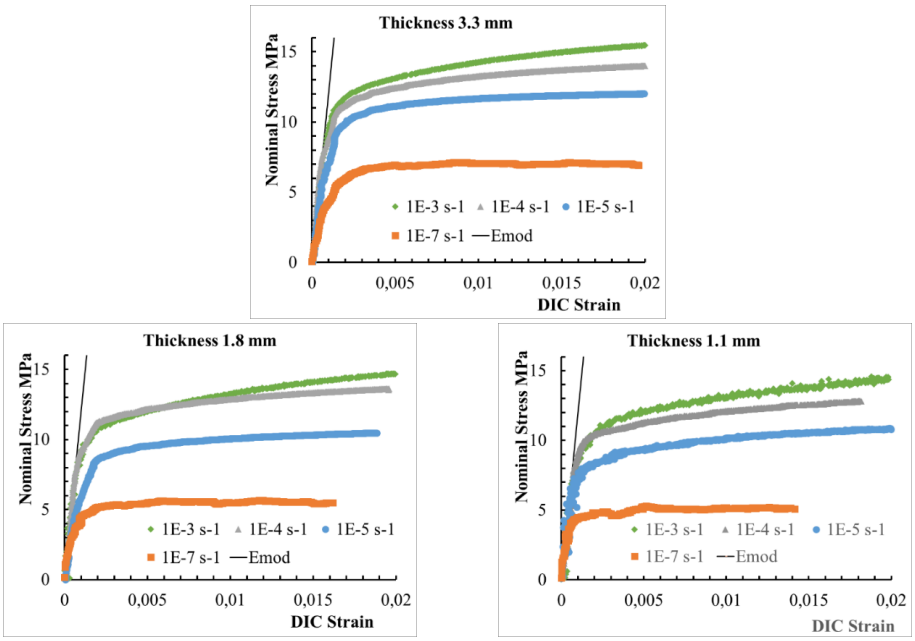

Figure 2.1.6. Comparison of the Digital Image Correlations results grouped for thickness.

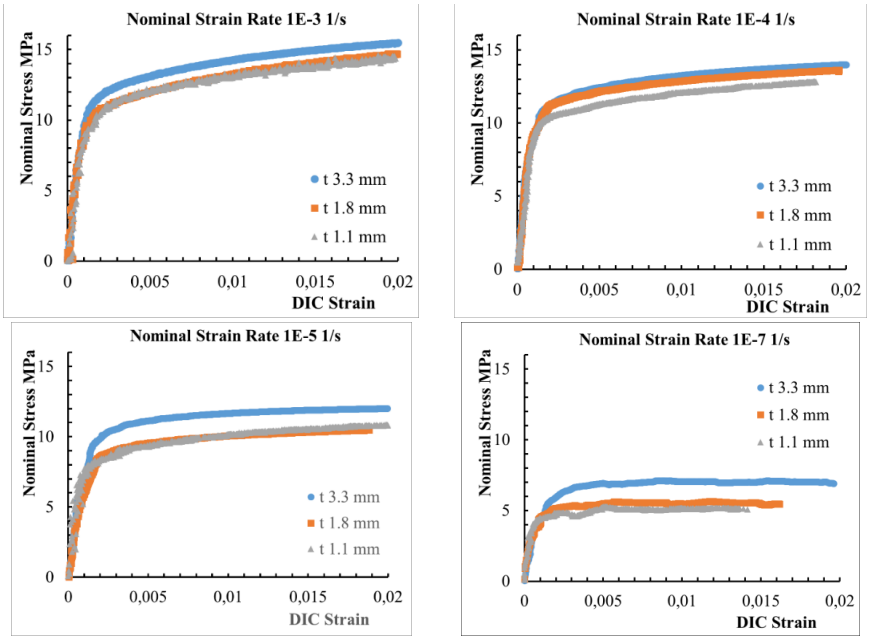

Figure 2.1.7. Comparison of the Digital Image Correlations results grouped for nominal strain rate.

2.1.5 Strain rate sensitivity of the young's modulus

By observing the initial stress-strain response of the material, and determining the Young's modulus as the slope of the curve, it has been experimentally observed a decrease of this value as strain rate is reduced. This trend is consistent with respect to previous works on Lead and Lead-free solder alloy, among those Motalab et al. [4], Pradeep et al. [3], Pang et al. [2], who showed a linear dependence between the elastic modulus and both temperature and strain rate. Furthermore, they implemented the Anand model to numerically replicate the experimental result. Pang et al. studied the behaviour of a 63Sn/37Pb solder alloy for different temperature and strain-rate values, suggesting the following equation:

$$E(T, \dot{\epsilon}) = (a_3 T + a_2) \log(\dot{\epsilon}) + (a_1 T + a_0) \qquad (2.1.1)$$

Pang's equation shows a good agreement with experimental data, since no temperature dependent test were conducted, only the strain rate dependent variables were computed. The result for 3.3 and 1.8 mm thick specimens are shown in figure 8.

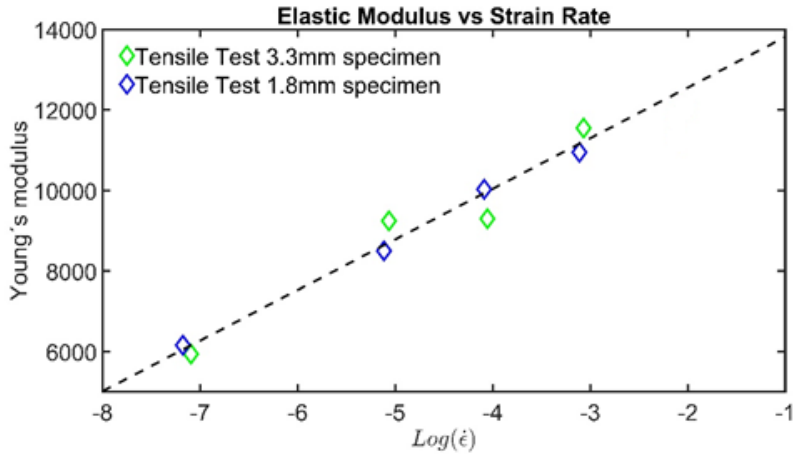

Figure 2.1.8. Variation of the apparent elasticity modulus as a function of the strain rate.

With, lacking data on the influence of the temperature:

- $(a_3 T + a_2) = 1257$ MPa
- $(a_1 T + a_0) = 15070$ MPa

It is possible to implement this result in the calibration of the material, adopting a user sub-routine which modifies the elastic modulus according to the strain rate at the previous iteration. It must be stressed that this is an engineering approach and does not correspond to the physics of the phenomenon. Although this procedure improves the capability of the models implemented in the following paragraphs to describe the initial part of the loading,

the results of the calibration presented are at constant elastic modulus, in order to investigate their capability to deal with the problem as they are provided.

2.1.6 Power Law creep model

A model to reproduce the mechanical response of the alloy to a deformation imposed has been tested using FEA in Abaqus environment. After having defined elastic and plastic behavior, the time dependent strain component has been defined as a power law, using the preset strain hardening form [12] :

$$\dot{\varepsilon}^{cr} = (A\tilde{q}^{n}[(m+1)\varepsilon^{cr}]^{m})^{\frac{1}{m+1}} \qquad (2.1.2)$$

Where:

$\dot{\varepsilon}^{cr}$ is the uniaxial equivalent creep strain rate, $\sqrt{\frac{2}{3}\dot{\varepsilon}^{cr}:\dot{\varepsilon}^{cr}}$

$\tilde{q}$ is the uniaxial equivalent deviatoric stress, A, n and m are to be calibrated to reproduce the right creep behavior. For a physically meaningful solution, A and n have to be positive and $-1 < m \leq 0$. In the Isight loop, figure 9, the three tensile simulations have been run simultaneously. Experimental and numerical response are compared after each calibration cycle in the data matching component with respect to two different quantities: the absolute difference between the experimental and simulation curves and the maximum absolute value. In such way both a global and local fit of the data is guaranteed.

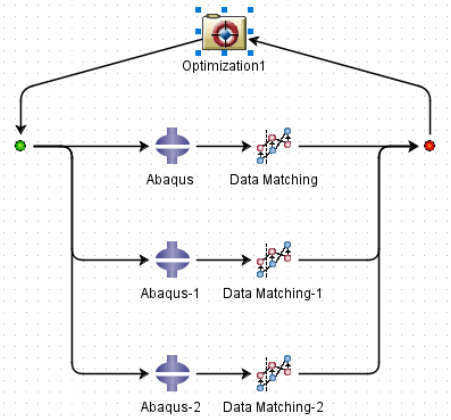

Figure 2.1.9. Optimization loop set in Isight for the calibration of the creep constants.

The model parameters as fitted are listed in Table 3,4. Table 3 summarizes the elasticity modulus, Poisson ratio and the three parameters of the power law model fitted with the aid of Isight. In table 4, the plastic curves for the material ideally in absence of creep are reported. These are individuated as a material response slightly stronger than the response at a nominal strain rate of 10E-3 s-1. This is a reasonable approach considering that the influence of the viscous deformation is very limited for the two highest strain rates tested and yields to fairly accurate results in the calibration of the creep models, as shown in figure 10. The same parameters are adopted, for the sake of uniformity, in the calibration of the Anand creep model in the next paragraph. The model adopted is feasible for the description of primary creep behavior. The secondary creep is characterized by a constant creep strain rate for a given stress level. The tests are executed at constant strain rate and a plateau is observed in the Stress-Strain curve for the tests at a nominal strain rate of 1E-7 1/s. This indicates that these tests lasted long enough so that the material entered the secondary creep phase, thus making the model unfit for the scope. This can be clearly seen in Figure 10, where the slope of the numerical stress-strain curve at the nominal strain rate of 1E-7 1/s is always greater than zero, giving a poor fitting for the slowest deformation.

Thickness [mm]	E [MPa]	ν	A	n	m
1.1 – 1.8	12000	0.431	7.27818E-10	5.10577	-0.389647
3.3	12000	0.431	5.27817E-10	5.22075	-0.468147

Table 2.1.3. Power law model constants as fitted for power law model.

Thickness [mm]			
1.1 – 1.8		3.3	
σ [MPa]	ε_{pl}	σ [MPa]	ε_{pl}
7.0	0.0	7.4	0.0
7.6	8.46e-05	7.9	6,00E-05
7.9	0.000134662	8.45	0.00013
8.5	0.000256403	9.05	0.00021
9.1	0.000418085	9.8	0.00031
9.8	0.000636959	10.5	0.00044
10.45	0.000935883	10.95	0.00057
10.8	0.00112436	11.3	0.00068
11.45	0.00166643	11.6	0.0008
11.8	0.00215645	11.8	0.00093
12.3	0.00337669	12.05	0.00108
12.8	0.0049784	12.26	0.00129
13.4	0.00703124	12.55	0.00158
13.7	0.00821398	12.9	0.00198
14.6	0.0125104	13.15	0.0024
15.5	0.0182811	13.47	0.0031
15.8	0.0205588	13.95	0.0042
16.4	0.0261663	14.3	0.0052
16.7	0.0301544	14.6	0.0064
17.3	0.0438478	14.9	0.0075
17.9	0.0719805	15.25	0.0088
18.5	0.122769	15.65	0.011
18.8	0.157931	16.6	0.0173
19.4	0.244784	17.3	0.0248
20.0	1.0	20.0	1.0

Table 2.1.4. Plastic table adopted for power law and Anand model calibration.

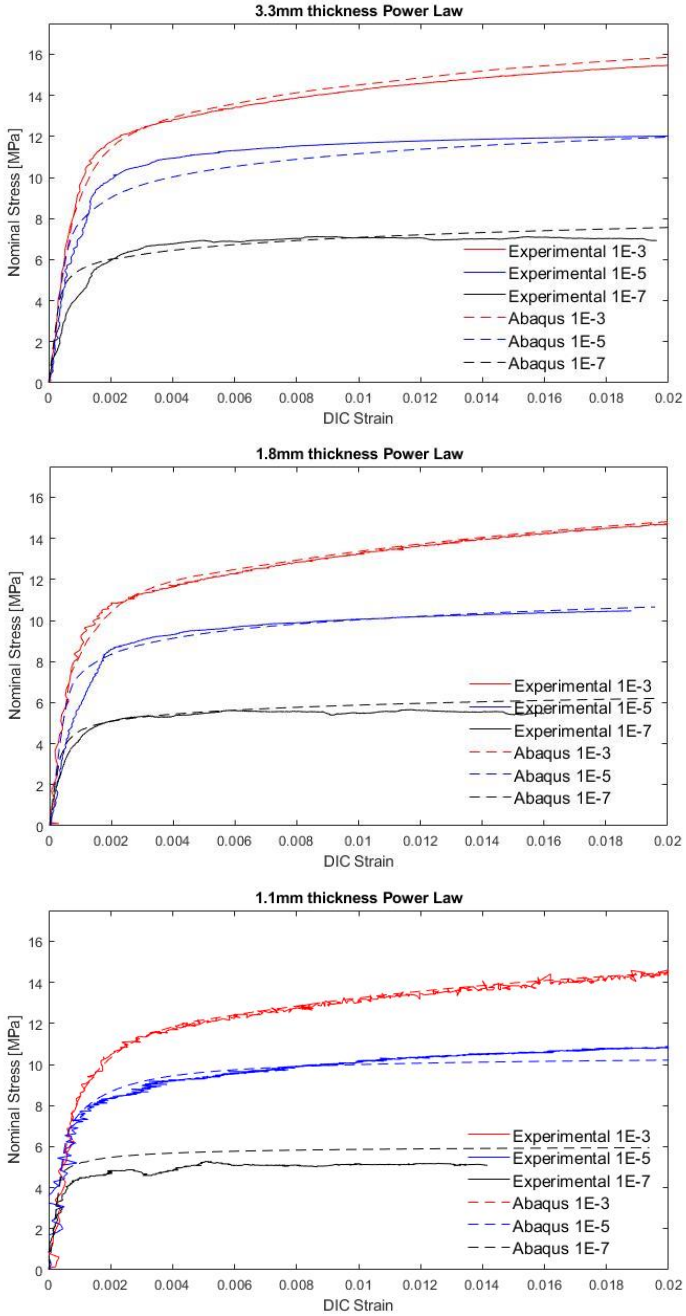

Figure 2.1.10. Power law model fitting compared with experimental results for three different strain rates.

2.1.7 Anand creep model

The model utilized describe both primary and secondary creep was initially proposed by Anand, et al. [13]- [14] for predict the rate-dependent deformations of metal in the high temperature range. Although it was originally developed to describe hot-working processes, it shows great result in predicting creep behavior for a wide range of alloys, mainly in the electronics field [15, 16, 17]. In the microelectronics industry is commonly used to predict and verify the reliability of solders exposed to thermal cycling, and the necessary model constants are available in literature for a large number of materials. The model constitutive equation considers both strain hardening and temperature dependent behavior and it has been showing good predicting ability with respect to primary and secondary stage creep transition. The Anand model implemented in Abaqus presents fifteen parameters, six more with respect to the model proposed by Anand et al [13, 14]. A comparison between the original and Abaqus version of the model is reported in [18] , with the latter showing a more precise fitting of experimental response for a wide range of temperature. The relation between stress and strain rate is model by the flow equation:

$$\dot{\epsilon}^{cr} = A * exp\left(-\frac{Q}{R(\theta - \theta^{z})}\right)\left[\sinh\left(\frac{\xi \bar{q}}{s}\right)\right]^{\frac{1}{m}} \tag{2.1.3}$$

Where:

- A is called "pre-exponential factor"
- Q is the activation energy
- m is the strain rate sensitivity exponent
- R is the universal gas constant
- ξ is a material parameter
- θ^{z} is the absolute value of the temperature
- $\tilde{q}$, $\dot{\varepsilon}^{cr}$ are defined above

Equation (3) is equal, except for the term s, to Garofalo's equation (4), that is commonly used for modelling the relationship between steady state stress and steady state creep strain [19].

$$\dot{\epsilon}_{ss}^{\ cr} = A * exp\left(-\frac{Q}{R(\theta)}\right)[sinh(\xi \sigma_{SS})]^{\frac{1}{m}} \tag{2.1.4}$$

The internal structure of the material is characterized by an internal variable, s. This has the dimension of a stress and represent the isotropic resistance opposed by the material to plastic flow. The evolution equation considers dynamic process such as strain hardening and recovery:

$$\dot{s} = h_0 \left|1 - \frac{s}{s^*}\right|^a sign\left(1 - \frac{s}{s^*}\right) \dot{\epsilon}^{cr} \quad (2.1.5)$$

With

$$s^* = \hat{s}\left[\frac{\dot{\epsilon}^{cr}}{A}\exp\left(\frac{Q}{R(\theta - \theta^z)}\right)\right]^n \quad (2.1.6)$$

And

$$h_0 = A_0 + A_1(\theta - \theta^z) + A_2(\theta - \theta^z)^2 + A_3\dot{\epsilon}^{cr} + A_4(\dot{\epsilon}^{cr})^2 \quad (2.1.7)$$

The initial deformation is described by:

$$s_0 = S_1 + S_2(\theta - \theta^z) + S_3(\theta - \theta^z)^2 \quad (2.1.8)$$

s^* represents the saturation value of *s* for a given strain rate and temperature. h_0 is the strain hardening or softening constant. $\hat{s}$ is a numerical coefficient, *n* and *a* are material parameters The six more parameters that are present in the Abaqus modified Anand model are *A1,A2,A3,A4 and S2,S3* [12].

The Isight optimization flowchart used in the calibration of the material is reported in figure 11 and, for the 3.3 mm thick specimen, also a relaxation test is included. Four different simulations were run simultaneously and the simulation response is compared after each cycle with experimental data. In the optimization component the Neighborhood Cultivation Genetic Algorithm has been used due to his ability to explore all the design space and find a global minimum value of the objective function in case of multi-object optimization [12]. Table 5 synthesizes the parameters obtained as result of the optimization loops and figure 12 illustrates the relative Stress-Strain curves ordered by thickness and strain range.

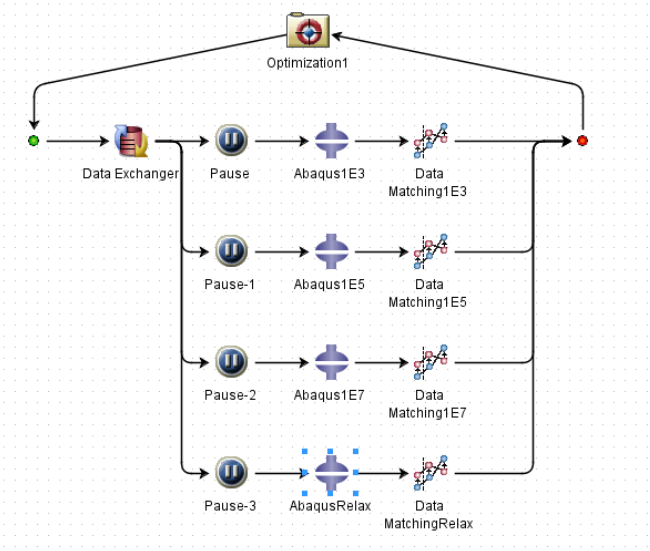

Figure 2.1.11. Optimization loop set in Isight for the calibration of the creep constants (top left). Anand creep model compared to experimental results.

	Thickness [mm]	
Parameter	1.1 – 1.8	3.3
S1	4.8749986	4.2073727
Q/R [K]	9599.5582	9845.9687
A	2499.9986	56524.519
ξ	4.5	3.6432953
m	0.41733489	0.43475551
A0	153587.88	158793.25
$\hat{s}$	4.6970472	6.8885417
n	0.037181053	0.011472397
a	2.9462357	2.2818810
S2	0	0
S3	0	0
A1	0	0
A2	0	0
A3	0	-261661.53
A4	0	686840.06

Table 2.1.5. Anand model constants as fitted for primary and secondary creep.

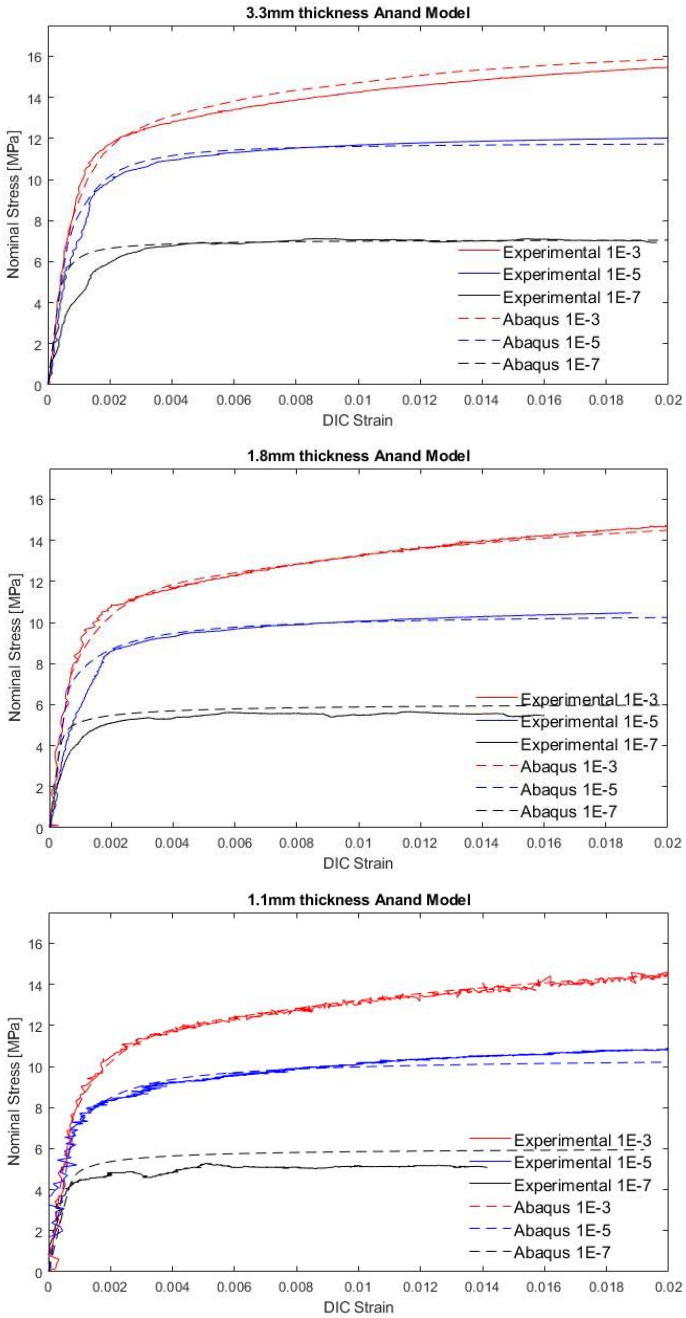

Figure 2.1.12. Anand model fitting compared with experimental results for three different strain rates.

2.1.8 Relaxation test

The Isight model was not able to optimize both the tensile and relaxation experiment simultaneously, if this was done considering a perfectly constant global strain during the relaxation phase. By using the parameters obtained from the tensile tests calibration, the numerical stress vs time curve was higher than the one obtained from experimental test. However, the DIC post-processing of the relaxation test showed that, during the hold/relaxation phase, a reduction of strain occurred, most probably due to a slipping in the clamps, figure 13b. By taking into account these effect the FEA simulation gave the correct relaxation behavior.

a) b)

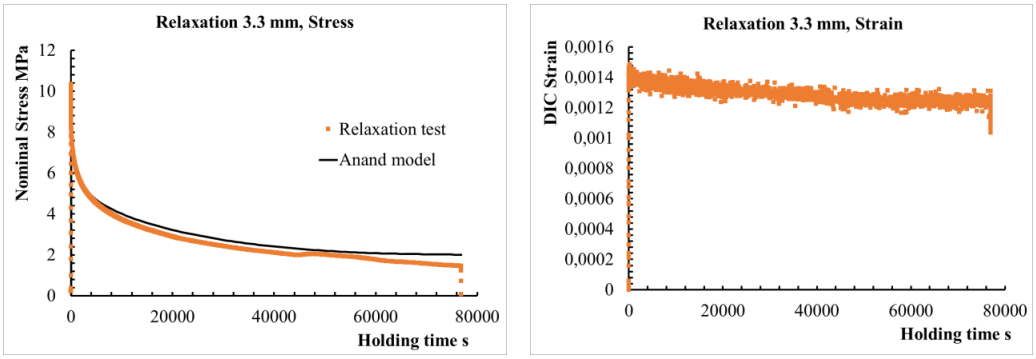

Figure 2.1.13. Relaxation test result: Stress vs Time curve (a) and DIC strain vs. time curve (b).

2.1.9 Conclusions

In this study, the behavior of a lead alloy at three different strain rate values was analyzed. Tensile test was conducted on three different geometries, finding a relation between thickness and steady state stress. Based on the test results, two different calibrations were performed, one for the 3.3 mm thick specimen and one suited for the 1.8mm and 1.1mm thick specimens. The derived constitutive laws were implemented in the commercial FEM code Abaqus. Two different models are adopted in this paper. The power law model, most suited for describing the primary creep region, which is attractive for its simplicity. The Anand model, on the other hand, is defined by fifteen parameters and is able to correctly represent also the secondary creep region and the temperature dependent response. Since no temperature dependent test were conducted only the strain rate behavior was calibrated. Isight was used in conjunction with Abaqus for optimizing the model. Due to the highly viscous and non-linear behavior of the material, DIC has been necessary for computing the actual strain values on the specimen's surfaces. In particular, during the relaxation test made on the 3.3 mm thick specimens, a reduction of the

longitudinal strain is observed. Considering this trend, the result is in agreement with numerical simulations. For explaining the thickness effect a metallographic investigation has been done, finding bigger average grain size in the 3.3mm specimen. This result explains the different value of steady state stress reached in the experimental test, due to the higher creep resistance for the thicker extrusion. To summarize the main conclusions are:

- The power law creep model is desirable for its simplicity and well performed at the higher strain rates.
- The Anand creep model performed better for the lower strain rates.
- The Anand creep model is indicated also for the time stress response at constant deformation.
- The extrusion thickness resulted proportional to the average grain size, giving an improved resistance for a higher thickness.
- The digital image correlation is an irreplaceable technique when dealing with very ductile alloys.

Acknowledgements

The present work was financed by Nexans Norway AS and the Research Council of Norway (IPN in ENERGIX Project number 256367) and performed within the project: Next-generation damage based fatigue of cable sheathing (REFACE).

References

[1] M.E. Kassner, Fundamentals of Creep in Materials (Third Edition), Butterworth-Heinemann, 2015, ISBN 9780080994277.

[2] "H. L. J. Pang, Y. P. Wang, X. Q. Shi and Z. P. Wang, "Sensitivity study of temperature and strain rate dependent properties on solder joint fatigue life," Proceedings of 2nd Electronics Packaging Technology Conference (Cat. No.98EX235), 1998, pp. 184-189.".

[3] "Pradeep Lall, Di Zhang, Vikas Yadav, David Locker, High Strain-Rate Constitutive Behavior of SACI05 and SAC305 Leadfree Solder, 1EEE , 2015".

[4] M. Motalab, Z. Cai, J. C. Suhling and P. Lall, "Determination of Anand constants for SAC solders using stress-strain or creep data," 13th InterSociety Conference on Thermal and Thermomechanical Phenomena in Electronic Systems, San Diego, CA, 2012, pp. 910.

[5] "Farghalli A. Mohamed, Terence G. Langdon, The transition from dislocation climb to viscous glide in creep of solid solution alloys, Acta Metallurgica, Volume 22, Issue 6, 1974, Pages 779-788, ISSN 0001-6160".

[6] "Kassner, M. E. (2000). Five-power-law creep in single phase metals and alloys. Oxford: Pergamon.".

[7] "P. Feltham. On the Mechanism of High-Temperature Creep in Metals with Special Reference to Polycristalline Lead. Proc Phys Soc. 69,12-B. 1956".

[8] "M K Sahota, J R Riddington. Compressive creep properties of lead alloys. Materials and Design. 21: 159-167. 2000".

[9] "DG Harvard. Fatigue of Lead Cable-Sheathing Alloys. Ontario Hydro research. 1972".

[10] "CW Dollins, CE Betzer. Creep Fracture and Bending of Lead and Lead Alloy Cable Sheathing. Engineering experiment station bulletin 440. 1956".

[11] F. D. W. L. P. Anelli, "The fatigue life of lead alloy E as a sheathing material for submarione power cables.," *Societa' cavi Pirelli*, pp. 86 SM 393-3, 1986.

[12] "Dassault Systèmes, SIMULIA User Assistance 2017, 2017".

[13] "Anand, L., "Constitutive Equations for the Rate-Dependent Deformation of Metals at Elevated Temperatures," Journal of Engineering Materials and Technology, Vol. 104(1), pp. 12-17, 1982.”".

[14] "Brown, S., Kim, K., and Anand, L., "An Internal Variable Constitutive Model for Hot Working of Metals," International Journal of Plasticity, Vol. 5(2), pp. 95-130, 1989".

[15] "Z.N. Cheng, G.Z. Wang, L. Chen, J. Wilde and K. Becker Viscoplastic Anand model for solder alloys and its application Soldering & Surface Mount Technology 12/2 [2000] 31±36".

[16] "Liang Zhang, Ji-guang Han, Yonghuan Guo, Cheng-wen He. 2014. Anand model and FEM analysis of SnAgCuZn leadfree solder joints in wafer level chip scale packaging devices. Microelectronics Reliability 54:1, 281-286.".

[17] "B. Rodgers, B. Flood, J. Punch, F. Waldron. Experimental determination and finite element model validation of the anandviscoplasticity model constants for SnAgCu 490-496.".

[18] "Swaminathan, Shriram et al. “Calibrating Material Constants from Experimental Data for Lead-free Solder Materials Using a Parametric Optimization Approach.” (2011).".

[19] "Garofalo, F., 1963. An empirical relation defining the stress dependence of minimum creep rate in metals Trans. Metall. Soc. AIME, 227 (1963), pp. 351-356".

2.2 Paper II

Room temperature creep mechanism of a Pb-Sn-Sb lead alloy

Luigi Mario Viespoli[a*], Audun Johanson[b], Antonio Alvaro[c], Bård Nyhus[c], Filippo Berto[a]

[a]*Department of Mechanical and Industrial Engineering, Norwegian University of Science and Technology (NTNU), Norway*
[b]*Nexans Norway, Innspurten 9, 0663 Oslo, Norway*
[c]*Sintef Industry, Richard Birkelands vei 2B, 7031, Trondheim, NorwayAbstract*

Abstract: Lead alloys are the most common materials adopted for the production of subsea power cable sheathing. The sheathing is a layer of stable and watertight metal, which serves to prevent the electrical failure of the cable. During the predicted operational life of the cables of several decades, these experience strains due to the installation process, the oceanic currents and the thermal expansion of the cable. The low melting temperature of such alloys, around 600 K, imply that creep deformation will occur when subjected to loading even at room temperature. The goal of the present study is to investigate the tensile behavior of the Pb-Sb-Sn alloy of interest in order to predict the correlation between strain rate and stress level. A mechanical characterization was performed through tensile testing at different strain rates of specimens cut from power cable sheathing. Due to the extreme ductility of the material, the use of digital image correlation was necessary to compute an acceptable approximation of the in-plane strain field on the surface of the specimens. The results were implemented in finite element method environment using Abaqus and Isight to calibrate a creep model able to reproduce at best the behavior of the material. Such model was also positively tested in the case of a relaxation test. In addition, a tensile test of several steps at different loads was executed with the aim of extrapolating and interpreting the steady state creep exponents at different creep regimes and the indications that these can provide on the deformation mechanisms of the alloy.
Keywords*:* lead; creep; plasticity mechanisms; modelling; digital image correlation

* Corresponding author. Tel.: +47-459-13-281
E-mail address: luigi.m.viespoli@ntnu.no

2.2.1 Introduction

Power cables used for submarine applications necessitate a watertight layer to prevent failure from electrical short circuit. Due to their properties of chemical stability and ductility, lead alloys have been employed for decades for the manufacturing of the sheathing layer. Due to the melting point inferior to 600 K, such alloys operate in a relatively high temperature regime. Creep deformation, stress relaxation and recrystallization are phenomena relevant at room temperature operation, Kassner et al (2015) [1]. Similar materials have been often studied in the microelectronics field, in which the interest is focused on the creep-fatigue interaction of solders, Pang et al. (1998) [2], Lall et al. (2015) [3], Motalab et al. (2012) [4]. Creep mechanisms which depend on grain boundary sliding present an increased resistance to deformation and a higher yield stress for an increased grain size, Fargalli et al. (1974) [5], Kassner et al. (2000) [6], Viespoli et al. (2019) [7]. Most of the research on the specific topic of the creep and fatigue behavior of lead alloys for the production of cable sheathing reaches to several decades ago, Feltham et al. (1956) [8], Sahota et al. (2000) [9], Harvard (1972) [10], Dollins and Betzer (1956) [11], Anelli et al. (1986) [12]. Up to date design has been performed on the base of experience and acquired know how. New interest for this research has in the recent years risen from the industry with the aim of a deeper understanding of the mechanisms driving the deformation and damage, Johanson et al. (2018) [13], of such alloys for a more conscious, efficient and sustainable production. The manuscript presents the result of a series of tensile tests giving insight on the deformation mechanisms possibly active during the installation and operation of the power-line, which sees decades of low strain rate, strain controlled deformation cycles caused by sea currents and tides and thermal cycling due to the periodic power request.

2.2.2 Material tensile characterization and modelling

2.2.2.1 Anand creep model

For the numerical reproduction of the mechanical response of a metallic alloy subjected to creep deformation at elevated temperature several models have been proposed. Of these, the one proposed by Anand, Anand (1982) [14], Brown et al. (1989) [15], is able to reproduce the creep behavior in the primary and secondary stage, that is the steady state creep regime. The constitutive equations characterizing the model include the effects of both temperature and strain hardening. The stress-strain correlation is expressed by the flow equation:

$$\dot{\bar{\varepsilon}}^{cr} = A \cdot \exp(-Q/R(\theta - \theta^z)) \left[\sinh\left(\xi \bar{q}/s\right)\right]^{1/m} \tag{2.2.1}$$

The different parameters included in the equation above are:

A , pre-exponential factor;
Q , activation energy;
m , strain rate sensitivity exponent;
R , universal gas constant;
ξ , material parameter;
θ^z , absolute temperature value;
$\bar{q}$, uniaxial equivalent deviatoric stress
$\dot{\bar{\varepsilon}}^{cr} = \sqrt{\frac{2}{3}\dot{\varepsilon}^{cr} : \dot{\varepsilon}^{cr}}$, uniaxial equivalent creep strain rate.

The response of the material depends on an internal value s, which is dimensionally a stress and corresponds to the resistance opposed to the plastic flow. The evolution of this variable considers strain hardening and recovery in the form:

$$\dot{s} = h_0 \left| 1 - s/s^* \right|^a \, sign\left(1 - s/s^*\right) \dot{\bar{\varepsilon}}^{cr} \tag{2.2.2}$$

Being:

$$s^* = \hat{s}\left[\dot{\bar{\varepsilon}}^{cr} / A \cdot \exp\left(Q/R\left(\theta - \theta^z\right)\right)\right]^n \tag{2.2.3}$$

And:

$$h_0 = A_0 + A_1\left(\theta - \theta^z\right) + A_2\left(\theta - \theta^z\right)^2 + A_3\dot{\bar{\varepsilon}}^{cr} + A_4\left(\dot{\bar{\varepsilon}}^{cr}\right)^2 \tag{2.2.4}$$

While the initial deformation resistance is:

$$s_0 = S_1 + S_2\left(\theta - \theta^z\right) + S_3\left(\theta - \theta^z\right)^2 \tag{2.2.5}$$

s^* is the saturation value of s at a certain strain rate and temperature. h_0 is the strain rate or softening constant, $\hat{s}$ is a coefficient and a and n are material dependent. The Anand creep model implemented in the finite element modelling software Abaqus is modified with the addition of the six parameters $A_1, A_2, A_3, A_4, S_2, S_3$, SIMULIA User Assistance (2017) [16].

2.2.2.2 Tensile testing and creep model calibration

Before the determination of the steady state creep exponents of the material, a tensile investigation and numerical calibration of the Anand model were executed, Viespoli et al. (2019). The lead alloy object of the investigation in the present work is an E alloy the composition of which is reported in Table 1. The material was received in the form of extruded tubes of 82 mm of diameter and 3.3 mm of wall thickness. Such tubes constitute the sheathing layer, that is the watertight barrier and provides electrical short-circuit

failure resistance to the subsea power cable. The alloy was cut and unfolded from a power cable section and machined to obtain the dog-bone geometry in Figure 1 a. For computing the real longitudinal strain of the material, overcoming the practical challenges caused by the elevated ductility of the alloy, the digital image correlation (DIC) technique was used, recording the tests with a Prosilica GC 2450 digital camera and post processing the results with the software eCorr, Figure 1 b and 1 c. To obtain the response of the alloy tensile testing at nominal strain rates of 1E-3, 1E-5 and 1E-7 s-1 and a relaxation test from the stress of 10 MPa were performed. The nominal strain rates were computed as the displacement speed of the testing machine clamps divided by the constant width length of the specimens, that is 44 mm. The results of the four tests were connected though an Isight loop with equivalent models realized in Abaqus environment, Figure 2 b, to calibrate the parameters of the Anand model. The Figures 2 a and c demonstrate the good agreement between the experimental results and the numerical model.

Pb	Sb	Sn
99.3	0.2	0.5

Table 2.2.1. Alloy chemical composition, weight percentage.

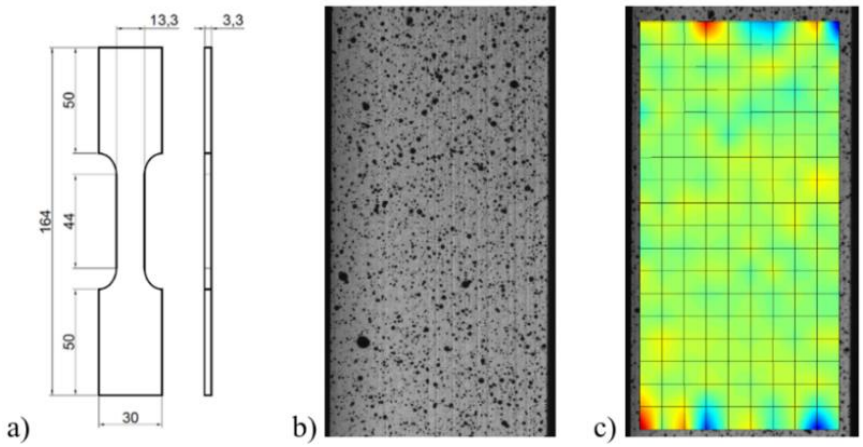

Fig. 2.2.1. (a) Specimen geometry (a); speckle pattern (b); DIC mesh and longitudinal strain pattern, which is homogeneous in the central section of the specimen (c).

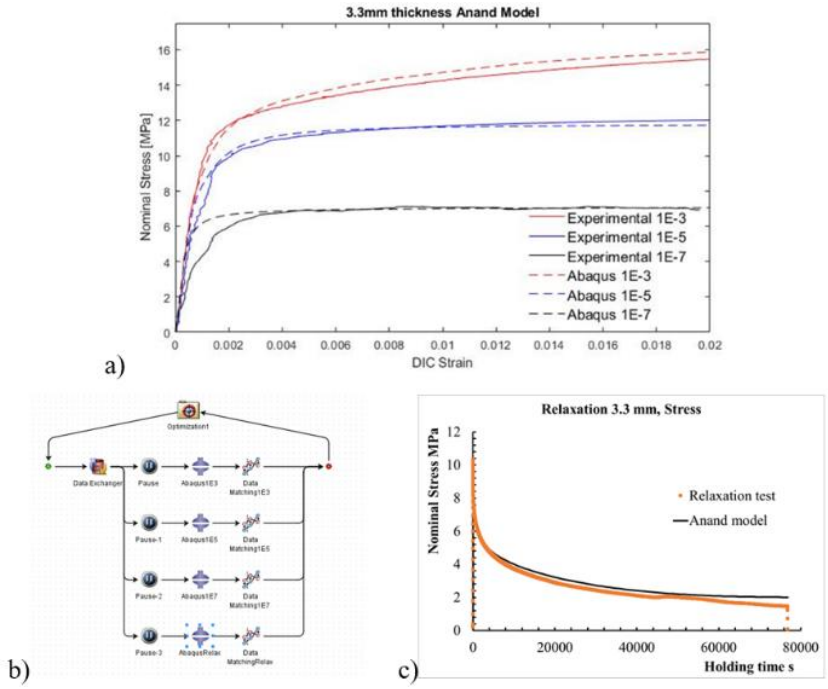

Fig. 2.2.2. (a) Tensile test and Anand creep model results; (b) Isight optimization loop; (c) relaxation test and Anand creep model results [7].

2.2.3 Creep mechanism investigation

2.2.3.1 Tensile testing and creep model calibration

Creep deformation can be caused by several different mechanism according to the material and the stress level active on the metal lattice. According to Dowling (1993) [17] an exponential correlation exists between the stress applied and the resulting steady state creep rate in the form of:

$$\dot{\varepsilon} = A_2 \sigma^m / d^q T \cdot \exp(-Q/RT) \tag{2.2.6}$$

The variables influencing the strain rate are the stress σ, the temperature T and the average grain diameter d. The remaining parameters, that is the coefficient A_2 , the exponents m and q and the activation energy Q depend on the material and on the creep mechanism active. In the case of low stress, but relatively elevated temperature, diffusional flow is active. This is characterized by m=1 and q=2 for vacancy diffusion through the crystal lattice and q=3 for vacancy diffusion along grain boundaries. The mechanism of grain boundary sliding is indicated by a value of the exponent equal to m=2, with the exponent q assuming the same values and meaning as in the former case. At more elevated stress

levels the mechanism of dislocation creep is active. Dislocation motion creep is indicated by an exponent m assuming values between 3 and 8, while q=0, that is a negligible dependence on the average grain size. For the tested alloy, the last point appears to be in contrast with the experimental evidence reported by Viespoli et al. (2019), in which the grain size influences the response also in the dislocation creep regime.

2.2.3.2 Step test results

In order to understand the fundamental mechanisms at the base of the creep deformation of the lead alloy it is then important to obtain the steady state creep exponent relating the applied stress to the strain rate. For collecting the necessary data to have information on the material behavior, a tensile test composed of several steps was executed. The specimen geometry and base material for this test were the same used in the initial tensile characterization for model calibration and the DIC technique was used to obtain the total longitudinal strain of the material. The different steps in the test, described in Table 2, were planned in terms of stress and time to provide results on the steady state creep behavior at different creep regimes. The deformation obtained in during the test is plotted against the time in Figure 3. The slope of each of the steps in positive (tensile) stress was determined in the regions in which the correlation between the strain and the time elapsed is linear, that is in steady state creep regime. The values of the steady state strain rate and the corresponding constant stress applied are plotted in Figure 4. To these values, two points are added from the tensile testing at a nominal strain rate of 1E-5 and 1E-7 s-1 reported in Figure 2 a. In these two tests at constant strain rate the applied stress reaches a constant value, conditions which corresponds do second stage creep. From the results obtained three regimes can be distinguished, characterized by three different stress exponents m. In the range 6 to 12 MPa the value found is m=8.43. This value is at the high end of the dislocation climb dominated creep deformation. In the range 5 to 6 MPa the exponent assumes the value m=5.52, lower but still in the range of the same deformation mechanism. For the lowest range of stress object of the test, that is between 3 and 5 MPa, and exponent m=0.907 is computed. This value is compatible with the diffusional creep mechanisms of vacancy diffusion along the grain boundaries of through the crystal lattice. To assess which of the two mechanisms is predominant it would be necessary to produce new results for the material in condition of different grain size, assessing then the value of the exponent q.

Step	Initial Stress [MPa]	Target Stress [MPa]	Time [s]	Initial Strain	Final Strain
1	0	8,5	250	0	0,001404836
2	8,5	8,5	15000	0,001404836	0,009813991
3	8,5	6	250	0,009813991	0,009658554
4	6	6	30000	0,009658554	0,010542822
5	6	5	250	0,010542822	0,010495558
6	5	5	30000	0,010495558	0,010825471
7	5	4	250	0,010825471	0,010778678
8	4	4	30000	0,010778678	0,010930828
*9	4	1,48	25000	0,010930828	0,010726642
10	1,48	-3	250	0,010726642	0,010356466
11	-3	-3	30000	0,010356466	0,009811369
12	-3	3	250	0,009811369	0,010246884
13	3	3	30000	0,010246884	0,010655562
14	3	-5	250	0,010655562	0,010003737
15	-5	-5	30000	0,010003737	0,008979056
16	-5	5	250	0,008979056	0,009693417
17	5	5	205200	0,009693417	0,013166749

Table 2.2.2. Alloy chemical composition, weight percentage.

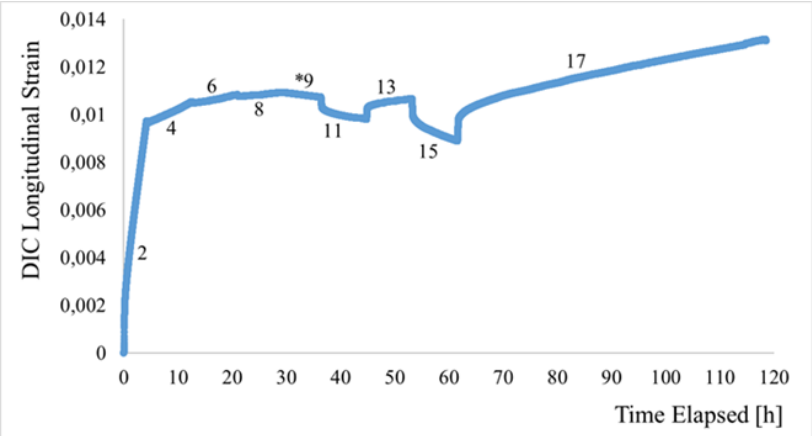

Fig. 2.2.3. Longitudinal DIC strain obtained in the step test. The numbers indicate the steps, *9 being the relaxation step.

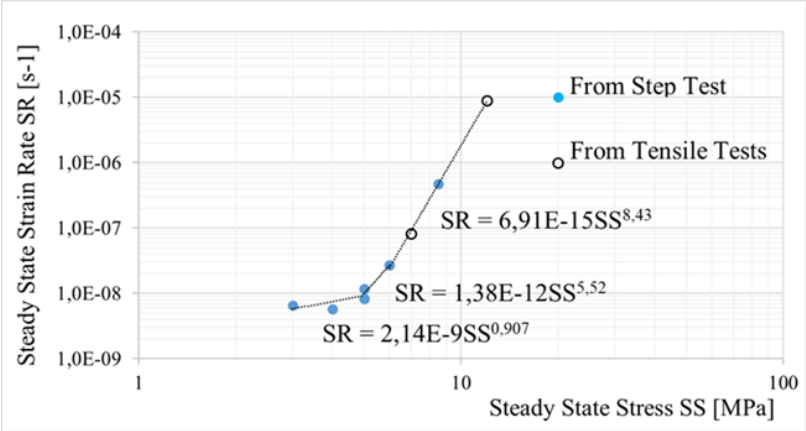

Figure 2.2.4. Steady state creep regimes and relative exponents as obtained from the analysis of the step test points in positive stress, plus the results of the tensile testing in which constant stress is reached.

2.2.4 Conclusions

The present work is the synthesis of a series of tests on dog-bone specimens of a lead E alloy industrially used for the production of the sheathing layer of subsea power cables. Firstly, the three tests at different nominal strain rates plus a relaxation test were performed to characterize the strain rate sensitivity caused by the creep mechanisms active and to calibrate the parameters of a numerical model based on the Anand creep model, which successfully approximated the mechanical response of the alloy to the deformation imposed. To study the mechanisms active during the time dependent deformation of the alloy the steady state creep behavior was investigated. From the results of a tensile test composed of several steps at different stress levels, each of which reached the secondary creep stage, the exponent correlating stress and strain rate for steady state creep was obtained between 3 and 12 MPa. The values assumed by such material parameter in the range of interest indicate that mechanisms of diffusional creep are active in the low stress range of 3 to 5 MPa, with a value of the exponent close to 1, while dislocation creep is the dominating mechanism for higher stresses, with values ranging from 5.5 to 8.4. Further testing for different average grain size would then be necessary in the low stress range to determine whether vacancy diffusion through the crystal lattice or vacancy diffusion along the grain boundaries is predominant.

Acknowledgements

The present work was financed by Nexans Norway AS and the Research Council of Norway (IPN in ENERGIX Project number 256367) and performed within the project: Next-generation damage-based fatigue of cable sheathing (REFACE).

References

[1] Kassner, M.E. Fundamentals of Creep in Materials (Third Edition). Butterworth-Heinemann, 2015.
[2]Pang, H.L.J., Wang, Y.P., Shi X.Q., Wang, Z.P. Sensitivity study of temperature and strain rate dependent properties on solder joint fatigue life. Proceedings of 2nd Electronics Packaging Technology Conference, pp. 184-189, 1998.
[3] Lall, P., Zhang, D., Yadav, V., Locker, D. High Strain-Rate Constitutive Behavior of SACI05 and SAC305 Lead-free Solder, IEEE, 2015.
[4] Motalab, M., Cai, Z., Suhling, J.C., Lall, P., Determination of Anand constants for SAC solders using stress-strain or creep data. 13th InterSociety Conference on Thermal and Thermomechanical Phenomena in Electronic Systems, San Diego, CA, pp. 910, 2012.
[5] Mohamed, F.A., Langdon, T.G. The transition from dislocation climb to viscous glide in creep of solid solution alloys, Acta Metallurgica, Volume 22, Issue 6, pp. 779-788, 1974.
[6] Kassner, M.E. Five-power-law creep in single phase metals and alloys. Oxford: Pergamon, 2000.
[7] Viespoli, L.M., Johanson, A., Alvaro, A., Nyhus, B., Sommacal, A., Berto, F. Tensile characterization of a lead alloy: creep induced strain rate sensitivity. Materials Science and Engineering: A, Volume 744, pp. 365-375, 2019.
[8] Feltham, P. On the Mechanism of High-Temperature Creep in Metals with Special Reference to Polycristalline Lead. Proc Phys Soc, 69,12-B, 1956.
[9] Sahota, M.K., Riddington, J.R. Compressive creep properties of lead alloys. Materials and Design, 21: 159-167, 2000.
[10] Harvard, D.G. Fatigue of Lead Cable-Sheathing Alloys. Ontario Hydro research, 1972.
[11] Dollins, C.W., Betzer, C.E. Creep Fracture and Bending of Lead and Lead Alloy Cable Sheathing. Engineering experiment station bulletin 440, 1956.
[12] Anelli, P., Donazzi, F., Lawson, W.G. The fatigue life of lead alloy E as a sheathing material for submarine power cables. Societa' cavi Pirelli, SM 393-3, 1986.
[13] Johanson, A., Viespoli, L.M., Nyhus, B., Alvaro, A., Berto, F. Experimental and numerical investigation of strain distribution of notched lead fatigue test specimen. MATEC Web Conf, 165, 2018.

[14] Anand, L., Constitutive Equations for the Rate-Dependent Deformation of Metals at Elevated Temperatures. Journal of Engineering Materials and Technology, Vol. 104(1), pp. 12-17, 1982.
[15] Brown, S., Kim, K., and Anand, L. An Internal Variable Constitutive Model for Hot Working of Metals. International Journal of Plasticity, Vol. 5(2), pp. 95-130, 1989.
[16] Dassault Systèmes, SIMULIA User Assistance, 2017.
[17] Dowling, N.E. Mechanical Behavior of Materials: Engineering Methods for Deformation, Fracture, and Fatigue. Pearson, 2013.

Chapter 3: Fatigue properties: micro, small and full scale

This chapter is composed of three conference papers focused on the fatigue testing of the material in three different conditions. The first observes the performance of the material under different strain rate displacement-controlled fatigue conditions. The second in focused on the observation of the tensile and cyclic deformation behaviour through in situ observation with scanning electron microscopy. The third collects a series of results of full-scale tests which will be object of further discussion in Chapter V.

3.1 Paper III

Subsea power cable sheathing: an investigation of lead fatigue performance

Luigi Mario Viespoli[1], Audun Johanson[2], Antonio Alvaro[1,3], Bård Nyhus[3], Filippo Berto[1]

[1]*Department of Mechanical and Industrial Engineering, Norwegian University of Science and Technology (NTNU), Norway*
[2]*Nexans Norway, Innspurten 9, 0663 Oslo, Norway*
[3]*Sintef Industry, Richard Birkelands vei 2B, 7034, Trondheim, NORWAY*

Abstract: The protection of subsea power cables against electrical failure is achieved by the use of a watertight layer. Due to its properties of chemical stability and ductility, lead has been the material of choice for this purpose for several decades. Due to the low melting temperatures of lead alloys, their behaviour is strongly influenced by time-dependent phenomena, such as creep and recrystallization, which become more prominent for lower strain rate deformations. In order to understand the performance of the alloys of interest under cyclic loading experienced during and after installation in combination with the different variables influencing its behaviour, extensive testing is necessary. This manuscript presents the results of fatigue tests at two different strain rates for an alloy of industrial interest. The tests are monitored with the aid of digital image correlation, which greatly reduces the uncertainty on the quantification of the real strain field. The post-mortem fracture surfaces are investigated through scanning electron microscopy and metallurgical characterization to help understanding the differences in the failure modes active in the different stress/strain regimes.

3.1.1 Introduction

The presence of a chemically stable and permanently watertight material layer is required to prevent the electrical failure of high voltage subsea power cables. This sheathing layer is often made of lead alloys, due to the ability of these materials to comply with the deformations imposed by the manufacturing process and the easiness of extrusion, important for the production process. Although power cables with lead sheathing are typically not used in dynamic riser systems, the lead sheathing in cables designed for static applications will be nevertheless subjected to various cyclic loads throughout its operational life including temporary dynamic suspension during installation or jointing and thermal deformation of the cable section. The low melting point of these alloys, inferior to 600 K, causesviscous phenomena to occur already at room temperatures. Creep deformation influences the static and fatigue performance of such alloys. The topic of

creep and its influence on fatigue has been thoroughly studied in the fields of energy production and microelectronics [1-11], while in the case of lead alloys used for the production of subsea power cables most of the works available in the open literature date back to several decades ago [12-16]. Research on this topic has risen to a new actuality due to the will of the industry community of optimizing the designs of subsea powerlines, with the clear spirit of producing a positive impact both on the environment and on production. Within the framework of this renewed interest, the microstructure and tensile behavior [17], steady state creep [18], the influence of local discontinuities on the fatigue resistance [19-20] and the full-scale fatigue performance [21] were investigated for two lead alloys of industrial interest. The aim of this manuscript is to integrate the aforementioned series of results with the results of fatigue testing at two different nominal strain rates and the fracture investigation focused on qualifying the correlation between the loading conditions and the dominant failure mode.

3.1.2 Fatigue testing

The scope of the fatigue testing was to characterize the fatigue performance of the commercial cable sheathing lead "E" alloy. The chemical composition of the alloy can be summarized as follows: 99.3 wt % Pb, 0.45-0.55 wt % Sn, 0.15- 0.25 wt % Sb, where the addition of Sb is made in order to improve the tensile and creep resistance of the alloy predominantly through solid solution hardening. The alloy is however slightly super-saturated and some precipitation hardening is expected. The tensile properties of this alloy are, at room temperature, strongly dependent on the strain rate [17]. In the case of monotonic tensile testing, for the strain rates of interest in this series of fatigue tests (1E-2 and 1E-3 s^{-1}), no important reduction in stress for a given strain level is recorded while a marked drop of tensile strength happens reducing the strain rate to 1E-5 and 1E-7 s^{-1} [17]. This most probably indicates a reduction of the influence of thermally activated dislocation motion for strain rates higher than 1E-4 s^{-1}. The conclusion that creep deformation for the present alloy is dislocation driven for strain rates over 1E-8 s^{-1} is drawn from the observation of the exponent correlating applied stress and the resulting strain rates, which is in excess of 5 for stresses over 5 MPa [18]. For cyclic testing the behaviour is different, and the stabilized cyclic properties are diverse already passing from 1E-2 to 1E-3 s^{-1} in strain rate, see figure 3. Considering the Ramberg-Osgood approximation for the stabilized cyclic curve in the form:

$$\varepsilon = \frac{\sigma}{E} + \left(\frac{\sigma}{K'}\right)^{n'}$$

The best fitting of the experimental data in figure 3 is given by E=15500 MPa, K'=54 MPa, n'=4.7 for the strain rate 1E-2 s-1 and E=15500 MPa, K'=53 MPa, n'=4.1 for the strain rate 1E-3 s-1. The specimens used for the fatigue testing were machined from high

voltage subsea cable sheathing extruded to a thickness of 1.8 mm. The original curvature of the sheathing was kept, in order to increase buckling resistance and to avoid the introduction of additional forming of the sheath, obtaining specimens corresponding to the geometry in figure 1. The tests were performed in tensile- compression loading mode which corresponds to the loading mode in the sheathing when the cable is subjected to bending. All tests were conducted in air at room temperature with a Zwick/Roell LTM Electrodynamic machine equipped with a 10 kN load cell. Digital image correlation (DIC) technique was used to control the longitudinal strain range according to the procedure schematically reported in figure 2: the test was started setting the positions values calculated based on tensile properties of the material at the target strain rate. During the first cycles, DIC images were immediately post-processed to obtain the actual strain range values from the surface of the specimen. If the values obtained differed from the target strain range (with a tolerance of about 5%), the clamp position was adjusted and the control repeated. It is assumed that small adjustments done in the initial part of the specimen's fatigue life have negligible effect on the result. This correction of the imposed displacement was necessary due to the highly plastic behaviour of the material to account for the unavoidable clamping pressure. The use of DIC is preferred to the use of an extensometer because of the absence of contact with the specimen during testing which may create concentrators on the specimen's surface which will drive the fatigue crack initiation. However, it was not possible to execute real time DIC post processing and control the machine in closed loop without manual intervention. The tests were performed in strain control because of the plastic behaviour even at very low strain ranges. Plasticity is increased by a reduction of strain rate. The same characteristic would lead to the material permanently deforming and settling to a new length if a displacement ratio different from -1 was to be used. A total of 23 specimens were tested, 9 at 1E-3 s^{-1} and 14 at 1E-2 s^{-1}, the results of which are reported in figure 4 in terms of cycles to failure vs longitudinal strain range, as computed by DIC in the central part of the specimen. Even if no strong stress-strain difference was detected in the tensile testing, time dependent damage is active and shows a different influence according to the strain rate: the increased duration of a cycle at 1E-3 s^{-1} compared to 1E-2 s^{-1} makes so that the former presents a reduced fatigue life than the latter in terms of cycles to failure. The observation of the evolution of the stress range in the initial part of the testing shows a negligible relaxation for the specimens tested at 1E-2 s^{-1}, while a reduction of the stress range of more than 10 % happened only for two of the specimens tested at 1E-3 s^{-1}, with the others showing limited relaxation as well. The difference detected is quantified in an increase of strain range from 2.46 % to 6.12 %. considering a 50 % failure probability at 2E-6 cycles. The reduction of resistance in terms of strain range is not constant, but inversely proportional to the load level: the fatigue curve slope is indeed 0.558 for 1E-3 s^{-1} and 0.346 for 1E-2 s^{-1} over the tested range.

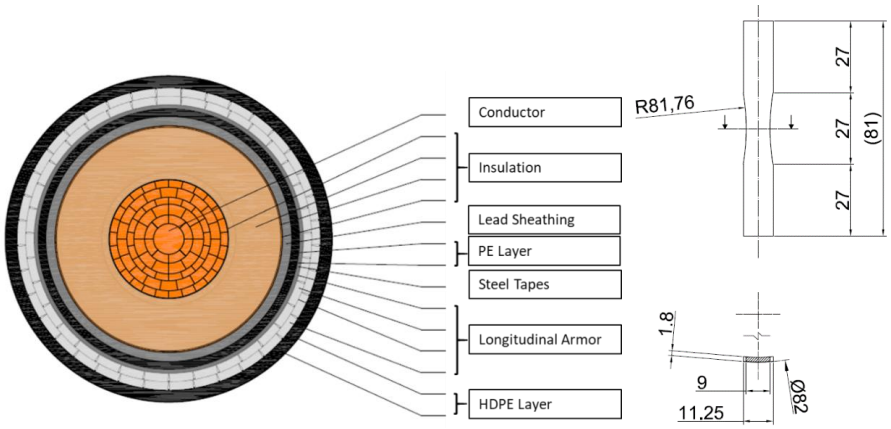

Figure 3.1.1 Cable section scheme and fatigue specimen geometry. Longitudinal direction of cable and specimen correspond.

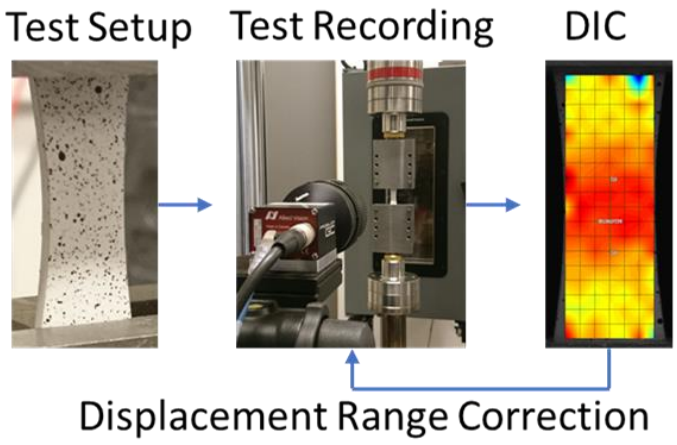

Figure 3.1.2 Strain range control logic.

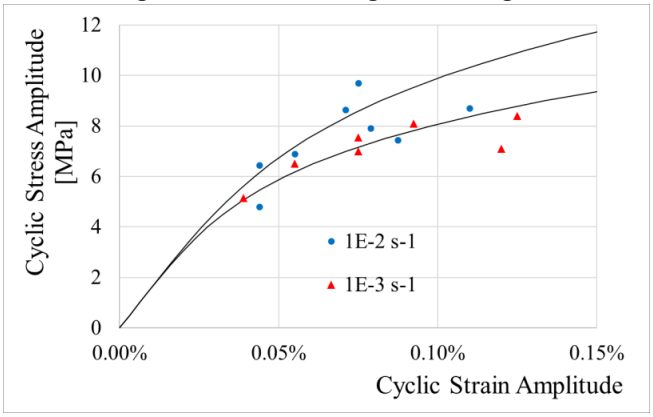

Figure 3.1.3 Ramberg-Osgood best fit of cyclic properties.

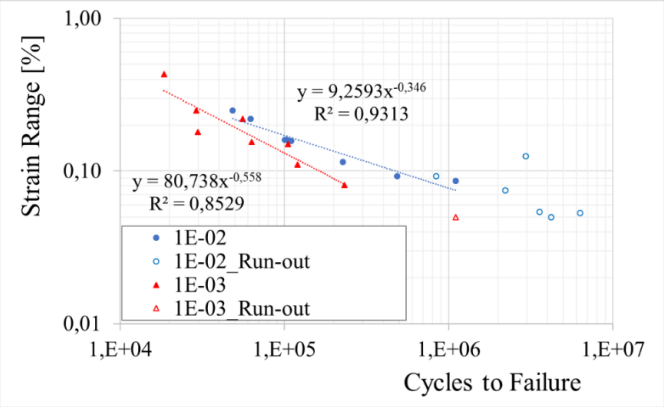

Figure 3.1.4 Summary of fatigue results.

3.1.3 Fracture surface investigation

Post-mortem metallography and fractography through scanning electron microscopy (SEM) was performed in order to understand the dominant failure mechanism/s and with the perspective of developing adequate damage models for the prediction of the fatigue performance of the alloys of interest. The specimens of choice for the fracture analysis presented were fatigue tested in the two extreme conditions of the testing parameters ranges: the highest strain rate and strain range providing results for lower creep influence on one hand and the lowest strain rate and strain range on the other hand, being majorly affected by creep inherent damage. The two cases correspond to 0.25 % strain range, 1E-2 s^{-1} strain rate and 0.15 % strain range, 1E-3 s^{-1} strain rate respectively. Figures 5 and 6 show the results of metallographic investigation of the afore mentioned specimens. Metallographic investigations were performed on the longitudinal direction of the specimens. In addition, figures 7 and 8 show SEM imaging of the fractures in the same order. The samples were prepared following the same procedure developed for [17]. It is evident for both specimens that crack propagation is dominated by grain boundary failure. In addition, several fatigue cracks nucleated and propagated, indicating diffused damage and not only a single dominant fracture. Most cracks develop in secondary branches following the grain boundary morphology. This damage behaviour appears to be more relevant in the case of increased creep influence, see figure 6, and is, in any case, analogous with the behaviour of another lead alloy investigated by the authors [19]. The SEM imaging of the fracture surfaces reveal a mixed behaviour crack propagation: both intergranular and transgranular cracking are present for the two extreme testing conditions. In particular, figure 7 shows crack initiation by grain boundary failure and subsequent presence of both failure mechanisms after approximately 400 μm of penetration.

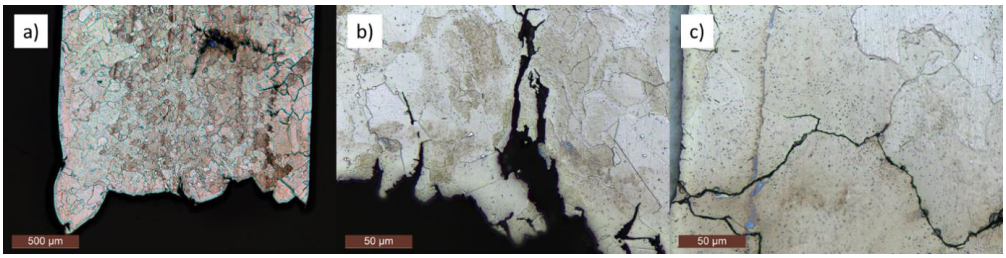

Figure 3.1.5 Metallography of fatigue fracture: 0.25 % strain range, 1E-2 s^{-1} strain rate. Side view of the fracture (a). Details of secondary cracking (b, c).

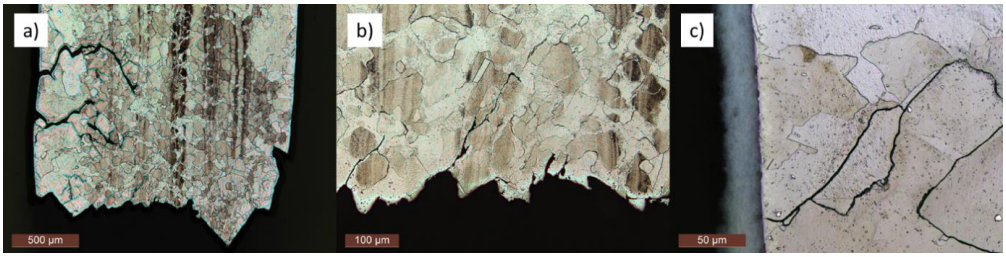

Figure 3.1.6 Metallography of fatigue fracture: 0.15 % strain range, 1E-3 s^{-1} strain rate. Side view of the fracture (a), note multiple non-fatal cracks. Details of secondary cracks propagating at the grain boundaries at an angle of 45º from the pulling direction (b, c).

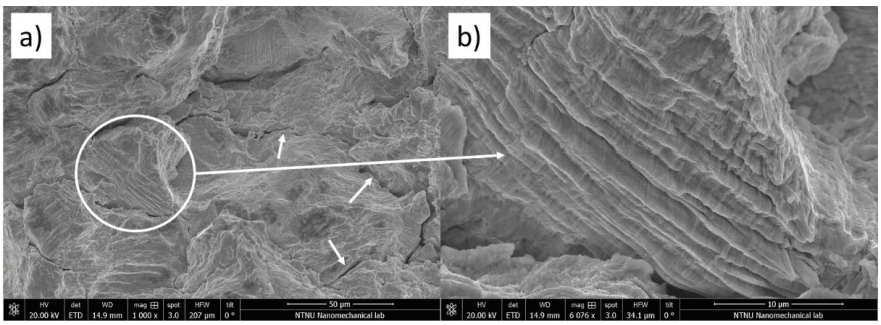

Figure 3.1.7 Fracture of specimen tested at 0.25 % strain range, 1E-2 s^{-1} strain rate. Both intergranular (a) and transgranular (b) fatigue crack propagation are present.

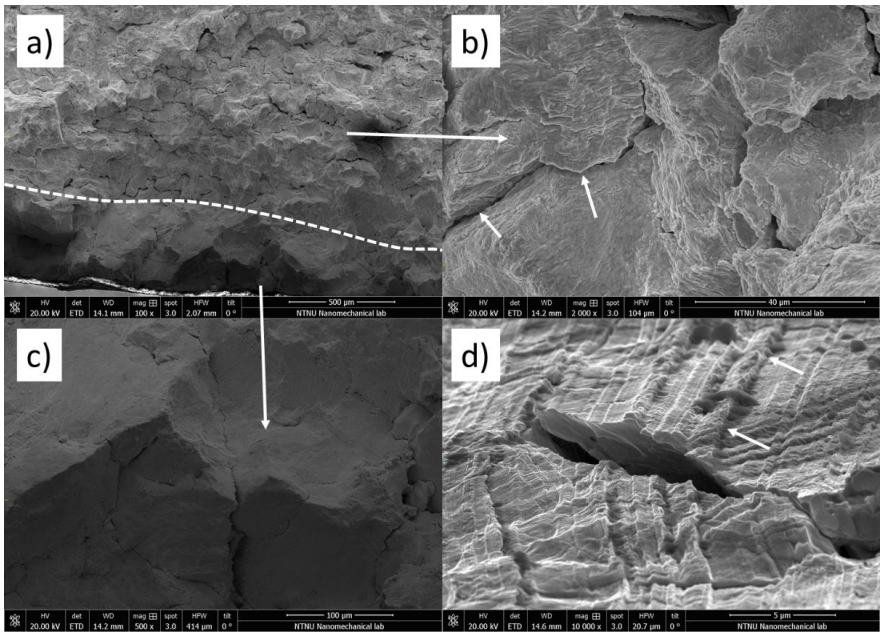

Figure 3.1.8 Fracture of specimen tested at 0.15 % strain range, 1E-3 s^{-1} strain rate. The fatigue crack (a) is initially dominated by intergranular propagation (c) and then by a combination of intergranular and transgranular (b). Non-fatal secondary crack nucleated at the surface and extrusion grooves (d).

3.1.4 Discussion

Two series of Pb-Sn-Sb alloy (E- alloy) used for the production of subsea power cables were fatigue tested in air at room temperature in strain control at different strain rates to obtain an evaluation of the influence of stress dependent damage and investigate the consequent damage mechanics. The tests were performed by a Zwick/Roell LTM Electrodynamic machine equipped with a 10 kN load cell and the correctness of the imposed strain level was verified by DIC analysis on the central portion of the specimens. The results clearly showed an important influence of the strain rate on the fatigue performance due to the strong impact of time dependent deformation and damage already at room temperature. Previous work on a same alloy has been published by Anelli et al. [16]. In his work all tests were done at ambient conditions under reversed bending. Testing strain ranges and frequencies ranged down to approximately 0.10 % and 2 cycles/ h. The resulting frequency dependent fatigue model is readily available for fatigue calculations and often used as input data for such calculations for subsea power cables. Although the experimental methodology used in this work is different, it is clear that the 5 % probability of failure curve proposed by Anelli overpredicts the fatigue life by up to two orders of magnitude compared to the low strain range results presented by the authors.

This difference appears to increase towards reduced strain range and rates. It is in other words highly critical to select an appropriate experimental approach as well as an accurate damage model. The abovementioned difference can in part be explained by the choice of loading mode which is consistent with the results presented by the authors in Johanson et al. [21], which showed that the fatigue life of lead appeared to increase when tested by reversed bending compared to the tensile-compression loading mode, the latter being more representative of the actual loading mode the sheathing being subjected to in real cable operation. Another major difference between the results herby and those reported by Anelli lies in the adoption by the latter of a frequency corrected fatigue model to account for creep. It is important to notice that the strain rate will drop when shifting from higher to lower strain range at a given cyclic frequency. As already stated in a previous work by the authors, Johanson et al. [21], it is suggested to adopt the strain rate rather than the frequency as central parameter when testing fatigue properties of materials for which time-dependent damage phenomena interact one another as in the case of lead in order to develop the base for an accurate mechanistically-based fatigue-creep damage model to adequately predict the lead sheath fatigue life for many operational scenarios. The fracture investigation, both by metallography of polished and etched samples at the height of the final fracture and by SEM imaging of the fracture surfaces, reveals how failure is dominated by grain boundary loss of cohesion at several points of the specimen. Creep characterization, implementation of opportune creep-fatigue interaction models for the prediction of the behaviour at very low strain rates, which are in fact representative of the operational conditions and development of alloys able to maintain elevated ductility, while reinforcing grain cohesion are important topics for research in the field. Ongoing work is directed toward overcoming some of these challenges.

3.1.5 Conclusions

The main conclusions on the fatigue testing performed on samples of lead E alloy subsea power cable sheathing can be summarized in the following points:

- The fatigue performance of the alloy is influenced by creep deformation. A shift of the strain rate causes an important shift in fatigue life in terms of number of cycles, with slower deformation causing cracking after fewer cycles.
- The crack propagation in lead is typically both intergranular and transgranular, with a lower strain rate increasing the formation of secondary cracks and having a detrimental impact on the grain boundaries.
- The development of a fatigue-creep interaction model based on the deformation and damage mechanisms active in the class of alloys of interest is a complex task, but necessary for a safe and knowledge-based prediction of the operational life of the components, whose real operating conditions are in fact dominated by low strain rates and elevated duration in terms of time.

Acknowledgements

The present work was financed by Nexans Norway AS and the Research Council of Norway (IPN in ENERGIX Project number 256367) and performed within the project: Next-generation damage-based fatigue of cable sheathing (REFACE).

References

(1) M.E. Kassner, *Fundamentals of Creep in Materials (Third Edition)*, Butterworth-Heinemann, 2015.
(2) H.L.J. Pang, Y.P. Wang, X.Q. Shi and Z.P. Wang, *Proceedings of 2nd Electronics Packaging Technology Conference* (Cat. No.98EX235), pp, 184-189, 1998.
(3) P. Lall, D. Zhang, V. Yadav, D. Locker, *Microelectronics Reliability*, Vol. 62, 2016, pp. 4-17.
(4) M. Motalab, Z. Cai, J.C. Suhling, P. Lall, Determination of Anand constants for SAC solders using stress-strain or creep data, *13th InterSociety Conference on Thermal and Thermomechanical Phenomena in Electronic Systems*, San Diego, CA, 2012.
(5) Farghalli A. Mohamed, Terence G. Langdon, *Acta Metallurgica*, Vol. 22, Issue 6, 1974, pp. 779-788.
(6) M.E. Kassner, *Five-power-law creep in single phase metals and alloys*, Oxford: Pergamon, 2000.
(7) Anand, L., *Journal of Engineering Materials and Technology*, Vol. 104(1), 1982, pp. 12-17.
(8) Brown, S., Kim, K., and Anand, L., , *International Journal of Plasticity*, Vol. 5(2), 1989, pp. 95-130.
(9) Dowling, Norman E., *Mechanical Behaviour of Materials: Engineering Methods for Deformation, Fracture, and Fatigue*, Pearson, 2013.
(10) E.H. Wong, W.D. van Driel, A. Dasgupta, M. Pecht, *Microelectronics Reliability*, Vol. 59, 2016, pp. 1-12.
(11) Viespoli, Luigi Mario; Berto, Filippo, *Material Design & Processing Communications, Vol. 1 (6)*, 2019.
(12) P. Feltham, On the Mechanism of High-Temperature Creep in Metals with Special Reference to Polycrystalline Lead. *Proc Phys Soc*, 1956.
(13) M.K. Sahota, J.R. Riddington, *Materials and Design*, Vol. 21, 2000, pp. 159-167.
(14) D.G. Harvard, *Fatigue of Lead Cable-Sheathing Alloys*, Ontario Hydro research, 1972.
(15) C.W. Dollins, C.E. Betzer, *Creep Fracture and Bending of Lead and Lead Alloy Cable Sheathing*, Engineering experiment station bulletin 440, 1956.
(16) P. Anelli, F. Donazzi, W.G. Lawson, IEEE Transactions on Power Delivery, Vol. 3, 1988, pp. 69-75. (17) Viespoli, Luigi Mario; Johanson, Audun; Alvaro, Antonio;

Nyhus, Bård; Sommacal, Alberto; Berto, Filippo, *Materials Science & Engineering: A*, Vol. 744, 2019, pp.365-375.
(18) Viespoli, Luigi Mario; Johanson, Audun; Alvaro, Antonio; Nyhus, Bård; Berto, Filippo, Room temperature creep mechanism of a Pb-Sn-Sb lead alloy, *Procedia Structural Integrity*, Vol. 18, 2019, pp. 86-92.
(19) Viespoli, Luigi Mario; Johanson, Audun; Alvaro, Antonio; Nyhus, Bård; Berto, Filippo, , *Engineering Failure Analysis*, Vol. 104, 2019, pp. 96-104.
(20) Johanson, Audun; Viespoli, Luigi Mario; Nyhus, Bård; Alvaro, Antonio; Berto, Filippo, Experimental and numerical investigation of strain distribution of notched lead fatigue test specimen, *MATEC Web of Conferences*, 2018.
(21) Johanson, Audun; Viespoli, Luigi Mario; Alvaro, Antonio; Berto, Filippo, Small and Full-Scale Fatigue Testing of Lead Cable Sheathing, *ISOPE International Offshore and Polar Engineering Conference Proceedings*, 2019.

3.2 Paper IV

Tensile and fatigue behavior of a Pb-Sn-Sb alloy investigated via small-scale *in-situ* mechanical testing in SEM

Di Wan[a,a], Luigi Mario Viespoli[a], Audun Johanson[b], Anette Brocks Hagen[c], Filippo Berto[a], Antonio Alvaro[a,c]

[a]*Department of Mechanical and Industrial Engineering, Norwegian University of Science and Technology, Richard Birkelands vei 2B, 7491 Trondheim, Norway*
[b]*Nexans Norway, Innspurten 9, 0663 Oslo, Norway*
[c]*Department of Materials Integrity and Welding, SINTEF Industry, 7456 Trondheim, Norway*

Abstract: Pb-Sn-Sb alloys (E-alloy) are commonly used in subsea power cable sheathing. Due to the relatively low melting temperature, *i.e.* around 600 K, this type of alloy is prone to experience microstructural time-dependent evolution such as recovery, relaxation, recrystallization and creep deformation even at room temperature, in contrast to other conventional materials for which involve these mechanisms are activated only at high temperatures. To better understand the deformation mechanisms of Pb-Sn-Sb alloys, small-scale *in-situ* mechanical testing inside a scanning electron microscope (SEM) has been conducted under both monotonic loading and cyclic loading conditions. Thanks to the *in-situ* imaging technique, the deformation behavior as well as the damage mechanisms were revealed with high resolution. The possible deformation mechanisms, including the creep behavior, has been discussed and the results can provide necessary input to damage calculations and modelling work of the studied alloy system used for cable sheathing.

***Keywords**:* Pb-Sn-Sb alloy; creep; fatigue; *in-situ* test; SEM.

3.2.1 Introduction

Lead alloys are commonly used in subsea cable sheathing due to their easy manufacturing, excellent chemical stability and mechanical ductility [1, 2]. A common understanding of this material is that due to its low melting point (~600 K or 327 °C), the deformation behavior includes relaxation, recovery, recrystallization or creep even at room temperature, in contrast to conventional metallic materials which experience these behaviors only at high temperatures. These time-dependent phenomena lead to a sensitive

strain rate-dependency of lead alloys in terms of the constitutive behavior and damage during deformation. The real-life scenarios involving cyclic motion will both vary in strain rate and entail cycles with strain rates far below practical limits if testing due to time constraints, *i.e*. it is a clear need to better understand the inherent damage models in order to improve the necessary extrapolations needed for fatigue- and creep damage calculations. Due to the complexity of the issue, the industry has for long time relied on the experience derived from the operational history rather the inadequate available literature on the topic. Among the earlier works we mention an investigation by the University of Illinois of the mechanical behavior of lead for cable sheathing at a range of temperatures, showing a strong strain rate dependency on the evolution of the plastic curve and on the tensile strength [3] and a study on the impact of chemical composition of the alloy, thermal treatments and repeated loading [4]. The impact of grain size on the creep behavior of polycrystalline lead was studied by Feltham [5] while tests on the fatigue behavior of commercial alloys were performed by Harvard [6]. Further works are available on the fatigue behavior [7] and the compression response [8]. Being most of the research available is outdated and inadequate to understand real life fatigue calculations, as well as significant manufacturing and cable design improvements, a novel interest for the performance of lead alloys has risen in the industry. In the recent years novel results have been produced with up to date tools, describing the tensile performance and the fatigue response in presence of geometrical discontinuities of a selection of lead alloys of interest [9-11], together with a statistical estimation of the sheathing's life in full scale tests [1]. The present work aims to present some interesting preliminary result to expand and improve the understanding of the mechanisms leading to failure under various loading conditions.

3.2.2 Materials and Experimental

The material investigated in this study is a Pb-Sn-Sb alloy (E-alloy) with the chemical composition shown in Table 3.2.1. The material was extracted from as-extruded lead tubes which involve direct quenching upon extrusion. Followed by > 1 year of storage. The as-received material has a face-centered cubic (FCC) phase with a small fraction of secondary precipitates (identified as SnSb particles by energy dispersive X-ray spectroscopy/ EDX) and was manufactured into dog-bone shaped tensile specimens with the dimension described in figure 3.2.1 with the longitudinal direction parallel to the extruded direction of the raw material. The metallographic investigation of this material can be found in Ref. [11]. The specimens are prepared by grinding, polishing, etching and ion-polishing at 2 kV for 10 min plus 1 kV for 10 min. Before testing, the specimen was analyzed by electron backscatter diffraction (EBSD) technique in a Quanta 650 FEG scanning electron microscope (SEM, ThermoFisher Inc., USA) with an accelerating voltage of 20 kV and a working distance of about 15 mm. The initial microstructure of the material as revealed through EBSD maps is shown in Figure 3.2.2. An average grain

size of about 25 μm is observed, and the grains are mostly in equiaxed shape. No specific sharp texture is observed from the normal direction - inverse pole figure (ND-IPF) map. A lot of twin boundaries (TBs, defined by Σ3 boundaries) together with low-angle grain boundaries (LAGBs, 2-15°) and high-angle grain boundaries (HAGBs, >15°) are revealed by the EBSD analysis. The residual strain after sample preparation revealed by kernel average misorientation (KAM, defined as the average misorientation of first nearest points including the kernel scanning point) map is not significantly strong. The specimen was considered as in well-annealed state before testing.

Element	Pb	Sb	Sn
wt.%	99.3	0.2	0.5

Table 3.2.1. Chemical composition of the tested material.

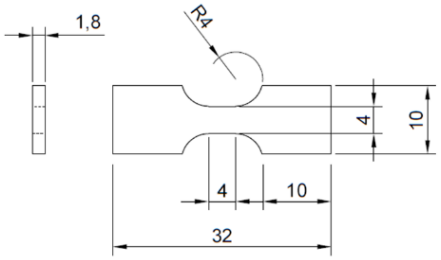

Figure 3.2.1 Sample geometry for tensile testing. (unit: mm).

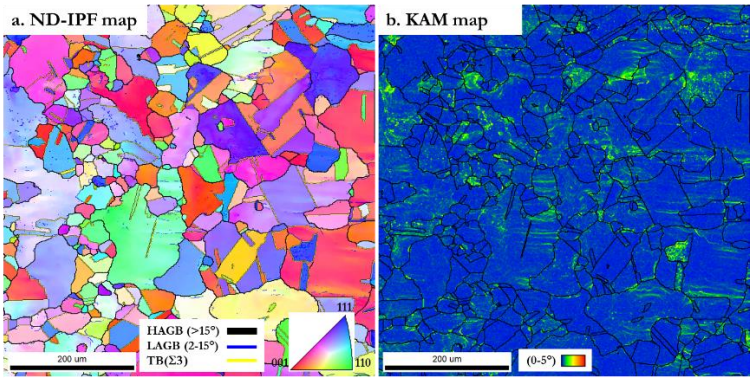

Figure 3.2.2 EBSD analysis of the tested material: a. normal direction - inverse pole figure (ND-IPD) map with high-angle grain boundaries (HAGBs), low-angle grain boundaries (LAGBs) and twin boundaries (TBs, defined by Σ3 boundaries), b. kernel average misorientation (KAM) map with 0-5°. (digital version in color).

Mechanical loading was applied by a tensile/compression module (Kammrath & Weiss GmbH, Germany) inside the SEM. Monotonic tensile tests with an initial nominal strain rate of from 5×10^{-5} s^{-1} to 5×10^{-3} s^{-1} were performed. For cyclic loading test, a nominal strain amplitude ($\Delta\varepsilon$) of approx. ±1.1% with an initial nominal strain rate of 5×10^{-3} s^{-1} was applied. The deformation procedure of specimens was recorded by *in-situ* SEM imaging at a chosen magnification to reveal the microstructural change during testing. Energy dispersive X-ray spectroscopy (EDS) was used to confirm the chemical composition information of the specimen at an accelerating voltage of 20 kV and a working distance of about 10 mm. The post-mortem fracture features were also investigated by SEM to confirm the fracture mechanism.

3.2.3 Results

3.2.3.1 Mechanical data

3.2.3.1.1 Monotonic loading

Figure 3.2.3 shows the nominal stress – strain curves for monotonic tensile tests on three different specimens with different nominal strain rates. The first two tests were done with a fixed nominal strain rate at 5×10^{-3} s^{-1} and 5×10^{-4} s^{-1}, respectively (referring to the black and the red curves). The third test was started with 5×10^{-5} s^{-1} but accelerated after the ultimate tensile strength has been clearly passed (*i.e.* after a clear drop in the nominal stress has been recorded). The accelerated testing ranges are divided by black dashed lines in Figure 3.2.3 and the corresponding nominal strain rates are marked accordingly. It is clear that the mechanical properties of the studied Pb-Sn-Sb alloy have a strong dependency on the strain rate. The yield strength (by 0.2% plastic deformation criterion) as well as the ultimate tensile strength increases with an increasing strain rate, and these values are recorded in Table 3.2.2. An interesting fact is that the final elongation/ nominal strain is quite similar (about 110%) between the different testing cases.

Nominal strain rate / s^{-1}	Yielding strength/ MPa	Ultimate tensile strength/ MPa
$5\times10^{-5,*}$	8.2	16.1
5×10^{-4}	8.8	17.4
5×10^{-3}	10.8	20.7

**The properties for 5×10^{-5} s^{-1} were got from the first segment of the blue curve in Figure 3.2.3.*

Table 3.2.2 Mechanical properties of the tested Pb-Sn-Sb alloy.

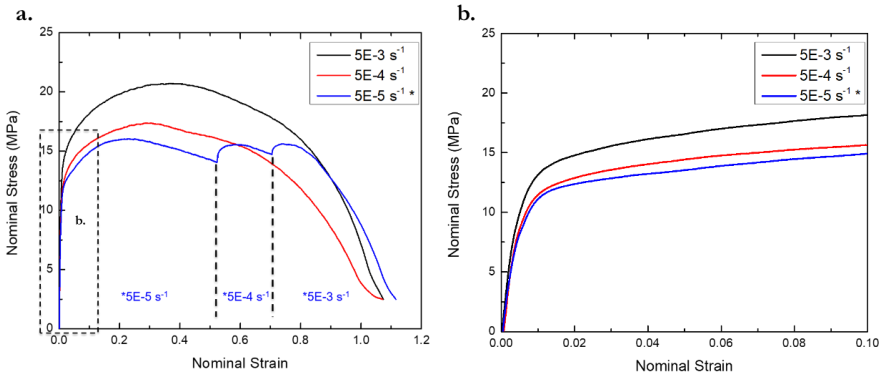

Figure 3.2.3 a. Nominal stress – strain curves for monotonic loading tests with strain rates ranging from 5×10^{-5} s^{-1} to 5×10^{-3} s^{-1}. The black and red curves were from the tests with a fixed strain rate at 5×10^{-3} s^{-1} and 5×10^{-4} s^{-1}, respectively. The blue curve started with 5×10^{-5} s^{-1}, and the loading was accelerated after the drop in the stress has been recorded. The segments are divided by black dashed lines and the corresponding nominal strain rates are marked. b. A magnified area focusing on the first stage of deformation (nominal strain less than 0.1). (digital version in color).

3.2.3.1.2 Cyclic loading

The cyclic loading test was conducted under an elongation-controlled mode with a fixed displacement rate (corresponding to an initial nominal strain rate of 5×10^{-3} s^{-1}). The corresponding global strain amplitude was $\Delta\varepsilon \sim \pm1.1\%$. The testing results are shown in Figure 3.2.4 and revealed that when loaded a fixed displacement (strain) range, the specimen showed gradually softening in the stress response. According to Figure 3.2.4.b, the stress level was continuously decreasing (in absolute value) with respect to time or number of cycles, and there was no significant sign of reaching a stable value. The stress – strain loops are also shown in Figure 3.2.4.c (for the first cycle) and in Figure 3.2.4.d (for the full test). A small turbulence can be found in the tensile part of the loop for all cycles, which was a systematic error that came from the tensile module. The loops consistently show softening during the cyclic loading.

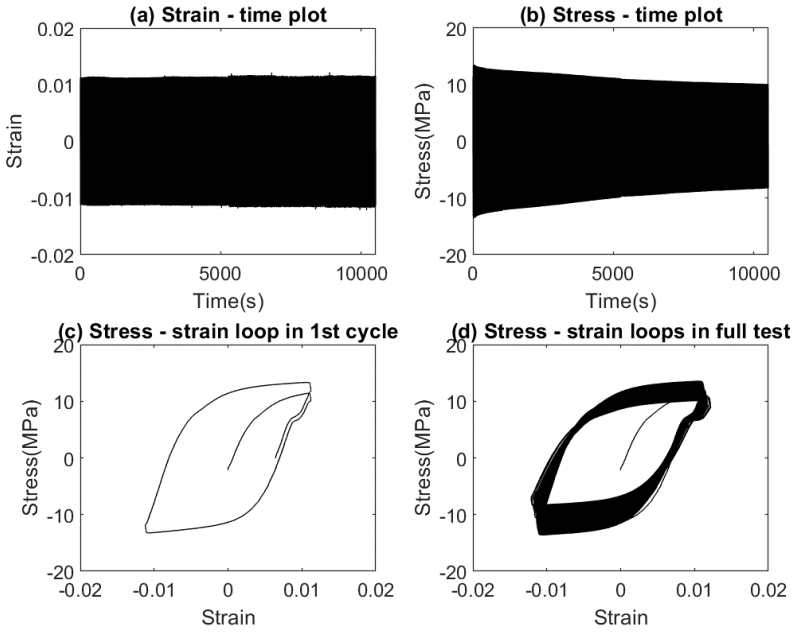

Figure 3.2.4 Mechanical testing results for the cyclic loading test. (a) strain – time plot; (b) stress – time plot; (c) stress – strain loop in 1st cycle and (d) stress – strain loops in full test.

3.2.3.2 Microstructure evolution

3.2.3.2.1 Monotonic loading

To track the microstructure evolution, the micrographs were taken by *in-situ* SEM imaging during the monotonic tensile test at 0.2 μm/s (nominal strain rate 5×10^{-5} s^{-1}). The results are divided into three stages according to different characteristics: an early stage (defined as global nominal strain from 0 to ~0.18), an intermediate stage (with global nominal strain from ~0.6 to ~0.8) and a final stage (global nominal strain from ~0.8 to ~1.1/ final failure). The SEM micrographs are presented in Figure 3.2.5 to 9.

Figure 3.2.5 shows the early stage microstructure evolution during the tensile test. Before loading, the specimen showed a relatively flat and smooth topography with the presence of only some precipitates, as is also marked as a reference point in the figures. After loading, the grain boundaries first started to appear (*e.g.* the white curved segments in Figure 3.2.5.b). As strain level increased, the grain boundaries became more and more significant, and some slip lines became revealed on the surface as parallel lines (indicated

by parallel dashed lines inside the grains). The slip lines were mostly parallel inside one grain and were parallel neither to the loading direction nor to the transversal direction. Both the grain boundaries and the slip lines became more significant as the strain level increased. The same phenomena continued through the whole stage.

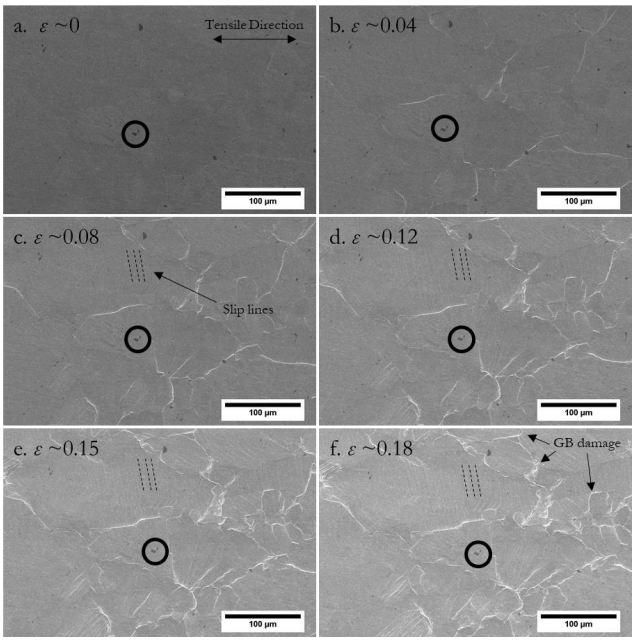

Figure 3.2.5 SEM micrographs from the in-situ investigation of microstructure evolution during tensile test at early stage. The corresponding global nominal strain levels are indicated in each sub-figure. The black circle indicates a same reference point in the view. The global tensile direction is horizontal.

Figure 3.2.6 shows the intermediate stage of deformation. Similar to what was observed during the early stage, the slip lines and the grain boundaries still evolved as the strain increased. Additionally, new slip lines in a different direction were observed in one grain containing previously developed slip lines. Both the new and the old slip lines were inclined to the tensile direction and the transversal direction. Moreover, the grain boundaries started to detach from each other, and early-stage damages can be found in the grain boundary areas (as indicated in Figure 3.2.6.c). However, no clear proof can be found for developing damage around precipitates and/or precipitate/matrix debonding.

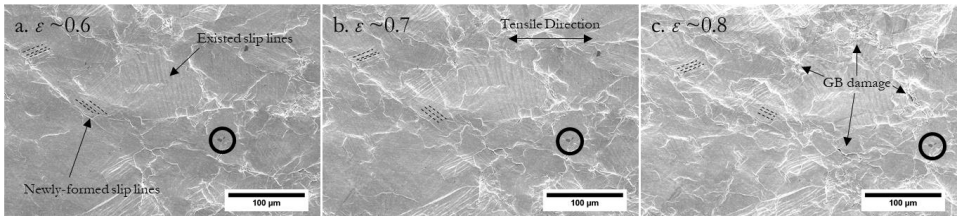

Figure 3.2.6 SEM micrographs from the in-situ investigation of microstructure evolution during tensile test at intermediate stage. The corresponding global nominal strain levels are indicated in each sub-figure. The black circle indicates a same reference point in the view. The global tensile direction is horizontal.

Figure 3.2.7 shows the final stage of the monotonic tensile test up to the final failure of the specimen. As observed at the end of the intermediate stage, the slip lines were inclined to the tensile direction and the transversal direction, and the grain boundary areas were relatively severely deformed. When the material was subjected to further elongation, the slip lines turned into thicker deformation bands whose direction was almost parallel to the transversal direction (perpendicular to the tensile direction), as shown in Figure 3.2.7.b. The final fracture did not start from the grain boundaries, but instead, the principal crack started from one side of the specimen in the necked area and propagated along the deformation bands in the transversal direction. From the in-situ observations, the crack was not growing in a continuous way, but accompanied with discontinuous small damage coalescence in the crack wake which finally determined the saw-tooth appearance observable at the final fracture area (Figure 3.2.7.c).

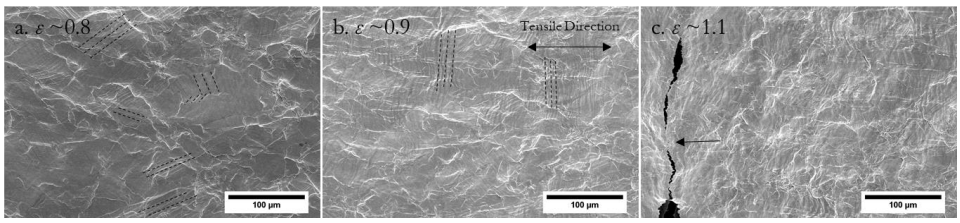

Figure 3.2.7 SEM micrographs from the in-situ investigation of microstructure evolution during tensile test at final stage. The corresponding global nominal strain levels are indicated in each sub-figure. The global tensile direction is horizontal.

3.2.3.2.2 Cyclic loading

The microstructure evolution during cyclic loading test was also investigated via *in-situ* imaging, analogously as was showed in the case of monotonic loading, and the results

are shown in Figure 3.2.8. Unfortunately, the specimen for the cyclic loading test was not prepared by metallographic techniques due to the early-stage technical limitations. Therefore, the results here reported are to be considered as preliminary and regarded as solely qualitative. Tests with higher resolution and better sample quality are in plan and will be conducted after the Covid-19 pandemic restrictions will be released.

Similar to the early stage deformation in the monotonic tensile test, the cyclic loading showed deformation mainly appearing at grain boundaries and inside grains. Additionally, deformation bands crossing grains can also be observed. Most of the deformation bands revealed a roughly 45° angle inclination with respect to the loading direction. As the number of cycles increased, the deformation became more and more significant, but no obvious global damages were found.

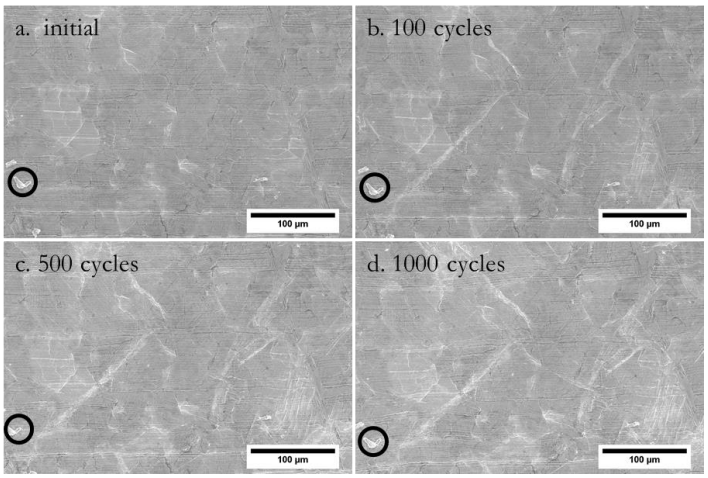

Figure 3.2.8 SEM micrographs from the in-situ investigation of microstructure evolution during cyclic loading test up to 1000 cycles. The black circle indicates a same reference point in the view. The global loading direction is horizontal. The horizontal lines are topographical defects from specimen manufacturing.

3.2.4 Discussions

3.2.4.1 Monotonic tensile behavior

From the tensile testing results, an obvious strain rate sensitivity can be concluded for the studied Pb-Sn-Sb alloy. Generally, the strain rate sensitivity can be correlated to a combination of several time-dependent mechanisms occurring during deformation. Due to the relatively low melting point of Pb alloys, *i.e.* approx. 600 K, room temperature deformation for Pb alloys is similar to what is usually observed at high temperature

deformation for conventional metallic materials such as aluminum or nickel. Therefore, the time-dependent procedures might have included some thermally activated deformation mechanisms such as diffusion, dislocation climbing, boundary migration, *etc*. Normally, these procedures can lead to a significant softening effect due to the fact that dislocations annihilate each other such that the global mobile dislocation density decreases. In a worse case, the damage mechanism of creep can be activated even at room temperature. These micro-mechanisms can explain the obvious strain rate sensitivity observed in the tensile tests.

The three deformation stages as described in the Results section can be linked to the dislocation slip behavior in the grains. In the first stage of early deformation, single slip systems are activated, and dislocations start to move on a specific slip plane. The result of slipping is a step on the specimen surface when dislocations slip out of the material, which is revealed as the slip lines appearing in Figure 3.2.5.b-f. As the strain level increases, additional dislocations take part in the slipping procedure, and more slip lines are formed. In the same grain, the slip lines are mostly parallel in given direction, indicating that the activated slip system is limited to a specific slip plane. In this stage, the stress level also increases, indicating that activating more dislocations to slip needs higher stress level. In the intermediate stage, the slip behavior becomes more complicated: the appearance of multi-directional slip lines on the specimen's surface is indicative of a multi-slip system activation. Through the activation of different slip systems, the grains can accommodate themselves regarding the neighboring grains and the whole specimen starts to deform according to the external loading. From Figure 3.2.6, it is revealed that some grains have changed their shapes to accommodate the geometrical continuity between different grains, and the slip lines are appearing in different directions even in a same grain. In this stage, the specimen has a decreasing stress (engineering stress) level, which means that the geometrical softening becomes more dominant in the deformation process. More specifically, global necking should have already happened, according to the mechanical data. In the final stage, the different slip systems rearrange themselves to form deformation bands perpendicular to the tensile direction, as shown in Figure 3.2.7. The severely deformed region in the necked area starts to form voids which subsequently grow, more and more rapidly as elongation is further increased, until they coalesce into forming a macro-crack. The arrow in Figure 3.2.7.c indicates ligament that still of the material that has not separated yet and the overall figure clearly reveal the void nucleation – growth – coalescence ductile failure mechanism typical of ductile metals.

It is however interesting to the observation that although the main topographical damages initiate and accumulate at the grain boundaries, they are not the main cause of the final failure. One possible damage accumulation at grain boundaries is initiated at lower stress/strain levels at which the deformation is completely dominated by the local microstructural features rather than the mechanical loading conditions. When the stress/ strain becomes higher, the mechanical effect overcomes the microstructural effect, such

that the global deformation follows the global mechanical loading. This can be dually compared to the early stage fatigue damage evolution in cyclically loaded specimens.

Another interesting observation pertains to mechanical twinning. From the initial microstructure observation by EBSD (*i.e.* Figure 3.2.2), a lot of annealing twin boundaries can be characterized. This shows a relatively lower stacking fault energy and thus a higher twinnability of this material in the as-received conditions. Since mechanical twinning is commonly regarded as a viable method to improve both the strength and the ductility of materials during deformation (*e.g.* twinning-induced plasticity/ TWIP steels use this criterion to improve the mechanical properties [12-16]), a deeper understanding on how mechanical twinning relates to the deformation mechanisms of the studied material can be an interesting topic. However, due to time limitation, this will be an outlook in a future work after the Covid-19 pandemic.

3.2.4.2 Cyclic loading behavior

The studied Pb-Sn-Sb alloy shows a clear cyclic softening behavior in the investigated testing range. This phenomenon is common also in some steels (*e.g.* [17, 18]), and is often explained by the reduction of dislocation density and the disappearing of sub-grain boundaries upon cyclic loading. In the present manuscript, due to time limitations, the investigation at the dislocation level was not conducted, but the microstructure evolution was revealed via *in-situ* imaging techniques. The appearance of deformation traces as observed in Figure 3.2.8 implies a dislocation slipping-dominant deformation mechanism during the cyclic loading. Since the shear stresses are most prominent at a degree of 45° to the loading direction, most of the deformation lines are along this direction, confirming the shearing nature of the deformation. However, these deformation bands are not long enough to go through the whole specimen, but rather they are limited by the obstacles present in the material. Unfortunately, it is not straightforward to identify which one of the typical metallurgical obstacles (grain boundaries, precipitates, etc.) are active due to a rough surface quality of the specimen, but based on the EBSD analysis, grain boundaries seem to be the most probable ones. Since the slip systems are defined by the crystallography of each single grain, dislocations are often slipping in different directions and on different planes when crossing grains. Therefore, most of the slip deformation cannot go through grain boundaries and will be accumulated in their vicinity. Moreover, due to the slip irreversibility during cyclic loading [19-21], only part of the deformation can be "relaxed" by the reversed dislocation motion in the "negative" half of the loading cycle. As a result, the deformation gradually and continuously accumulates at the obstacles, such as grain boundaries, and form early-stage damages and geometrical irregularities which constitute the early damage. This damage is in other words expected to add to expected creep induced void formations. Normally some extrusions/ intrusions can be observed on the surface of the specimens.

Another factor that needs to be accounted for is the fact that for this material creep damage may play a role already at room temperature in the way that during cyclic loading, the material recovers itself dynamically and the dislocation density keeps reducing (fatigue + creep interaction). To prove this hypothesis, new tests with different strain rates as well as advanced characterization techniques are needed. This is planned to be presented in a future work by the present authors.

3.2.4.3 Damage modes

Based on the investigations and the discussions, the damage modes of the studied material under the present testing conditions are summarized as follows. During monotonic tension, early-stage damage driven by microstructural constraints accumulates at grain boundaries and causes geometrical softening of the material. As stress and strain level increases, the deformation in more dominated by the global mechanical loading (Figure 3.2.9.a), and final failure starts from the geometrical irregularity in the necked area and proceeds via a void coalescence mode. The final fracture is a ductile type with a locally shear type, as can be seen in Figure 3.2.9.b. The fracture of the material is driven by the deformation lines as in the surrounding areas and follows a shear direction instead of the loading direction. During cyclic loading, the early-stage damages revealed as deformation lines (Figure 3.2.9.c) are also controlled by the crystallography and accumulate inside the grains until an obstacle such as a grain boundary is reached. Typical extrusions/ intrusions are formed on the surface of the specimen as parallel deformation lines (Figure 3.2.9.d) that can serve as geometrical irregularities, which can cause local stress concentration and a possible formation of cracks. Due to time limitation, the quantitative deformation analysis of the cyclically loaded specimen could not be completed. The possible fatigue – creep interaction is of high interest in the authors' research group and will be a topic in a future study.

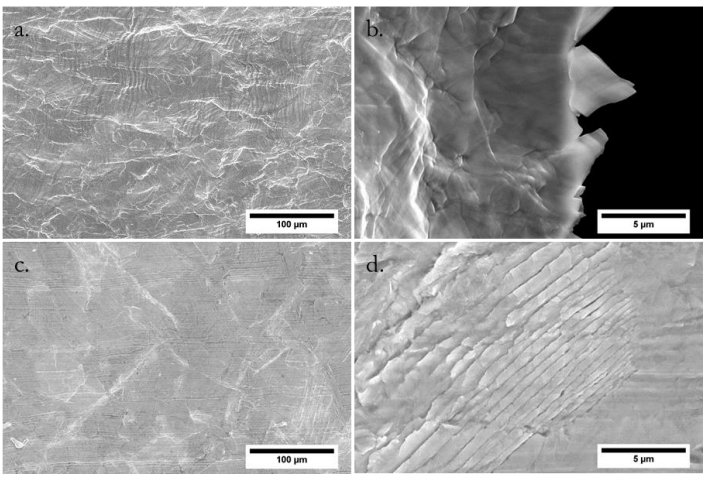

Figure 3.2.9 Damage modes micrographs. a. microstructure before failure at lower magnification (monotonic loading); b. a closer view of the final failure at higher magnification (monotonic loading); c. microstructure after cyclic loading at lower magnification (after 1000 cycles) and d. damage from cyclic loading at higher magnification (after 1000 cycles).

3.2.5 Conclusions

The tensile and fatigue behavior of a Pb-Sn-Sb alloy was investigated through small-scale mechanical testing coupled with *in-situ* imaging techniques in SEM. The tensile tests were conducted under different strain rates, and the cyclic loading test was conducted in a displacement-controlled mode at a strain amplitude of about $\Delta\varepsilon \sim \pm 1.1\%$. With the help of *in-situ* imaging, the microstructure evolution was captured during the mechanical loading. Nevertheless, the current manuscript summarizes only the preliminary results, and deeper analyses, in particular toward that of the mechanisms related to fatigue – creep interaction and dynamic recovery, will be conducted in the close future. The main conclusions from this initial investigation can be drawn as follows:

- The mechanical property of the studied Pb-Sn-Sb alloy has a strong dependency on the strain rate in the studied range (from 10^{-5} s^{-1} to 10^{-3} s^{-1}) with a clear softening phenomenon as the strain rate is decreased.
- The strain rate mainly changes the strength level (both the yielding strength and the tensile strength), while the strain to failure remains similar.
- In monotonic tensile testing, early-stage damages occur at grain boundaries, while the final failure starts from the necked area constrained by the global mechanical condition.

- The material shows a cyclic softening behavior when subjected to cyclic loading, and the formation of extrusions/ intrusions as a result of persistent slip bands is observed.
- Dynamical recovery can be a possible mechanism for both monotonic loading and cyclic loading. This is the outlook of the present work and will be conducted in the close future.

Acknowledgements

The authors would like to thank the financial support from Nexans Norway AS and the Research Council of Norway (IPN in ENERGIX, Project number 256367) and performed within the project: Next-generation damage based fatigue of cable sheeting (REFACE).

References

[1] A. Johanson, L.M. Viespol, A. Alvaro, F. Berto, Small- and Full-Scale Fatigue Testing of Lead Cable Sheathing, The 29th International Ocean and Polar Engineering Conference, International Society of Offshore and Polar Engineers, Honolulu, Hawaii, USA, 2019, p. 6.
[2] L.M. Viespoli, A. Johanson, A. Alvaro, B. Nyhus, F. Berto, Room temperature creep mechanism of a Pb-Sn-Sb lead alloy, Procedia Structural Integrity 18 (2019) 86-92.
[3] H.F. Moore, N.J. Alleman, The creep of lead and lead alloys used for cable sheathing, a report of an investigation conducted by the Engineering Experiment Station, University of Illinois in coöperation with the Utilities Research Commission, University of Illinois at Urbana Champaign, College of Engineering …, 1932.
[4] C.W. Dollins, C.E. Betzer, Creep, fracture, and bending of lead and lead alloy cable sheathing, University of Illinois at Urbana Champaign, College of Engineering …, 1956.
[5] P. Feltham, On the Mechanism of High-Temperature Creep in Metals with Special Reference to Polycrystalline Lead, Proceedings of the Physical Society. Section B 69(12) (1956) 1173-1188.
[6] D. Harvard, Fatigue of Lead Cable-Sheathing Alloys, Ontario Hydro research (1972).
[7] P. Anelli, F. Donazzi, W. Lawson, The fatigue life of lead alloy E as a sheathing material for submarine power cables, IEEE Transactions on power delivery 3(1) (1988) 69-75.
[8] M.K. Sahota, J.R. Riddington, Compressive creep properties of lead alloys, Materials & Design 21(3) (2000) 159-167.
[9] A. Johanson, L.M. Viespoli, B. Nyhus, A. Alvaro, F. Berto, Experimental and numerical investigation of strain distribution of notched lead fatigue test specimen, (2018).
[10] L.M. Viespoli, A. Johanson, A. Alvaro, B. Nyhus, F. Berto, Strain controlled medium cycle fatigue of a notched Pb-Sn-Cd lead alloy, Eng. Fail. Anal. 104 (2019) 96-104.

[11] L.M. Viespoli, A. Johanson, A. Alvaro, B. Nyhus, A. Sommacal, F. Berto, Tensile characterization of a lead alloy: creep induced strain rate sensitivity, Mater. Sci. Eng., A 744 (2019) 365-375.
[12] O. Grässel, L. Krüger, G. Frommeyer, L.W. Meyer, High strength Fe–Mn–(Al, Si) TRIP/TWIP steels development — properties — application, Int. J. Plast. 16(10-11) (2000) 1391-1409.
[13] O. Bouaziz, N. Guelton, Modelling of TWIP effect on work-hardening, Mater. Sci. Eng., A 319-321 (2001) 246-249.
[14] S. Allain, J.P. Chateau, O. Bouaziz, A physical model of the twinning-induced plasticity effect in a high manganese austenitic steel, Mater. Sci. Eng., A 387-389 (2004) 143-147.
[15] S.-J. Lee, J. Kim, S.N. Kane, B.C.D. Cooman, On the origin of dynamic strain aging in twinning-induced plasticity steels, Acta Mater. 59(17) (2011) 6809-6819.
[16] B.C. De Cooman, Y. Estrin, S.K. Kim, Twinning-induced plasticity (TWIP) steels, Acta Mater. 142 (2018) 283-362.
[17] P. Sulich, W. Egner, S. Mroziński, H. Egner, Modeling of cyclic thermo-elastic-plastic behaviour of P91 steel, Journal of Theoretical and Applied Mechanics (2017).
[18] M.F. Giordana, P.F. Giroux, I. Alvarez-Armas, M. Sauzay, A. Armas, Micromechanical modeling of the cyclic softening of EUROFER 97 steel, Procedia Engineering 10 (2011) 1268-1273.
[19] H. Mughrabi, Dislocation wall and cell structures and long-range internal stresses in deformed metal crystals, Acta Metall. 31(9) (1983) 1367-1379.
[20] H. Mughrabi, Cyclic Slip Irreversibilities and the Evolution of Fatigue Damage, Metall. Mater. Trans. B 40(4) (2009) 431-453.
[21] H. Mughrabi, Cyclic slip irreversibility and fatigue life: A microstructure-based analysis, Acta Mater. 61(4) (2013) 1197-1203.

3.3 Paper V

Small- and Full-Scale Fatigue Testing of Lead Cable Sheathing

Audun Johanson[1], Luigi Mario Viespoli[2], Antonio Alvaro[3], Filippo Berto[2]

[1]*Nexans Norway,*
[2]*Dept. Of Mechanical and Industrial Engineering, Norwegian University of Science and Technology (NTNU), Norway*
[3]*Dept. of Materials and Nanotechnology, SINTEF Industry, Norway*

Abstract: The fatigue behavior of a PbSnSb alloy used in subsea power cable sheathing was studied using small- and full-scale experiments. The aim of the work was to understand the transferability between the scales and suitable testing methods. Creep phenomena are addressed by considering the cyclic strain rate as well as the small-scale loading mode. The fatigue test results show significant difference between different loading modes and scales. It is also evident that fatigue- creep interaction is highly important.

Keywords: Lead Sheath; Fatigue; Creep; Subsea Power Cables.

3.3.1 Introduction

Subsea power cables operating above 36 kV require an impermeable water barrier to prevent humidity in the isolation system. In the case of Mass-Impregnated (MI) or Cross-Linked High-Density Polyethylene (XLPE) insulation systems as normally used for high voltage submarine power cables, humidity can compromise the systems electrical integrity. Lead-based alloys are normally used as a water barrier due to ease of extrudability and ductility. Lead-based alloys are also associated with favourable low-cycle fatigue properties when compared to higher strength materials such as copper or aluminium. However, due to its combination of very poor high cycle fatigue properties and low creep resistance, multiple cyclic scenarios can challenge the fatigue-creep life of the sheathing. Critical scenarios include cable installation and offshore jointing. These operations imply a temporary dynamic suspension between the seabed and a floating vessel where the cable will be subjected to bending due to wave motion on the cable and vessel. Additional bending fatigue damage can be introduced from vortex- induced vibrations (VIV) in the temporary catenary or free-spans along the cable route. Another case arises from the insulation temperature fluctuations during operation. Thermal expansion and contraction of the oil in MI insulation or the XLPE will cyclically strain the lead sheath in radial direction. The high relative temperature for lead-alloys at room

temperature (~0.5 T_m) and low creep resistance for typical cable sheathing alloys cause a significant strain rate dependency under loading [1,2]. These properties also depend on the alloying elements and the microstructure.
The fatigue performance of a Lead-Tin- Antimony (PbSnSb) - alloy as cable sheathing on MI- and XLPE power cables have been investigated. The alloy is common in the subsea power cable industry, but its fatigue and creep properties, probably due to the numerous challenges inherent to testing and metallurgical investigation, have been subject to limited research. The existing literature, which is quite scarce, include the work of Anelli (1986) [3] who investigated the frequency dependency of the alloy. In a recent publication by the authors, the importance of microstructure of this alloy with respect to its strain rate dependency at room temperature, Viespoli et al., 2019 [4].
In this work cyclic fatigue testing on both small- and component/full- scale level have been conducted. The material has been subjected to two different loading modes: reverse bending and tension- compression. Particular attention is payed to the influence of creep by considering the strain rate sensitivity.

3.3.2 Materials and methods

3.3.2.1 Materials and Test Specimens

This study investigates an extruded PbSnSb alloy with composition given in Table 1. The as-extruded grain size is approximately 70 μm by the average grain intercept method.

Pb	Sn	Sb
99.3	0.45	0.25

Table 3.3.1. Composition of test material.

Four types of test specimens have been investigated in this study:
(1) 3.0 mm thickness as- extruded 3.0 mm rectangular specimens for reverse bending;
(2) 3.0 mm thickness as- extruded rounded hourglass shaped specimens tension-compression tests;
(3) MI full scale power cable;
(4) XLPE power phases.
Figure 1 show the MI power cable and XLPE power phase cross-sections.

3.3.2.2 Small Scale Test Procedures

Reverse Bending. Cyclic reverse bending testing has been carried out to investigate the fatigue life under such loading mode and effect of strain rate.
Forty-four reverse bending tests over 11 different test parameters have been performed (the test parameters are summarized in Table 2). The test object target strain range ($\Delta\varepsilon$)

is controlled by fixing the test object horizontally and vertically displacing it against a shaper with a defined curvature (Figure 2).

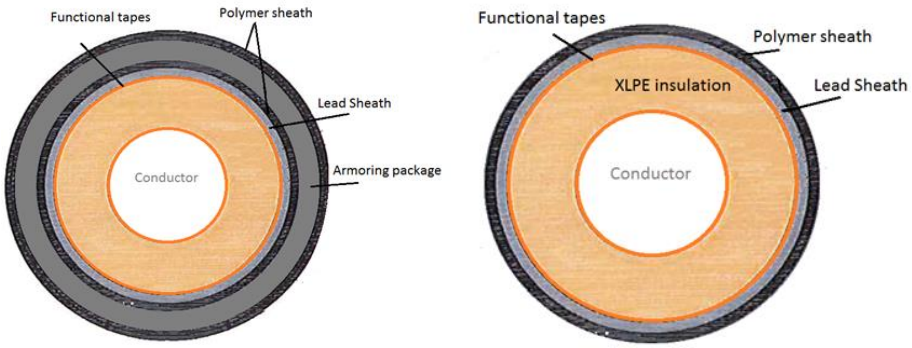

Fig. 3.3.1. (Upper) MI power cable test object; (Lower) XLPE power phase test object. A XLPE power cable often consists of 3 XLPE power phases stranded together where axial armoring is applied on the outside of the 3- phase cross- section. Functional tapes indicate one or more layers of helically wounded tapes for various purposes.

The strain range is calculated according to Eq. 1.

$$\Delta\varepsilon_{nom} = C_{Shaper} t_{test\ Object} \tag{3.3.1}$$

Where C and t are the measured curvature and thickness of each individual test object, respectively.
Failure is measured by electrical resistance of each samples whereby an increase is caused by fracture and separation of the specimen. All tests are conducted at room temperature.

Tension-compression. Cyclic loading testing in tension-compression has been conducted to investigate the fatigue life under such loading mode.
Eight tests at different Δε and constant strain rate (i.e. 1e-2 1/s), were carried out. Triangular shaped load cycles were used in order to assure a strain rate as constant as possible for the duration of the whole test. The strain rate value was chosen with the intent of excluding creep and thus strain rate dependency (Viespoli, et al., 2019). Symmetric loading (R= -1) is employed for all tests where and the strain is measured by Digital Image Correlation (DIC) technique. The test set-up is shown in Figure 3.

Shaper curvature [1/m]	Δε (nom.)	Frequency [Hz]
1.00	0.32 %	1
		$3.3e^{-1}$
		$1.7e^{-2}$
		$2.8e^{-3}$
		$8.3e^{-3}$
0.67	0.21 %	1
		$1.3e^{-1}$
0.50	0.16 %	2
		1
		$3.5e^{-1}$
		$1.3e^{-1}$

Table 3.3.2. Test matrix. Four tests for each parameter parallel.

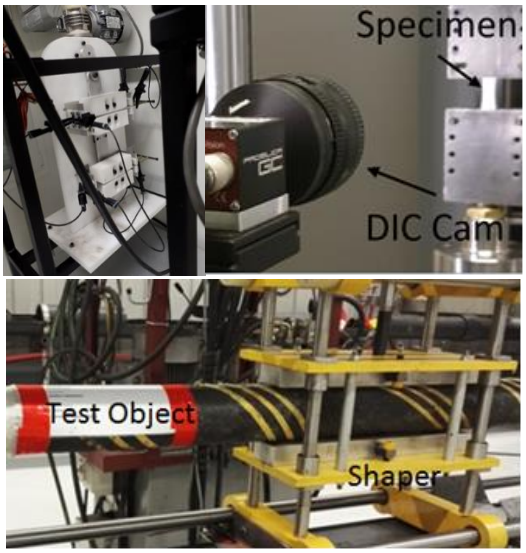

Fig. 3.3.2. (Left) Cyclic reverse bending set-up; (center) Tension- Compression set up and DIC strain measurement; (right) Full scale test set-up.

3.3.2.3 Full Scale Test Procedure

In total 27 XLPE power phases and 30 MI power cable test object where subjected to reverse bending. The set- up is shown in Figure 2. The test objects are tensioned to 5 kN in order to straighten the test object prior and during the test. 600 mm long shapers of defined curvatures are mounted with its curved side facing the test object from each side. The test object is bent by displacing the shapers vertically until the test object is in contact

with the shaper over 400- 500 mm at its minimum and maximum positions. The vertical shaper displacement amplitude is kept constant throughout the test.
The strain range is calculated from the measured test object sheathing diameter and radius of the shapers according to Eq. 1 where t is the test object diameter. Test temperature is maintained at room temperature. Due to the lack of a reliable failure detection system, all tests are run to a pre- specified number of cycles where post- test dissection and die-pen investigation of the lead surface is used to determine if the test object had failed. The test matrix is given in Table 3.

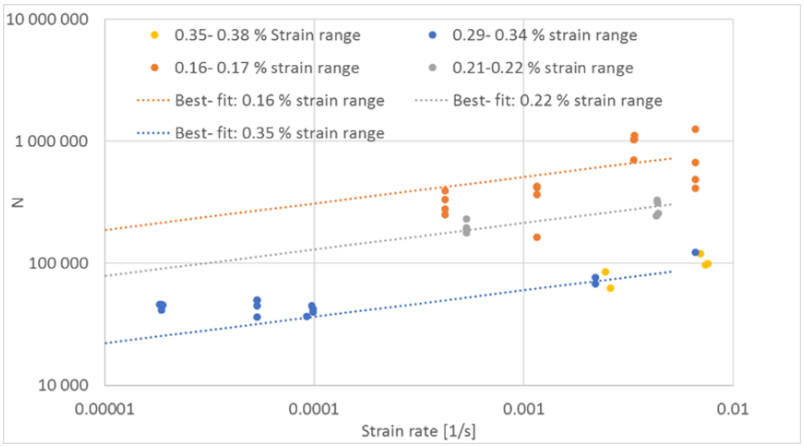

Fig. 3.3.3. Reverse bending fatigue results and best-fit fatigue- creep model. The damage model appears to over-predict the creep damage towards low strain rates, at which it results too conservative.

Shaper curvature [1/m]	Test Object/ OD [mm]	Δε (nom.)	Frequency [Hz]
0.110	MI/ 95.8	1.02 %	0.20
	MI/ 66	0.70 %	0.10
	XLPE/ 105.6/	1.11 %	0.20
0.037	MI/ 95.8	0.36 %	0.20, 0.33, 0.44
	MI/ 66	0.24 %	0.25
	XLPE/ 105.6/ 104.5	0.39 %	0.25
0.029	MI/ 66	0.19 %	0.25, 0.5, 0.67

Table 3.3.3. Test matrix. In total 30 MI full scale power cables and 27 XLPE power phases where tested.

3.3.3 Experimental results

3.3.3.1 Small-Scale Tests

Reverse bending. The fatigue life of the lead is clearly affected by both the tests frequency and the shaper curvature. The nominal strain ranges are obtained by using the specimen thickness together with Equation 1 and the approximate the strain rate according to Equation 2:

$$\dot{\varepsilon} = 2 \cdot f[Hz] \cdot \Delta\varepsilon \tag{3.3.2}$$

The modified frequency strain life equation (Wong, 2016) is adopted where the frequency value is replaced with the estimated strain rate calculated following Eq. 2.

$$\Delta\varepsilon = A(N\dot{\varepsilon}^{-p})^{\beta} \tag{3.3.3}$$

where A, β and p are constants of which p dictates the strain rate dependency. Figure 3 show the results together with the best fit solution of the damage model.
A strain rate dependency (p) of 0.21 was calculated by a fitting the test data to Equation 3.

Tension-compression. Equation 3 set the basis for the construction of the fatigue curve where the strain rate component is neglected, i.e. the high strain rate curve is constructed based on the strain life equation without frequency modification. Figure 4 is a plot of the tension- compression results and corresponding fatigue curve. Selected reverse bending results from tests conducted at comparable strain rates (~0.7e^{-2} 1/s) are also plotted in the same graph to facilitate a direct comparison.

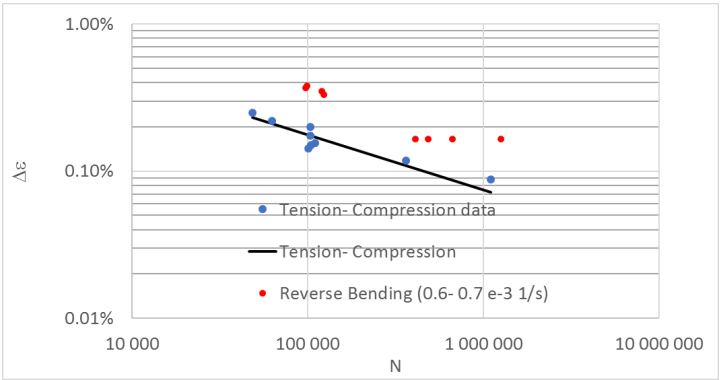

Fig. 3.3.4. Tension-compression results and calculated fatigue curve. The high strain rate reverse bending result (0.6- 0.7 e^{-2} 1/s) are also reported.

3.3.3.2 Full Scale Tests

MI power cables and XLPE power phases test results are shown in Figure 5 and 6. All the test results are normalized to the average strain rate for the tests according to the modified damage model identified from reverse bending results.

Fatigue Δε- N curves are estimated by the Maximum Likelihood Method (MLM) where the fatigue life follows a log-normal distribution. The method described in Pascual (1997) [5], but with fixed standard deviation and introduction of a component to account for unknown point of failure is adopted in this study.

Th likelihood function is described as follow:

$$L(\theta) = \prod_{i=1}^{n} F(X_i|\theta)^{\delta_i} R(X_i|\theta)^{1-\delta_i} \quad (3.3.4)$$

where F and R is the cumulative probability of failure and survival, respectively. δ assigned after dissection observation as follow:

$$\delta = \begin{cases} = 1, if\ the\ sample\ has\ failed \\ = 0, if\ the\ sample\ has\ not\ failed \end{cases}$$

The reliability function is given by:

$$R(X|\theta) = 1 - F(X|\theta) = 1 - 0.5\left[1 + erf\left(\frac{Ln(X_i) - \tilde{X}}{\sigma\sqrt{2}}\right)\right] \quad (3.3.5)$$

Assume the fatigue life can be described according to the Coffin- Manson relation:

$$\tilde{X} = \ln N = \ln A + m \ln \Delta\varepsilon \quad (3.3.6)$$

the fatigue parameters Ln (A), m and standard deviation, σ are estimated by maximizing the likelihood function. To simplify the calculations:

$$\ln L(\theta) = \sum_{i=1}^{n} Ln\left(R(X_i|\theta)^{\delta_i}\right) Ln\left(1 - F(X_i|\theta)^{1-\delta_i}\right) \quad (3.3.7)$$

By maximizing Equation 7 through a Raphson-Newton iterative scheme, the best-fit fatigue parameters are obtained.

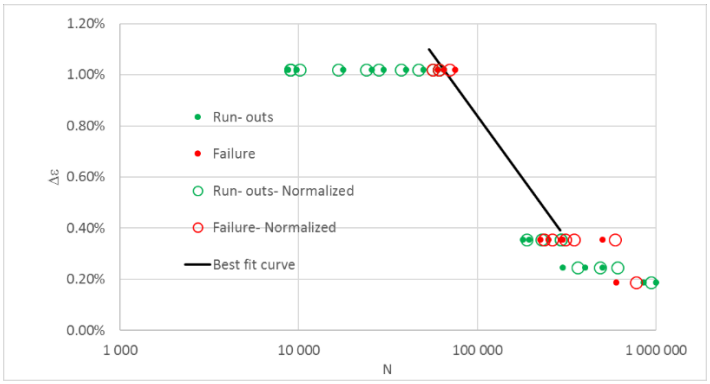

Fig. 3.3.5. Full scale results for MI power cables together with the results normalized to the average testing strain rate and the calculated maximum likelihood function.

Fig. 3.3.6. Full scale results for XLPE power phases together with the results normalized to the average testing strain rate and calculated the maximum likelihood function.

3.3.3.3 Post-Test Dissection Observations

The test objects were dissected after testing and any identified fracture by die-pen or visual inspection deemed the test result as failure. Tests exceeding the number of cycles given by the calculated fatigue curve tended toward an increasing severity and frequency of cracks. The characteristics of the test object prior to- and after failure differ between MI power cable test objects and XLPE power phases. High and low strain ranges also were a discriminant in the type of observed cracks. XLPE showed a tendency to initiate cracks from pre-existing discontinuities running in a helical direction whereby the cracks mainly propagate in circumferential direction for $\Delta\varepsilon$ tests > 1.0 % (reference to Figure 7). Cracks propagating along the discontinuities were also found. The majority of XLPE power phase tested for a strain range of approximately $\Delta\varepsilon$=0.4%, cracked following the

discontinuities as shown in Fig. 8. Another distinct feature for both tested Δε levels where deformation aligned with the same discontinuities is shown in Figure 9. Helical discontinuities of comparable or worse severity were found also for MI power cables (Figure 10). Cracks initiated also from these, but predominantly propagated along the sheathing circumference- not the helical direction of discontinuities. This is the case for all tested Δε. The large amount of deformation observable at the cracked location evident in all the failed XLPE power cables were absent. Figure 11 show the typical failure characteristics.

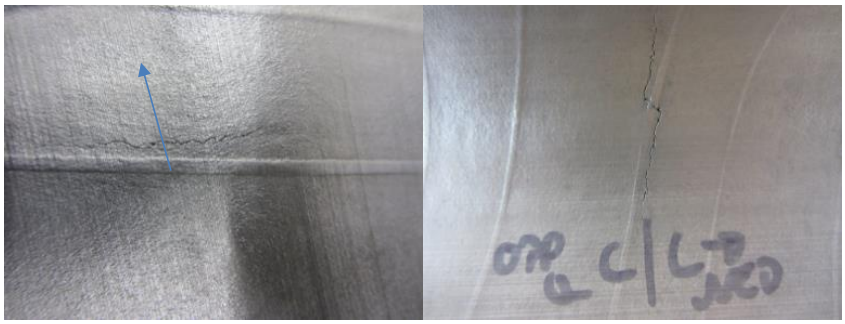

Fig. 3.3.7. (Upper) Inside of a XLPE power phase after 15,000 cycles at 1.1 % Δε; (Lower) Inside of a XLPE power phase after 25,000 cycles. Arrow indicate axial object direction.

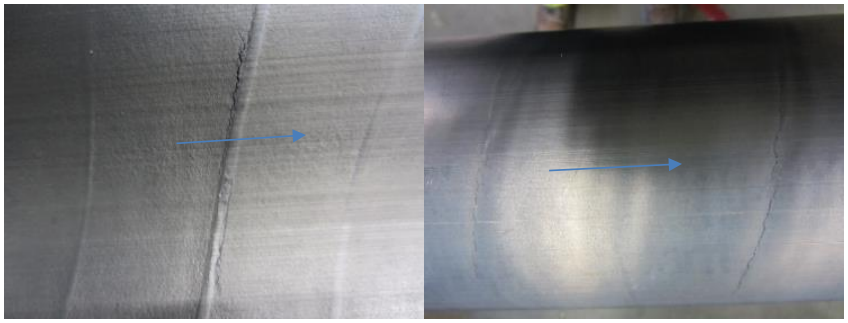

Fig. 3.3.8. (Upper) Inside of a XLPE power phase after 30,000 cycles at 0.4 % Δε; (Lower) Outside of the same test object. The blue arrow represents the axial direction.

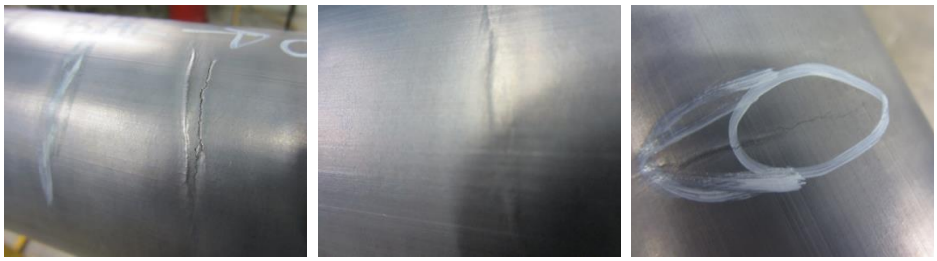

Fig. 3.3.9. (Left) Outside of a (failed) XLPE power phase after 15,000 cycles at 1.1 % Δε; (Center) Outside of a (run- out) XLPE power phase after 25,000 cycles at 0.4 % Δε; (Right) Outside of a (failed) XLPE power phase after 30,000 cycles at 0.4 % Δε.

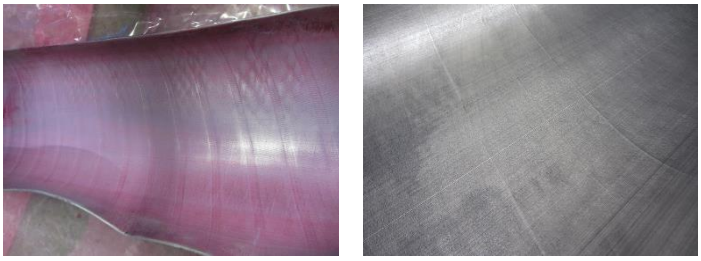

Fig. 3.3.10. (Left) Inside of (run-out) MI power cable after 65,000 cycles at 1.02 % Δε; (Right) Outside of a (run- out) XLPE power phase after 40,000 cycles at 0.40 % Δε.

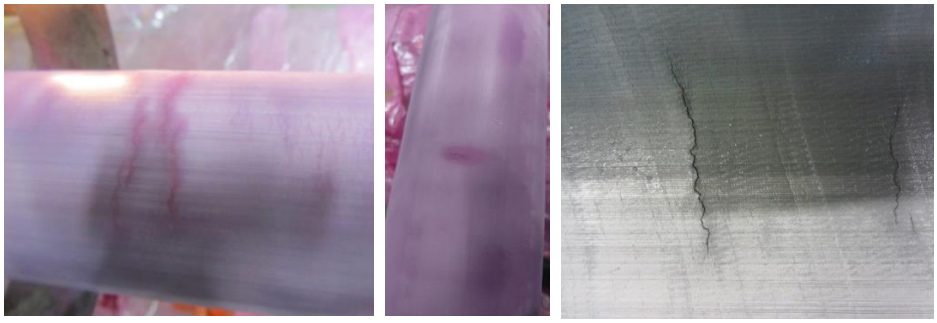

Fig. 3.3.11. (Left) Outside of a (failed) MI power cable after 75,000 cycles at 1.02 % Δε; (Center) Outside of a (failed) MI power cable after 60,000 cycles at 1.02 % Δε; (Right) Inside of a (failed) MI power cable after 300,000 cycles at 0.36 % Δε. The blue arrow represents the axial direction.

3.3.4 Conclusions

The fatigue life of lead strongly depends on loading mode. Reverse bending of small-scale test specimen results in significantly improved fatigue life compared to tension-compression (Figure 4 and 12). Power cable subjected to bending introduce mostly tension-compression type of load on its lead sheath. Based on this it is not advisable to base fatigue calculation of tubular sheathing from reverse bending of small-scale specimens.

The fatigue life of lead is greatly enhanced when tested in a MI Power cable design compared to small- scale. The tested MI power cable designs used axial and transversal armoring which would introduce hoop stress and potentially prevent local ratcheting. The latter is supported by the post- test dissections where the ridges observed on the XLPE power phases are absent. The extension of full- scale fatigue life can also be related to modification of the hysteresis under bending where compression from the armoring elements shift the hysteresis towards compression which could modify both crack-opening, closing and potentially arrest. Ongoing work is aimed towards understanding these mechanisms for lead alloys and cable design. The enhanced fatigue life of observed for MI power cables compared to small-scale results appears to be significantly reduced or absent for XLPE power phases. The XLPE power phase do potentially overlap with the small-scale data, but additional experiments towards the high-cycle region is required.

Over the range of strain rates investigated in full scale MI power cable testing, the strain rate dependency extracted from reverse bending fits relatively well. By increasing the strain rate sensitivity from 0.21 to 0.35, a minor improvement of fit for the MI power cables tests is observed, effectively reducing the scatter identified by the maximum likelihood method (Figure 13). This puts into question the applicability of the identified strain rate dependency for full scale results. As the strain rate sensitivity is not based on tests reflecting the correct loading mode or representing a physically meaningful description of the underlying fatigue-creep interaction, care should be taken when extrapolating the test results outside the test range.

The majority of the fractures on full scale tests appear to initiate in surface discontinuities. It is clear that the identified discontinuities do affect the fatigue life, but their effect appear to be different for MI and XLPE power cables. For XLPE cables the fractures locations are often associated with local deformation in the form of ridges intimate to the fracture location. The same observation is not made for neither reverse bending or tension-compression small-scale tests even if the fatigue life were similar. This could indicate that the apparent negative effect from discontinuities on the sheathing is offset by other positive effects such as the absence of an edge on tubular sheathing. This statement is supported by a previous study, which demonstrates a low influence of severe stress concentrators on the fatigue life of lead (Johanson et al., 2018).

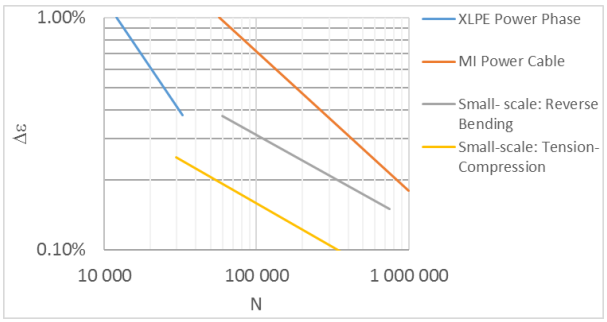

Fig. 3.3.12. Comparison of the XLPE, MI and small-scale fatigue curves. All curves are modified to a common strain rate corresponding to the average strain rate for all tests. Curves are plotted for their tested Δε range.

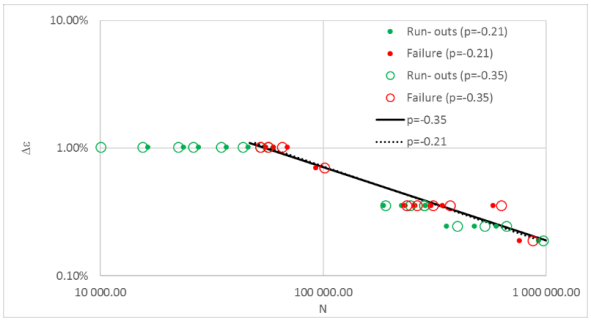

Fig. 3.3.13. The increase in strain rate sensitivity parameter (p) from 0.21 (as calculated from the small-scale experiments), to 0.35 determine a shift of the failure points below the calculated mean curve towards or above the curve. A higher strain rate sensitivity will in other words better explain the observations.

Acknowledgements

This work has been financed by Nexans Norway and the Research Council of Norway through ENERGIX Programme, Contract No. 256367/E20.

References

[1] E.H. Wong, W. v. (2016). Creep fatigue models of solder joints: A critical review. *Microelectronics Reliability*, 1-12.

[2] Johanson, A., Viespoli, L., Nyhus, B., Alvaro, A., & Berto, F. (2018). Experimental and numerical investigation of strain distribution of notched lead fatigue test specimen. *12th International Fatigue Congress.* Poitiers.

[3] P.Anelli, F. (1986). The Fatigue Life of Lead Alloy E as a Sheathing Material for Submarine Power Cables.
[4] Viespoli, L., Johanson, A., Alvaro, A., Nyhus, B., Sommacal, A., & Berto, F. (2019). Tensile characterization of a lead alloy: creep induced strain rate sensitivity. *Materials Science & Engineering A, 744*, 365-375.
[5] Pascual, F. (1997). Analysis of Fatigue Data with Runouts Based on a model with Non- constant Standard Deviation and a Fatigue limit parameter. *Journal of testing and evaluation, 25*(3), 292- 301.

Chapter 4: Influence of notches

This chapter is constituted of a journal paper and the relative journal extension on the fatigue properties of a lead alloy in presence of a geometrical discontinuity. The scope of the chapter is the assessment of the influence of manufacturing defects on the structural integrity of the sheathing.

4.1 Paper VI

Strain controlled medium cycle fatigue of a notched Pb-Sn-Cd lead alloy

Luigi M. Viespoli[1], Audun Johanson[2], Antonio Alvaro[3], Bård Nyhus[3], Filippo Berto[1]

[1]*Department of Mechanical and Industrial Engineering, Norwegian University of Science and Technology (NTNU), Norway*
[2]*Nexans Norway, Innspurten 9, 0663 Oslo, Norway*
[3]*Sintef Industry, Richard Birkelands vei 2B, 7031, Trondheim, NORWAY*

luigi.m.viespoli@ntnu.no
+47 459 13 281

Abstract: During the extrusion process of subsea power cable sheathing layer it is possible that metallic and/or non-metallic debris present in the processing environment enter the metal lattice originating discontinuities that might have a detrimental effect on the fatigue life and the overall integrity of the sheathing. In order to understand the influence of these production defects on the reliability of installed power-lines, a series of specimens directly retrieved from the extruded sheathing were fatigue tested at different strain rates and range both in presence and absence of a non-passing through notch simulating the geometrical discontinuity induced by a particle. In order to collect the necessary information for the understanding of the failure mechanism, Digital Image Correlation and Scanning Electron Microscopy were used to understand the influence of the testing condition on the material resistance and failure mode.
Keywords: Lead, creep-fatigue interaction, digital image correlation, notch sensitivity

4.1.1 Introduction

To prevent the failure of power lines for electric short circuit it is necessary to impede the penetration of water through the polymer wall. This is achieved by the addition of a layer of stable metal such as lead. The technology used for such application is not recent, but most of the studies performed are dated and many issues regarding the topic are still unclear, while the production of power cables greatly relies on previous experience. In the case of the alloy object of the study, which has a melting temperature of 590 K, operational temperature (i.e. room temperature) above its recrystallization temperature, time dependent plasticity phenomena must be taken into account [1] to provide a reliable prediction of the mechanical response of the material. The mechanisms of creep deformation of lead alloys were investigated by Feltham [2] with focus on the effect of

the inter-granular substructure and grain size. A qualitative classification of fitness for different kind of power cable application was performed by Harvard [3]. An investigation on the compressive creep behaviour of cable sheathing and the influence of alloy elements has been performed by Sahota et al. [4]. Dollins and Betzer [5] studied the influence of the production variables on the long term plasticity and fatigue behaviour of lead alloys. Anelli et al. [6] found a non-significant influence of grain size and temperature on the fatigue life of cable sheathing lead alloys E and Pb-Sb. Analyzing the behavior of the cable sheathing as a creep problem, several effects have to be considered. For the application of lead and lead-free solders, a variation of the apparent elastic modulus was detected in function of the temperature and strain rate which the material is subjected to [7,8,9]. Grain boundary sliding has a consistent contribution on the creep deformation of polycrystalline commercially pure metals [10, 11], leading to greater deformation in the presence of smaller grains. The influence of creep and microstructure on the tensile properties of a PbSnSb alloy used for the manufacturing of subsea power cables was investigated by Viespoli et al. [12] finding a correlation between the grain size and the stress level reached for a given strain rate. Johanson et al. [13] tested a batch of notched and un-notched lead fatigue specimens at two different strain levels and testing frequencies. The influence of sharp and blunt V-notches and semi-circular notches on the medium cycle fatigue, in the case of an aluminum alloy, was studied by Negru et al. [14]. With regards to the tests in [13], although the finite element modelling shows a significant increment of the strain range due to the notch, this was not determinant for the failure mechanism. In the present work, these results are recalled and integrated with new elements to enhance the understanding of the material behaviour. The material plastic response of the same alloy was obtained by performing tensile testing on flat dog-bone samples and extracting the strains by digital image correlation (DIC) post-processing. A second batch of four new fatigue tests was performed at two different strain rates and one strain range. These tests were recorded by a digital camera at selected intervals in order to reconstruct the strain pattern on the specimen's surface by DIC post-processing. The effective Von Mises strain range has been extracted from the crack initiation locations and correlated to the crack initiation number of cycles. The fracture surfaces were investigated by the use of a scanning electron microscope (SEM) to understand the damage progression mechanics.

4.1.2 Material and samples

In the manufacturing of lead sheaths for power cables, the unwanted presence of hard particles included in the material due to the production process may occur as showed in Figure 1. It is then important to understand the influence of these hard particles, which create a discontinuity in the material and intensify the strain field, on the overall fatigue life. The geometry of the notches to be introduced in the samples was decided from the observation of real defects on sheathing samples and machined by electro discharge

machine (EDM). The procedure adopted was to simulate the presence of the defect machining a small blind hole, acting as a notch, on the convex surface of the specimen. The effect of the discontinuity was investigated testing both notched and un-notched samples at the frequencies of 5 and 10 Hz for two strain ranges, 0.15 and 0.28%. The cable sheathing was extruded from material according to PB012K in EN 12548. The main alloying elements are tin (Sn) and cadmium (Cd). Minor additions of tellurium (Te) for grain stabilization are also present. The chemical composition, measured by optical emission spectroscopy on the extrusion material, is reported in Table 1. The test specimens were machined according to the specifications in Figure 2 from 80 mm nominal diameter tubes. The curvature in the transversal section was kept in order to prevent buckling in the compressive phase and limit the work hardening during the production of the sample.

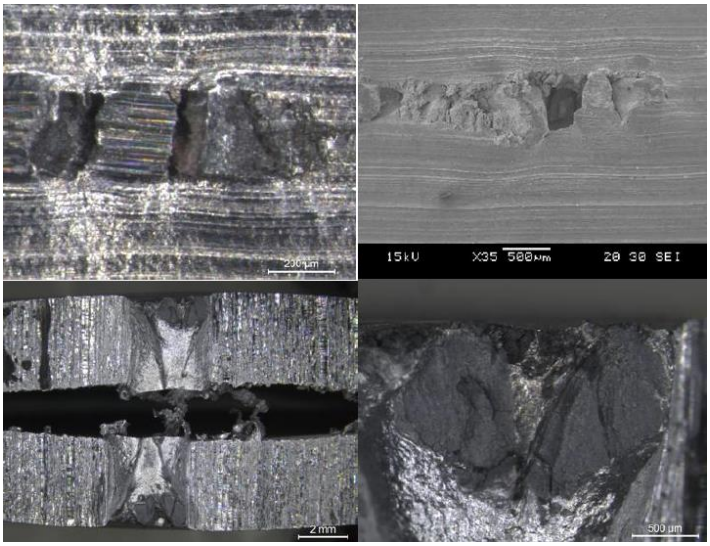

Figure 4.1.1. Magnifications of defects created in the extruding process.

Element	**Sn**	**Te**	**Cd**
Weight %	0.175-0.225	0.0008-0.0025	0.60-0.90

Table 4.1.1. Chemical composition of lead alloy 1/2C+Te.

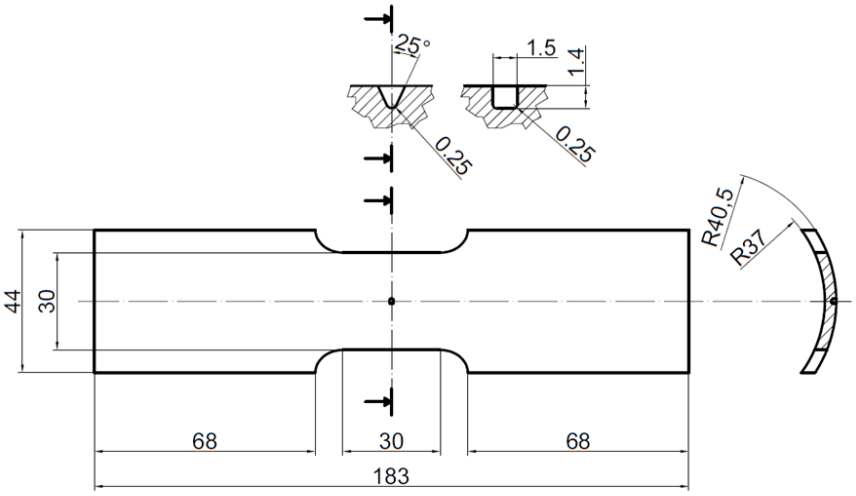

Figure 4.1.2. Nominal dimensions of the specimens and of the notch practiced.

4.1.3 Material tensile characterization

In order to have an estimate of the strain rate sensitivity in the chosen strain ranges, tensile testing at two different strain rates, 1E-2 and 1E-3 s-1, was performed. The tensile testing was executed on flat dog-bone samples, see Figure 3. The strains were obtained through DIC post-processing. The mechanical response of the material treated is strongly influenced by time dependent phenomena [12], thus it was necessary to perform a tensile characterization at two different strain rates in the range of the fatigue testing, but also compatible with the capabilities of the equipment. The fatigue testing was executed at two different strain ranges and two frequencies, as indicated in Table 2. The value indicated in Table 2 as nominal strain rate is the averaged strain rate value calculated considering a constant strain rate development through the whole cycle even if the imposed load cycle was of sinusoidal shape. Even if the testing conditions have a nominal strain rate 1.5 to 3 times greater than the highest adopted in the tensile testing, figure 4 shows the reduced influence of time dependent deformation in the strain rate range of interest. In fact, the two tensile curves obtained at 1E-2 and 1E-3 s-1 are mostly correspondent.

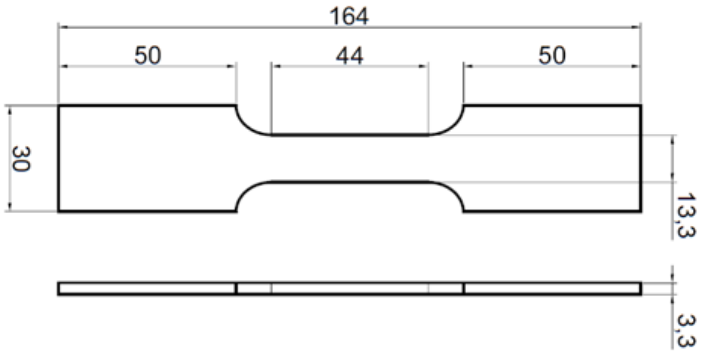

Figure 4.1.3. Geometry of the tensile specimens for material calibration.

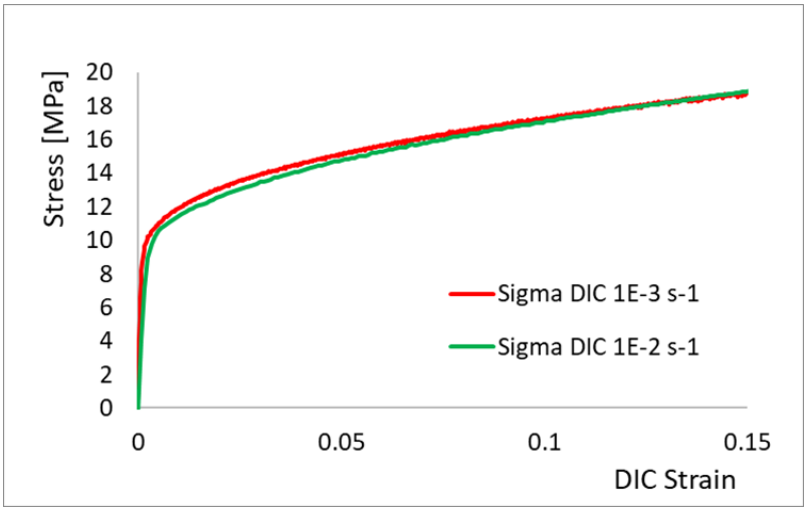

Figure 4.1.4. Tensile testing characterization.

Strain Range [%]	**Load Ratio R**	**Frequency [Hz]**	**Nominal Strain Rate [s-1]**
0.28	-1	5	2.8E-2
0.15	-1	5	1.5E-2
0.15	-1	10	3E-2

Table 4.1.2. Nominal fatigue testing conditions.

4.1.4 Fatigue testing

The fatigue testing was run in position control according to the conditions reported in Table 2, that is frequencies of 5 and 10 Hz and nominal strain ranges of 0.15 and 0.28 %. The load ratio adopted was equal to -1 in terms of displacement. Two different series of testing were executed, the second of which with the use of digital image correlation. In the first batch, nineteen specimens were tested without DIC [13]. The following procedure was adopted to determine the test parameters: an extensometer was used during the first upload phase to register the necessary machine displacement to be imposed as the cycle amplitude. The extensometer was then removed and, before the test was initiated, the marks left by the extensometer clips were removed by careful manual grinding to prevent early crack initiation. The results of the fatigue testing of this first batch are summarized in figure 6. At the highest strain range and lowest frequency, no influence of the presence of the notch was detected in terms of cycles to failure. For all the specimens the failures have started from the edge and propagated towards the middle of the specimen, passing through the notch in case of the notched ones. Stronger influence was observed for the tests at the lower strain range: both at 5 and 10 Hz, the notched samples had a shorter fatigue life than the respective un-notched. In addition the cracks were seemingly more randomly positioned: they did not start from the notch, but from the edges of the specimens, at the fillet radius or at the height of the notch, without a significant correlation with the presence of the discontinuity, see Figure 5.

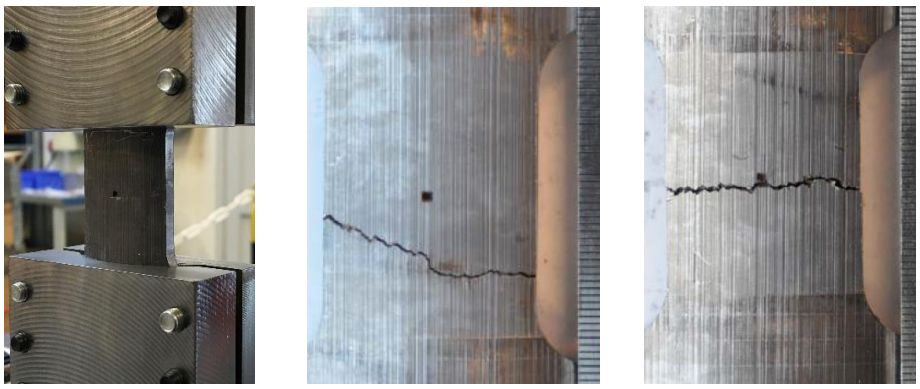

a) b) c)

Figure 4.1.5. The pictures show the sample in the custom-made, curved clamping system (a), two different crack paths on notched samples (b, c).

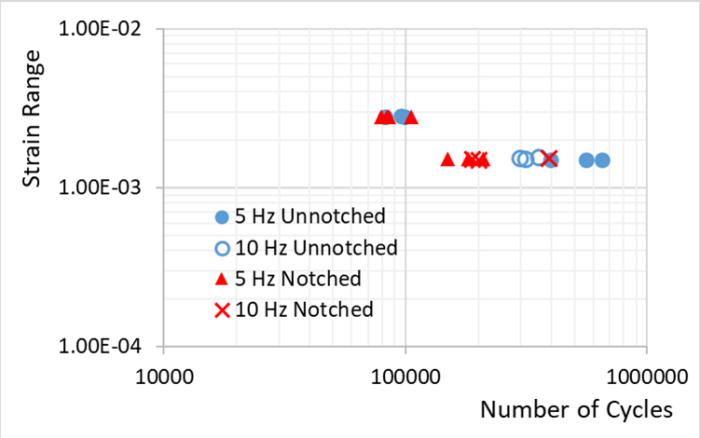

Figure 4.1.6. Summary of the fatigue testing results obtained by Johanson et al. [13]. Number of cycles to resistance drop to 200 N in the tensile phase of the cycle.

4.1.5 DIC Strain-Life results synthesis

The second batch of fatigue tests was performed at 5 and 10 Hz at a nominal strain range of 0.15 % following the same procedure and adopting the same equipment used for the first batch and having one notched sample for each testing frequency. In addition, these tests were recorded by a Prosilica GC 2450 digital camera to reconstruct the strain field on the specimens' convex surfaces by DIC post-processing, executed with the software eCorr. Being the acquisition rate of the camera limited to 10 Hz and due to limitations of the DIC software, it was not possible to either reconstruct the strain evolution within one single cycle or to record the points of maximum positive and negative strain. Therefore an acquisition period slightly longer than the fatigue cycle period was adopted and an equivalent strain cycle in DIC was obtained out of 40 real fatigue cycles: one image for each real cycle, but each at an higher angular position than in the previous one. Due to the huge amount of data the images were not captured during the whole test, but only at selected intervals. Following this procedure it was possible to compute the strain range in selected areas on the specimen's surface and adopt it as failure parameter. The crack initiation has been observed by means of visual imaging. The first initiation phase however has not been detected due to the discrete acquisition time frame during the tests. On the other hand it was possible to observe the moment before and after the onset of the crack growth. This has allowed to define, at least, an upper and lower threshold for crack initiation. The effective von Mises strain range was computed by the DIC post-processor and correlated to the crack initiation upper and lower threshold. These values where extracted from the crack initiation sites, Figure 7, and plotted in Figure 8. The software eCorr allows to directly compute the equivalent von Mises strain at the surface of the material, that is:

$$\varepsilon_{eff} = \sqrt{\frac{2}{3}(\varepsilon_1^2 + \varepsilon_2^2 + \varepsilon_3^2)} \quad (1)$$

In order to execute this calculus it is necessary to have an approximation of the third principal strain. Assuming negligible elastic strains and incompressible plasticity, approximation feasible due to the highly plastic behaviour of the alloy, this is equal to:

$$\varepsilon_3 = -(\varepsilon_1 + \varepsilon_2) \quad (2)$$

Equations 1 and 2 are reported from the software theory guide [15]. The values obtained following the described procedure on the second batch, Figure 8, are in line with the results obtained from the first batch, Figure 6, being slightly more conservative. In this case, contrarily to what had happened for the samples in the first batch, the notched sample tested at a frequency of 10 Hz presented cracks originating also from the notch, while the specimen tested at a frequency of 5 Hz did not present any cracking at the notch. The different behaviour could be due to an enhanced notch sensitivity of the material at higher strain rates, but other cracks were contemporarily generated also from other areas of the same sample subjected to a much smaller theoretical stress concentration factor, i.e. the fillet radius.

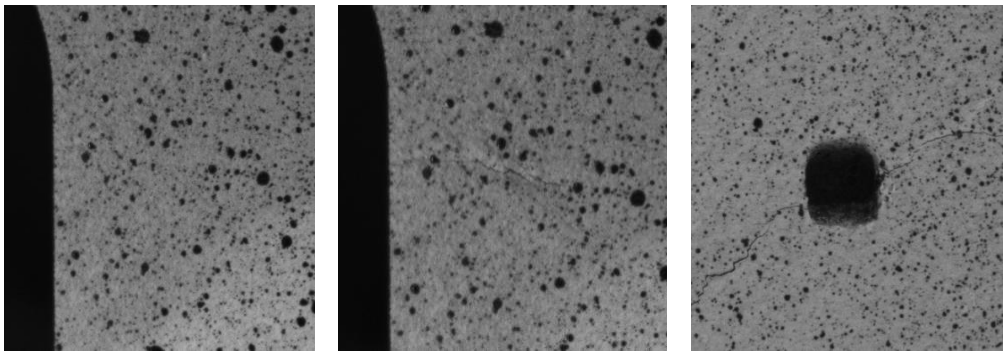

a) b) c)

Figure 4.1.7. DIC images of a sample before (a) and after (b) crack initiation in the proximity of the fillet radius. Cracks developing from the notch (c).

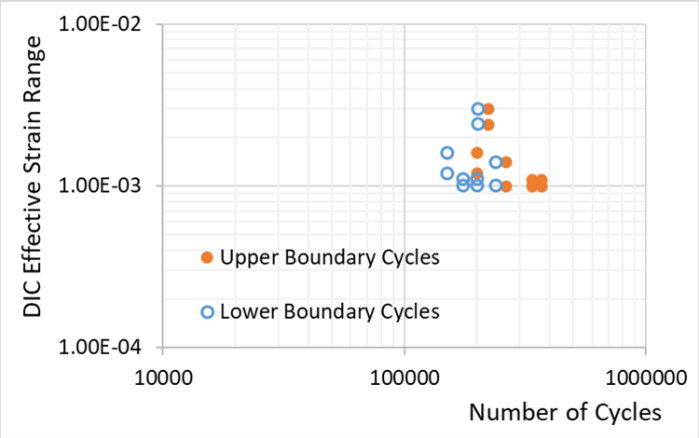

Figure 4.1.8. Summary of the strain range detected by DIC in the crack initiation sites. The number of cycles is to crack initiation and the lower and upper boundary cycles are the cycles of the DIC window immediately before and after the crack initiation.

4.1.6 Second batch failure analysis

The fracture surfaces of the samples tested in the second batch and recorded for DIC post-processing, were investigated in a scanning electron microscope. Figure 9 shows the crack initiation and propagation from the specimen surface orthogonal to the radial direction, being the radial direction the direction from the curvature axis of the specimen to the specimen's surface, while figure 10 shows the grain de-cohesion caused by the final plastic tearing. Although not clear from the SEM images, the cracks have propagated through the thickness of the specimen along a plane with an inclination of approximately 45º from the loading direction, so in the maximum shear plane, Figure 11. From this observation is deduced that the crack propagation in an alloy characterized by the described elastic-plastic properties in the case of fully reversed loading strongly depends on mode II propagation, in contrast with the effect that a similar load has on an alloy for which the assumptions of linear elastic fracture mechanics are valid, for which the crack propagation is mode I dominated. Figures 12 and 13 show the striations left on the fracture surface during the crack propagation and after the final plastic failure. In particular several secondary cracks are visible. In fact, what was observed in the failed specimens was not a single catastrophic crack, but rather a diffused damage interesting several areas in which the cohesion between the grains is diminished, due to the influence of creep damage on the failure mechanism. The observation of the pronounced strain-rate sensitivity on the tensile behaviour of the alloy, the kind of fatigue damage produced and the differentiation of the fatigue life obtained by a change of the testing frequency, particularly in the case of the un-notched samples tested at a nominal strain range of 0.15 %, indicate that the material is subjected to creep-fatigue interaction damage.

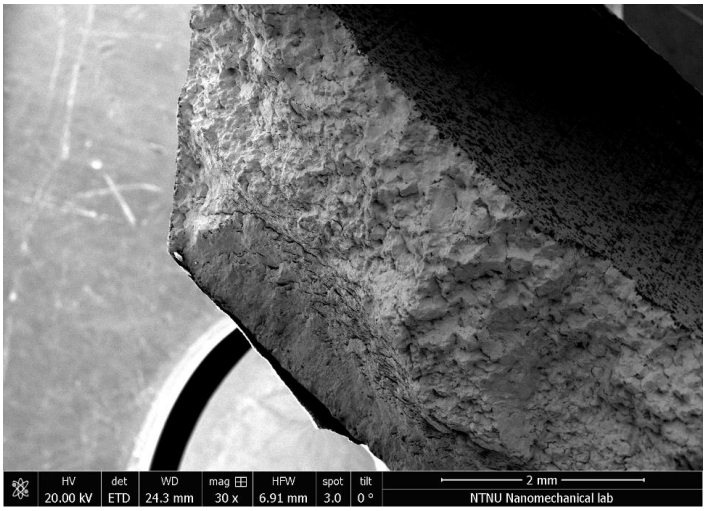

Figure 4.1.9. Crack initiation, propagation and plastic fracture on a specimen tested at 5 Hz and at a strain range of 0.15 %.

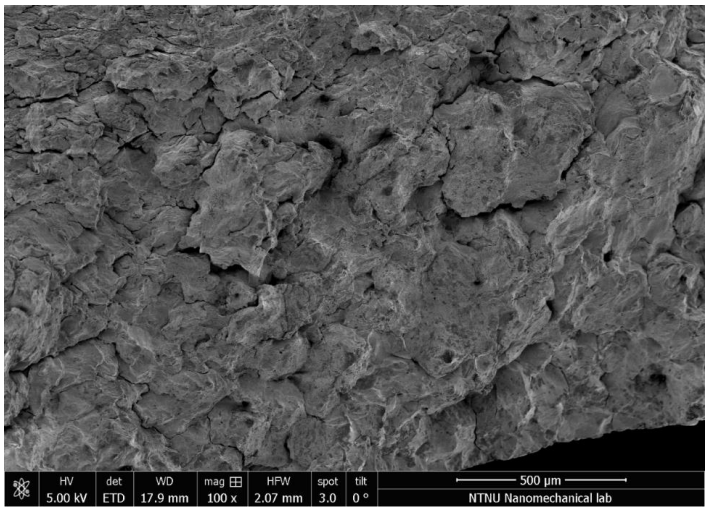

Figure 4.1.10. Grain de-cohesion at the final plastic fracture on a specimen tested at 10 Hz and at a strain range of 0.15 %. The fracture location both for the present figure and for the previous fig. 9 is analogous to the one presented in fig. 7b.

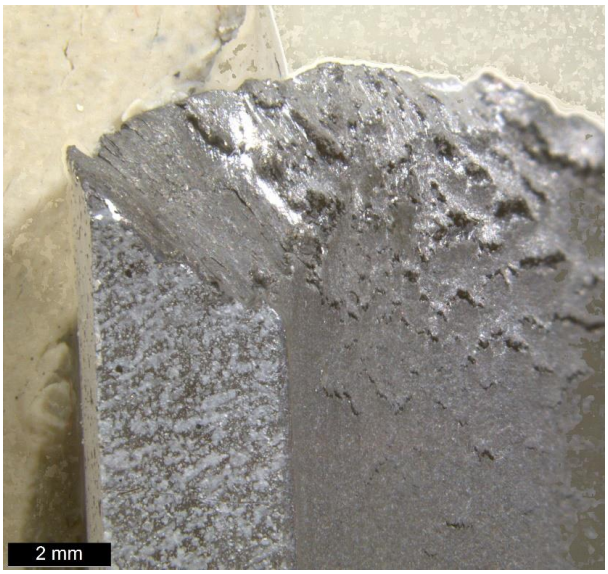

Figure 4.1.11. Side view of a failed specimen. The shear crack propagation, the multitude of diffused secondary cracks and the final plastic tearing executed at the end of the test are distinguishable.

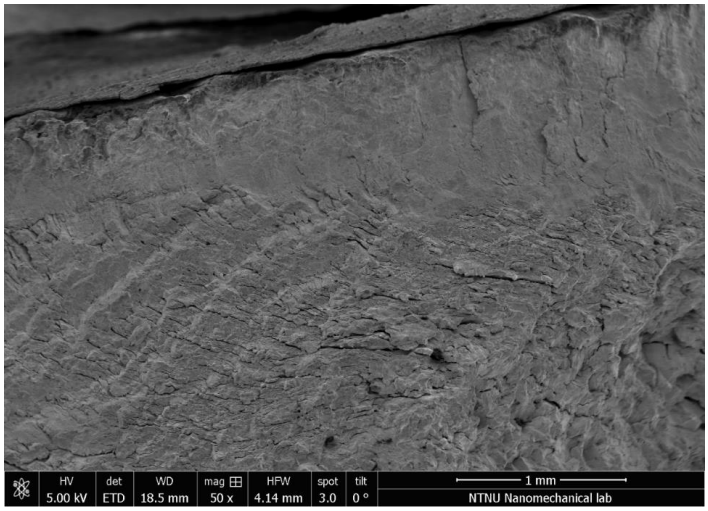

Figure 4.1.12. Crack initiation and propagation on a specimen tested at 10 Hz and at a strain range of 0.15 %. On the upper surface, the layer of paint for DIC can be seen.

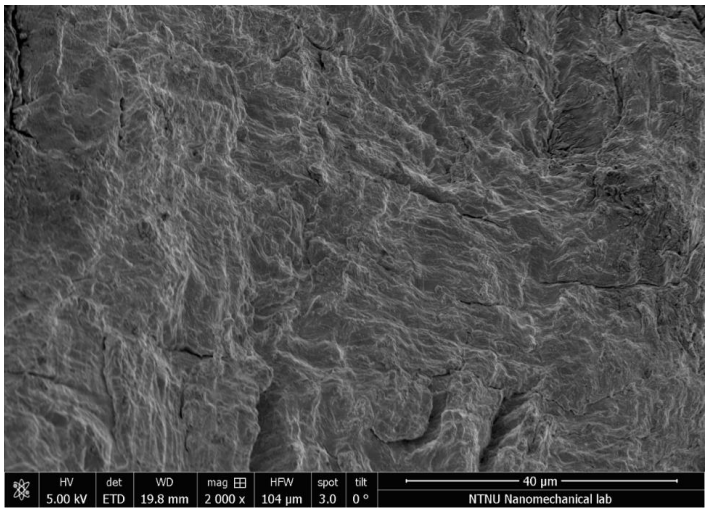

Figure 4.1.13. Crack propagation striations on a specimen tested at 10 Hz and at a strain range of 0.15 %. Secondary cracking can be observed.

4.1.7 Conclusions

The present work summarizes the results of static and fatigue testing performed on a number of Pb-Sn-Cd lead alloy specimen, material used in the production of sub-sea power-cable sheathing. The testing was performed in displacement control at two strain ranges and two frequencies. Due to the presence of defects in the components after the extrusion process, a blind notch was machined in part of the specimens. Some of the tests have been recorded by a digital camera for obtaining an approximation of the real strain field with DIC post-processing. The fractures of these samples were then investigated in SEM. The results obtained demonstrate how the highly plastic behavior of the alloy tested yields to a minimal notch sensitivity, with fatigue cracks starting from other location at a much inferior geometrical stress concentration factor. That is, the presence of small defects in the cable sheathing, although to be avoided, does not constitute a high threat to the structural integrity of the same. The propagation of the fatigue cracks at an angle of 45º from the loading direction, that is along the maximum shear plane, means that the propagation of a fatigue crack in a plastic material in fully reversed load is strongly influenced by mode II fracture propagation.

Acknowledgements

The present work was financed by Nexans Norway AS and the Research Council of Norway (IPN in ENERGIX Project number 256367) and performed within the project: Next-generation damage based fatigue of cable sheating (REFACE).

References

[1] M.E. Kassner. Fundamentals of Creep in Materials (Third Edition). Butterworth-Heinemann, ISBN 9780080994277. 2015.
[2] P. Feltham. On the Mechanism of High-Temperature Creep in Metals with Special Reference to Polycristalline Lead. Proc Phys Soc. 69,12-B. 1956.
[3] D.G. Harvard. Fatigue of Lead Cable-Sheathing Alloys. Ontario Hydro research. 1972.
[4] M.K. Sahota, J.R. Riddington. Compressive creep properties of lead alloys. Materials and Design. 21: 159-167. 2000.
[5] C.W. Dollins, C.E. Betzer. Creep Fracture and Bending of Lead and Lead Alloy Cable Sheathing. Engineering experiment station bulletin 440. 1956.
[6] P. Anelli, F. Donazzi, W.G. Lawson. The fatigue life of lead alloy E as a sheathing material for submarine power cables. Societa' cavi Pirelli, pp. 86 SM 393-3. 1986.
[7] H.L.J. Pang, Y.P. Wang, X.Q. Shi and Z.P. Wang. Sensitivity study of temperature and strain rate dependent properties on solder joint fatigue life. Proceedings of 2nd Electronics Packaging Technology Conference (Cat. No.98EX235), pp. 184-189. 1998.
[8] P. Lall, D. Zhang, V. Yadav, D. Locker. High Strain-Rate Constitutive Behavior of SACI05 and SAC305 Lead-free Solder. IEEE. 2015.
[9] M. Motalab, Z. Cai, J.C. Suhling, P. Lall, Determination of Anand constants for SAC solders using stress-strain or creep data. 13th InterSociety Conference on Thermal and Thermomechanical Phenomena in Electronic Systems, San Diego, CA, pp. 910. 2012.
[10] A. Farghalli, Mohamed, Terence G. Langdon. The transition from dislocation climb to viscous glide in creep of solid solution alloys. Acta Metallurgica, Volume 22, Issue 6, pp. 779-788, ISSN 0001-6160. 1974.
[11] M.E. Kassner. Five-power-law creep in single phase metals and alloys. Oxford: Pergamon. 2000.
[12] L.M. Viespoli, A. Johanson, A. Alvaro, B. Nyhus, A. Sommacal, F. Berto. Tensile characterization of a lead alloy: creep induced strain rate sensitivity. Materials Science and Engineering: A, Volume 744, pp. 365-375. 2019.
[13] A. Johanson, L.M. Viespoli, B. Nyhus, A. Alvaro, F. Berto. Experimental and numerical investigation of strain distribution of notched lead fatigue test specimen. MATEC Web Conf. 165 05003. 2018.
[14] R. Negru, D.A. Șerban, L. Marșavina, A. Magda. Lifetime prediction in medium-cycle fatigue regime of notched specimens. Theoretical and Applied Fracture Mechanics. Volume 84, Pages 140-148. 2016.
[15] http://folk.ntnu.no/egilf/ecorr/doc/definitions/strain/logstrains.html

4.2 Paper VII

Experimental and numerical investigation of strain distribution of notched lead fatigue test specimen

Audun Johanson1,*, Luigi Mario Viespoli2, Bård Nyhus3, Antonio Alvaro3 and Filippo Berto2

1Nexans Norway, Innspurten 9, 0663 Oslo, Norway
2Department of Mechanical and Industrial Engineering, Norwegian University of Science and Technology (NTNU), Norway
3Sintef Materials and Chemistry, Richard Birkelands vei 2B, 7031, Trondheim, NORWAY

Abstract. The work here presented focuses on the test methodology related to effect of stress concentrators in strain controlled structures. Cable sheathing as used in subsea power cables are investigated by cyclic fatigue testing, Digital Image Correlation (DIC) and 3D Finite Element Analysis. Focus is put on the strain distribution in conventional specimen geometries and under the presence of artificial notches. It is evident that standardized fatigue testing provides limited input to the final fatigue life of strain controlled power cable sheathing- taken into account both intended and unintended stress concentrators. The limitations can be explained by measured strain distribution inherent in most fatigue test specimens. The use of DIC and 3D FEM provides valuable insight into both the theoretical and practical stress and strain distribution. This can help in understanding and overcoming geometrical test constraints, when compared to the actual component loading mode.

4.2.1 Background and Scope

Lead alloys sheathing is used as water barrier on high voltage subsea power cable. Subsea power cables are subjected to various cyclic loads during manufacturing, installation and operation. Cyclic loading of cable sheathing falls in the typical high cycle regime, but under global strain control in combination with non-linear and time dependent material response.
Cable sheathing design and manufacturing is associated with multiple discontinuities which intensify the local stress and strain field. Such discontinuities might be inherent design features such as intimate contact with various strips such as transversal steel armouring, or local defects associated with the sheathing extrusion process such as indigenous oxides or intermetallic, or exogenous particles. Studies of such effects and fatigue properties of power cable sheathing is limited and rarely provide suitable input

for fatigue life calculations of power cable sheathing where appropriate loading mode and design features are taken into account [1]. Discontinuities in components subjected to mechanical loading will cause concentration(s) in the local stress and strain field and shorten the fatigue life of the component. Such effect is dependent on the material in question, particularly inelastic and relaxation properties as well as work hardening. These are associated with lead alloys [2]. Otherwise said, both the monotonic and the cyclic behaviour of lead alloys exhibit a significant strain rate dependence. Effects of discontinuities are therefore not equivalent at any strain rate. Usually lab scale testing regarding such effects are often done by implementing a well-defined notch detail on the test specimen. Due to the aforementioned material characteristic behaviour, the interpretation of results thereof is non-trivial as the component loading mode with respect to the detail-of-interest is not necessarily reproduced in smaller scale. Additional complications arise from the fact that the lab specimens geometry introduce deformation incompatibility zones, such as specimen edges and fillet radiuses, that do not exist for the real component which put into question the direct lab testing results transferability to the real component case. In this case, both the distribution of strain and strain rate must be carefully accounted for to ensure the suitability of the lab scale results. The following work aims to investigate the strain distribution and fatigue failure of notched test specimens extracted from cable sheathing.

4.2.2 Material and experimental procedure

4.2.2.1 Materials

The test material is extracted from as- manufactured power cable where the tubular lead sheathing was extruded from raw material according to PB012K in EN 12548. The chemical composition is reported in Table 4.2.1. The procedure has been adopted to account for the presence of the defect in the lab specimen. A 0.5 x 0.5 x 0.4 sheathing thickness notch was made by electro discharge machining (EDM) on the convex surface of the curved specimen (Figure 4.2.1). The design of the notch/discontinuity has been made based on a potential surface penetrating inclusion originating from the extrusion process. Due to the small thickness of the sheathing (3.3 mm), the sheathing curvature in the transversal section has been kept for later fatigue testing in order to prevent buckling in the compressive phase and thus increase the maximum achievable strain range, as well as limiting the induced work hardening when preparing the sample (Figure 4.2.2).

Element	Sn	Ca
Weight %	0.175- 0.225	0.60- 0.90

Table 4.2.1 Chemical composition of lead alloy PB012K.Setting Word's margins.

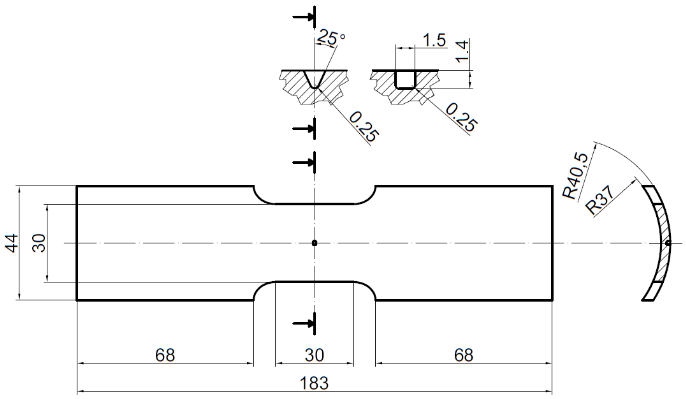

Fig. 4.2.1 Nominal dimensions of the specimens and of the notch detail.

Fig. 4.2.2. The pictures show the sample un-notched (left), notched (middle) and in the custom-made, curved clamping system (right).

4.2.2.2 Fatigue test procedure

The effect of the discontinuity has been investigated by comparing cyclic tension-compression fatigue testing directed towards reversed bending of a power cables.
The tests have been run in position control, moving the head between two set points, which have been related to the strain range target values (0.15 or 0.28%) prior to the test controlled by a mechanical extensimeter. The extensometer was removed after the set-

point definition due to sample indents (which where polished away). The recorded positions obtained before each test, in average corresponded to 0.008 and 0.0041 mm for a strain of 0.28 and 0.15%, respectively, has been kept constant during the complete the test duration. An appreciable decrease in the nominal amplitude was found for notched specimens Figure 4.2.3, suggesting the presence of the notch affects the global response of the specimen.

For two of the tests at higher strain amplitude, the extensometer was applied on both sides of the specimen in order to verify whether or not an out-of-plane deformation occurred. The fatigue tests were performed following a frequency stepping up (0.5, 1, 2 and then 5 or 10 Hz, according to the target frequency). During the test, load and displacement were recorded every 100 cycles and the number of cycles to failure was considered at the moment in which the tensile load fell below 0.2 kN, This was the highest lad value at which a through-thickness growing crack was visually detectable.

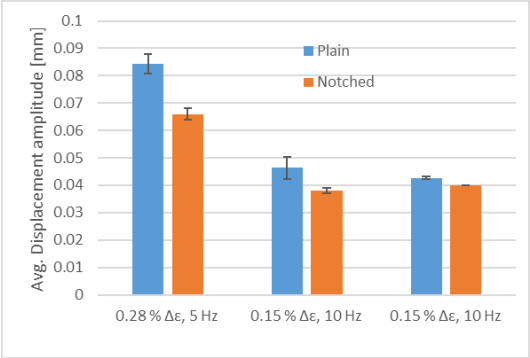

Fig. 4.2.3 Average displacement amplitude for plain and notched specimens.

4.2.2.3 Strain rate dependency

Creep and relaxation will cause a strain rate dependency of the test material. Fatigue testing will be conducted at frequencies exceeding the DIC acquisition rate meaning that a lower testing strain rate must be chosen for this work. A series of tensile tests at various strain rates were conducted to identify the onset of appreciable strain rate dependency and thereby a common material law for finite element modelling. Tensile test where performed on dog- bone specimens (Figure 4.2.4).

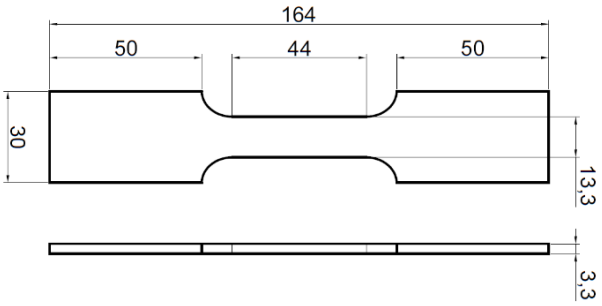

Fig. 4.2.4 Geometry of flat dog- bone tensile specimens.

The Stress-Strain curves obtained are shown in Figure 4.2.5. It is evident how, for strain rates higher than 10^{-4} s^{-1}, the effect of creep at room temperature is negligible, especially in the range of interest for the fatigue testing (up to 0.28% of nominal strain). Subsequently, the DIC material characterization on the flat dog-bone samples in Figure 4.2.4 and the DIC analysis on the curved samples in , have been performed at a nominal strain rate of 10^{-3} s^{-1}.

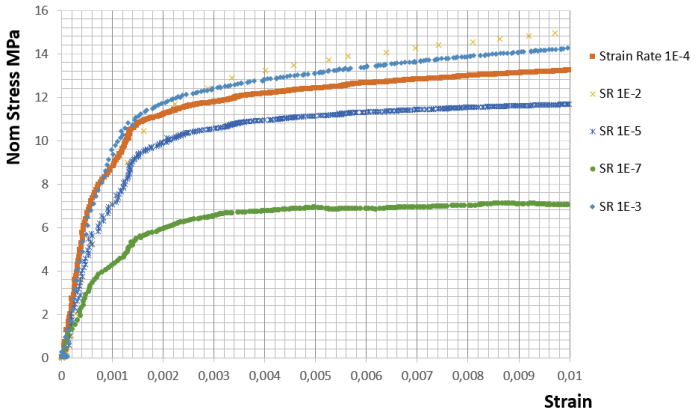

Fig. 4.2.5 Nominal Stress vs Strain curves for tensile dog-bone samples of lead alloy at different nominal strain rates. At a rate higher than 10^{-4} s^{-1} the creeping effects are negligible within the cyclic strain range to-be investigated.

The stress distribution in the specimen during the fatigue testing in relation to the failure location and final fatigue life from the fatigue testing, is investigated by finite element analysis, where monotonic tensile testing under Digital Image Correlation (DIC) is used to validate the calculated strain distribution. Speckle pattern where applied on both flat dog-bone specimens and curved dog-bone specimens (Figure 4.2.6) which were tested in a servo-hydraulic Zwick machine. A nominal strain rate of $1e^{-3}$ where applied which assumes to constitute the lower bound strain rate below which relaxation/ creep effects

takes effect; in other words, above such strain rate value the material strain rate sensitivity is negligible.

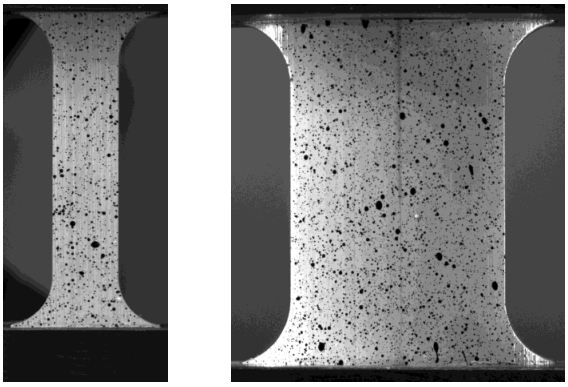

Fig. 4.2.6 A frame of the DIC images acquired for the flat tensile dog-bone (left) and of the curved specimen, un-notched, of the same geometry used for the fatigue testing (right).

4.2.3 Experimental results

The test results are summarized in the plot in Figure 4.2.7. Result at the higher strain range, i.e. 0.28% show practically no difference in terms of fatigue life due to the presence of the notch. For the test performed at 0.15% and 5Hz, the presence of the notch infers a decrease in the average fatigue life of about 65%, i.e. from an average value of 536,000 cycles to 181,000 cycles. However, by stepping up the frequency from 5 to 10 Hz, the detrimental effect induced by the presence of the notch seems to be reduced as in fact is rather the average fatigue life of the un-notched specimens to drop of about 40%, from 536,000 to an average of 323,000 cycles. No significant difference is found for the notched specimens.

Post-mortem analysis of the specimens also reveals a difference when it comes to the crack location. In 7/ 9 un-notched specimens the crack initiated from the specimen fillet radius, 8/ 10 notched specimens failed by the crack initiating from the outer edge, but in correspondence of the notch height/ location. Note that 2/ 3 unnotched 0.28 % strain range samples failed from the middle edge position. i.e. the trend more evident for the 0.15 % strain range samples. This indicates that the presence of the notch induces a variation in the stress/strain field strong enough to alter the position of the initiation point but still the specimen edge constitutes the "weakest" point when it comes to either crack initiation or crack- initiation and growth. The investigation of this effect and the primary aim for continued DIC and FEM analysis reported in the following paragraphs. The strain distribution in the different regions of the specimen (Figure 4.2.8) together with the resulting stress-strain plot obtained through post-processing of the DIC images. Tensile

testing under DIC has permitted to record the true Stress-Strain characteristic of the alloy. This provides the material constitutive behaviour for the elastic-plastic FEM analysis on both the un-notched and the notched sample.

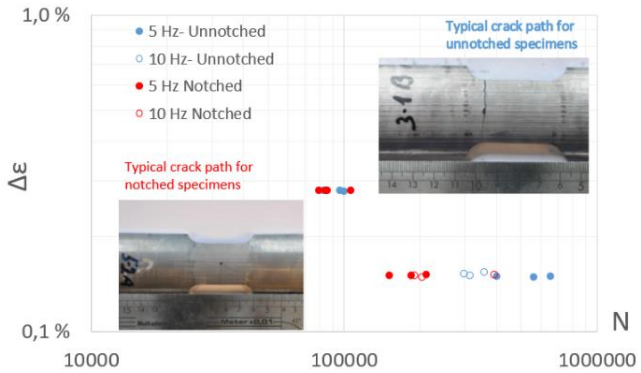

Fig. 4.2.7 Fatigue test results and representation of the typical failure modes.

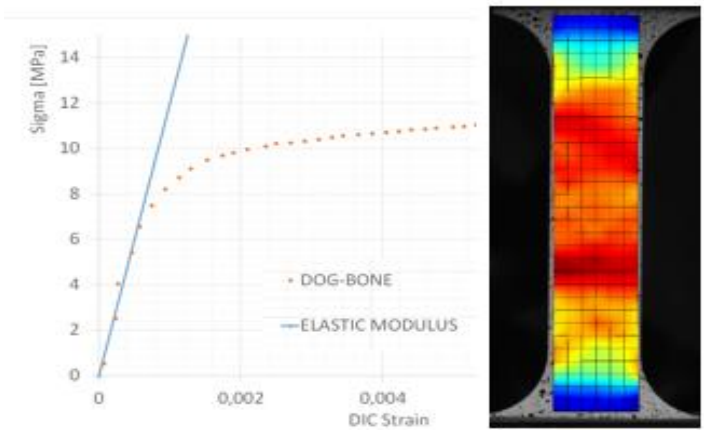

Fig. 4.2.8. Obtained tensile curve and strain distribution as acquired by DIC.

4.2.4 Finite element analysis

The aim of the analysis is to give basis for a better understanding of the influence of the notch on the failure dynamics and to eventually reproduce numerically the behavior of the alloy. The comparison between the DIC and FEM analysis is executed at the same nominal/global strain, i.e. measured from the displacement of the boundary divided by the free length in the FEM analysis. For the test, the real border effects and eventual deformation of the sample close to the clamping area does not allow precise strain estimation. Therefore, the nominal strain is obtained from DIC on a vector which covers

the full length of the sample. The evaluation of the equivalent nominal strain is then made by considering the FEM analysis. The results obtained show, at the same equivalent loading condition and in the same scale, that the FEM analysis is feasible to reproduce the strain field in magnitude and shape, with a concentration of the strain for the un-notched sample in correspondence of the fillet radius and the clamping area. The results of the FEM analysis on the notched geometry (Figure 4.2.9, Figure 4.2.10), shows a much higher strain, at comparable equivalent boundary displacement, which justifies the final fracture passing through the notch, but there is no evidence from the numerical stress field of the reason why fatigue fractures in the notched specimens have been observed to initiate on the edge of the sample, at the height of the notch, but not from the notch itself.

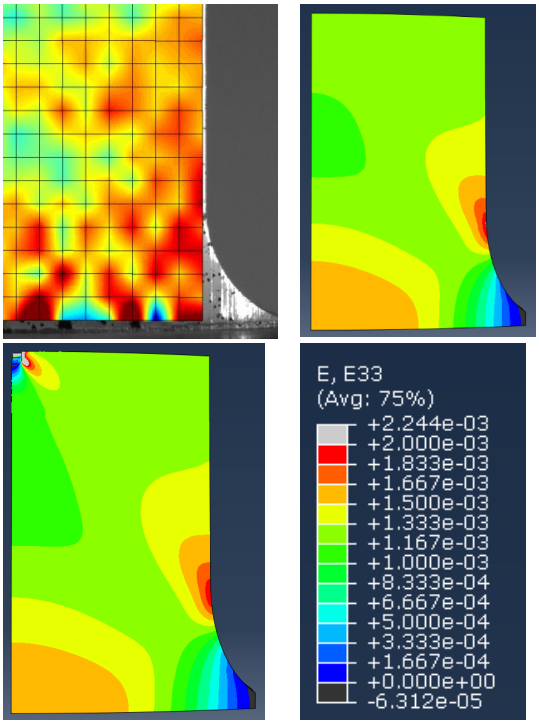

Fig. 4.2.9. Strain field along the longitudinal direction of a quarter of the un-notched specimen, DIC (upper left) and FEM (upper right). In figure (lower right), the same strain field for the notched specimen. The scale adopted for the strain is the same for all captures (lower left). All strain fields correspond to a nominal strain of $1.1e^{-3}$.

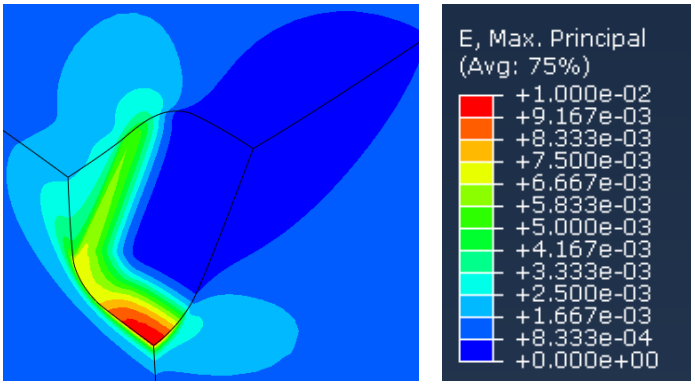

Fig. 4.2.10. Maximum principal strain in the area of the notch, at the same nominal strain of the captures in Figure 4.2.9. The scale shows an important strain intensification due to the notch.

4.2.5 Conclusion and further work

It is evident from the fatigue test results that the impact of the notch is higher for low strain ranges. This relation appears to be dependent on test frequency. However, the imposed test frequencies imply a strain rate exceeding appreciable creep. Understanding of the impact of frequency, particularly taking in account the expected fatigue life reduction due to creep is critical and the subject of ongoing work.

Location of failure initiation also supports a different effect of the notch for the two tested strain range levels, where high cyclic strain range fail from the middle region of the test specimens both with and without a notch. For lower cyclic strain range, failure only occur in the middle region when the notch is present. The Numerical calculations and tensile test experiments under DIC show that the strain concentration on specimen fillets is significantly higher than the nominal strain range and supports failure from this location. Numerical calculations show that the notched detail is associated with the highest strain concentration which justifies both the reduction in fatigue life and change in failure location. However, as the final crack do not tend to initiate at notch and the test results appear inconsistent with the analysis. As the lead alloy is expected to undergo irreversible deformation at the imposed strain ranges, hardening and local blunting can be mechanisms that cause re-distribution of the strain and differentiates the monotonic and cyclic strain fields- thus explains a change in failure initiation. However: no evidence of blunting or major changes of the notch geometry is observed. Regardless, the material law used in the numerical study as well as the DIC strain is obtained from monotonic cases. The cyclic material response will differ. Ongoing work is put into the development of a dynamic material law and in obtaining the DIC recording to have a quantification of the strain distribution variation and development during the actual fatigue test. The inconsistently between local strain concentration and failure initiation can also be related

to the crack initiation and growth dynamics- meaning that the strain field must not only favour crack initiation but continued growth.
Finally, it should be noted that failure initiation from the specimen edge is a test artefact with respect to the final application as such details are absent for tubular components. Crack initiation from the sample edge indicates that even if the relative effect of a notched- unnotched component is larger than for the notched -unnotched test specimen, the laboratory scale fatigue test result for both notched and unnotched samples are conservative compared to the real component. Despite of this, care should be taken in assessing fatigue life ductile components such as power cable sheathing, by standardized testing.
The work supports the use of numerical calculations coupled with experimental validations using DIC to both interpret fatigue results and design fatigue test specimens. This is critical for accurate fatigue life predications of component subjected to cyclic loading- particularly in the presence of local details and strain distribution.

Acknowledgment

The authors wish to thank the NEXANS Norge as and Research Council of Norway for the financial support through ENERGIX Programme, Contract No.256367/E20.

References

1. International Lead Zinc Research Organization, Inc. (ILZRO), *"Program on Technology Innovation: Grain Growthin Lead Alloy Sheathin and its Influence on the Life of Lead- Sheathed Power Cables,"* EPRI, Palo Alto, Ca, (2007).
2. S. Guruswamy, *Engineering Properties and Applications of Lead Alloys*, New York: Marcel Dekker, (2000).

Chapter 5: Component modelling

This chapter investigates the impact of the cable's layout, in particular of the steel tape armouring winded around the sheathing on the stress state of this component under different loads. The analysis if performed through finite element modelling and the results discussed in light of the data provided in Chapter III.

5.1 Paper VIII

Tape winding angle influence on subsea cable sheathing fatigue performance

Luigi Mario Viespoli[1*], Luigi Panza[1-2], Audun Johanson[3], Antonio Alvaro[1-4], Aurelio Somà[2], Filippo Berto[1]

[1]*Department of Mechanical and Industrial Engineering, Norwegian University of Science and Technology (NTNU), Richard Birkelands vei 2B, 2034, Trondheim, Norway*
[2]*Dipartimento di Ingegneria Meccanica e Aerospaziale, Politecnico di Torino, Italy*
[3]*Nexans Norway, Innspurten 9, 0663 Oslo, Norway*
[4]*Sintef Industry, Richard Birkelands vei 2B, 7031, Trondheim, NORWAY*

*luigi.m.viespoli@ntnu.no

Abstract: A fundamental component of subsea power cables is the thin galvanized steel tape winded around the dielectric and sheathing layer in order to prevent permanent thermal cycling induced deformation. The pressure state induced by the resistance offered by such tapes against radial reformation reduces the triaxiality ratio of the stress state of the lead sheathing layer. It is known that a reduced triaxiality has a beneficial effect on ductility and fatigue life of metals. In the present work a series of finite element simulations are performed in presence of galvanized steel tapes at three different winding angles and without such reinforcement at all, obtaining a qualitative indication of its effect on the stress state induced in the sheathing layer. Loading conditions as internal pressure related to thermal dielectric expansion and cable bending are modelled. The numerical qualitative results are discussed in connection to a series of full-scale fatigue tests performed on subsea power cables with and without the support of steel tapes.

Keywords: subsea power cable, viscous deformation, fatigue, triaxiality factor, lead alloy

5.1.1 Introduction

The fatigue behavior of subsea high voltage cable sheathing, produced by extrusion of lead alloys, is affected by the design of the cable and by time dependent deformation and damage mechanisms. The operational temperature for the sheathing layer lies around room temperature or slightly above. The low melting point characterizing the lead alloys industrially adopted for the production of this component is generally inferior to 600 K, barely twice as much as the operational temperature.

Being the use of lead alloys as extrusion material for cable sheathing a specialized topic, often laying in the boundaries of the industrial secrecy and a relatively old technology, the amount of available literature regarding the subject is limited and most of it was produced several decades ago. An investigation on creep behaviour of cable sheathing lead alloys was published by the University of Illinois evidencing, at three different temperatures, time dependent deformation even for very low stresses and a marked effect of pulling speed on tensile resistance [1] and the effect of alloying elements, thermal treatments and cyclic loading [2]. The creep behaviour of polycrystalline lead and the influence of mean grain diameter was investigated by Feltham [3], while the fatigue properties of some alloys of interest for the cable industry was published by Havard [4]. Testing on the topic of fatigue life of lead alloys for subsea power cables was performed by Società Cavi Pirelli [5] while Sahota and Riddington investigated the response to compressive loads for various lead alloys [6].
In the recent years, the industrial will to obtain a deeper understanding of the materials used in production and optimize alloys and design for economic and environmental purposes has led to a new series of investigations with modern techniques. The studies performed regarded the tensile behaviour and microstructure [7], influence of production defects on fatigue life [8,9], steady state creep [10] and fatigue results of full-scale testing [11].
Research papers focused on the FEM analysis of subsea power cables are not numerous, especially for what regards the mechanical aspect. Some interesting contributions are the works of Huang et al. [12,13].
The present work utilizes the material properties obtained in the tensile testing and the creep model calibrated with such testing [7] to perform a qualitative numerical investigation on the influence of the compressive stresses introduced in the sheathing layer by the winding of tensioned steel tapes. The full-scale fatigue results [11] are discussed in light of the influence of stress triaxiality on the fatigue life of metallic alloys.

5.1.2 Short notes on triaxiality

Experimental evidence in creep-fatigue models and multi-axial fatigue conditions shows that a triaxial stress state influences the fatigue life of a ductile metal and such influence is accounted for in some failure models. For example, the Strain Range Partitioning (SRP) method applied under multi-axial conditions [14] uses the concept of Multiaxiality Factor (MF) for the assessment of the creep-fatigue damage. The same MF is used in the total equivalent strain range method modified by multiaxiality factor [15] for the evaluation of the fatigue life. In both theories, MF is defined as a function of the Triaxiality Factor (TF). TF is the ratio between the mean stress σ_m, representative of the hydrostatic state of material, and the Von Mises equivalent stress σ_{eq}, representative of the deviatoric state of material.

$$TF = \frac{\sigma_m}{\sigma_{eq}} \tag{5.1.1}$$

The Multiaxiality Factor is so defined [14]:

$$\begin{aligned} MF &= TF \qquad\qquad for\ TF \geq 1 \\ MF &= \frac{1}{(2-TF)} \qquad for\ TF \leq 1 \end{aligned} \tag{5.1.2}$$

For example, the strain-life equation of total equivalent strain range method modified by Multiaxiality Factor is: [15]

$$\Delta\varepsilon_{eq} = MF^{-b/c} B\left(N_f\right)^b + \frac{C}{MF}\left(N_f\right)^c \tag{5.1.3}$$

Where B, C, b and c are material constants. It's possible to observe that when MF > 1 the fatigue curve downshifts towards lower strain ranges, while when MF < 1 the fatigue curve shifts upwards. The same reasoning is valid for what concerns the SRP method under multiaxial conditions, where MF contributes to move the fatigue line influencing the creep damage by modifying the creep ductility.

5.1.3 Subsea cable fatigue scenarios and full-scale testing

Lead testing and fatigue performance appear to be particularly sensitive to loading mode and interaction with other components. As such it is necessary to validate the fatigue life by component of full-scale setting where the appropriate loading mode is reflected.
Fatigue and creep damage arise from multiple sources during the cable operational life. This includes bending due to wave motion during offshore installation or recovery operations, High frequency bending in the case of free-spans on the seabed, or slow frequency radial displacement under thermal fluctuation. We focus on testing by reversed bending to simulate the former scenarios. The lead sheathed power phase is axially load controlled while displaced in the parallel direction by shapers with fixed radius. A given shaper radius will induce a corresponding Δε in the lead sheath in relation to the lead sheath's diameter. Although the actual strain was not measured, the contact between the shaper and test object was visually controlled.
All testing was conducted at room temperature. Power phases with and without transversal armor where tested. The former corresponds to typical Mass Impregnated High Voltage Direct Current cable (MI HVDC), where the latter corresponds to Cross-linked Polyethylene (XLPE) power phases [11].

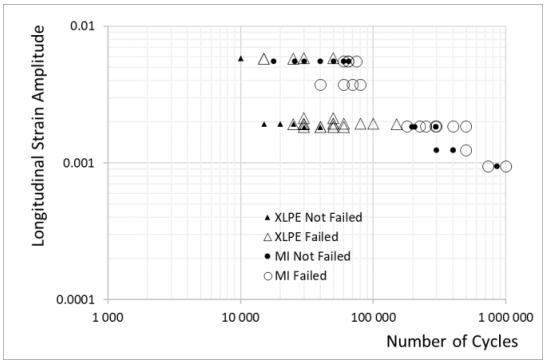

Figure 5.1.1. Full scale fatigue testing results. The MI cable have considerably better fatigue performance [11].

5.1.4 Cable modelling

5.1.4.1 Schematization of the cable

In order to better understand the results obtained in the full-scale testing campaign a series of numerical simulations were performed. A Nexans 525 kV Mass-impregnated (MI) HVDC subsea cable was chosen as model geometry for the simulation. The fifteen components of the cable are listed in table 1 and the multi-component finite element model was created by assembling a series of eight parts, listed in table 1 as A to H. This simplification of the structure severely reduces the computational costs and does not affect negatively the validity of the simulations results since the layers which are not modelled do not provide, due to the very small thickness, any mechanical resistance. Conductor, reinforcements, insulants and armours were modelled as continue bodies. The FE model corresponds to a cable length of 2 m, that is over the pitch length of the longitudinal armour.

Part	Components	Description	Material	t (mm)	Rint (mm)	Rext (mm)
A	1	Conductor	Copper			23.15
	2	Conductor screen	Carbon black paper tapes	0.4	23.15	23.55
B	3	Insulation	Impregnated paper tapes	20.15	23.55	43.7
	4	Insulation screen	Carbon black paper and metallized paper tapes			
	5	Serving	Copper woven fabric tape			44.6
C	6	Lead Sheath	E-Alloy	3.3	44.6	47.9
D	7	PE Sheath	PE	3.3	47.9	51.2
	8	Bedding	Semi conductive nylon tape			
E	9	Reinforcement	Galvanized Steel	0.8	51.2	52
	10	Bedding	Semi conductive nylon tape			
F	11	Armor wires	Galvanized Steel GR34	3	52	55
	12	Bedding	Plastic coated nylon tape			
G	13	Armor wires	Galvanized Steel GR34	3	55	58
	14	Bedding	Plastic coated polyester tape			
H	15	Outer Sheath	HDPE	6	58	64

Table 5.1.1. MI HVDC cable cross section component list and dimensions. Parts A to H correspond to the assembly components in the FE model.

Material properties

The material properties are chosen to model the assembly in a meaningful way, with the main focus on the rate dependent behaviour of the lead sheathing. Severe simplifications had to be made on some of the other component. However, since the scope of the work is to gain a better understanding of the qualitative influence of the reinforcement tapes and their configurations on the cable fatigue behaviour and these simplifications allow to perform the modelling efficiently with respect to the aforementioned objective. The

description of the material properties for each part included in the model is presented in this paragraph and the mechanical properties are the listed in tables 2,3 and 4.
The conductor (A) is made of very commercially pure copper and its mechanical behaviour was modelled as isotropic linear elastic material so that only two parameters are necessary: the elastic modulus and the Poisson's coefficient. These values can be easily found in the literature. On the other hand, modelling the individual strands helically wound is highly demanding from a computational point of view and not necessary for the scope of this analysis, which focused on the lead sheathing. Therefore, the coupling of the torsional and of the flexural behaviour in the two longitudinal planes due to the helical winding of the strands is neglected.
The insulation system (B) is a challenging component to model in a practical and realistic way since it requires several assumptions to be approximated by a simple assembly component. In mass impregnated cables, Kraft paper impregnated by high viscosity oil is used as main electrical insulation layer. Typically, the range of temperature experienced by the cable during the service is between the seabed temperature for the outer layer and 50 to 80ºC for the insulation [13], low enough to consider the oil always with high viscosity. The choice of the authors was to approximate it by a simple isotropic elastic component. Although the authors are aware that this constitutes a heavy approximation, the scope of the study is to investigate the influence of steel tapes winding angle on the lead sheathing layer. The insulation is then simply considered as a solid between the conductor and the external layers. [13] It is necessary to calculate an equivalent elastic modulus the B part from the constitutive components, the Kraft paper, the oil giving compression stiffness and the outer copper woven fabric tape. Such components are treated as parallel springs because subjected to the same curvature Γ caused by the bending load M_f.

$$k_{f,i} = E_i \, I_{f,i} \tag{5.1.4}$$

$$M_f = \Gamma \, k_{f,eq} = \Gamma \, \sum\left(E_i \, I_{f,i}\right) = \Gamma \, E_{eq} \, I_{f,eq} \tag{5.1.5}$$

$$E_{eq} = \frac{\sum\left(E_i \, I_{f,i}\right)}{I_{f,eq}} \tag{5.1.6}$$

Where $k_{f,i}, E_i, I_{f,i}$ are respectively the bending stiffness, the elastic modulus and the bending inertia of the single parts and $E_{eq}, I_{f,eq}$ are respectively the equivalent elastic modulus and the equivalent bending inertia of the system. The equivalent Poisson's ratio ν_{eq} was computed as a volume weighted average of the ratios of the components.

$$\nu_{eq} = \frac{\sum\left(\nu_i \, V_i\right)}{V_{eq}} \tag{5.1.7}$$

Where ν_i, V_i, V_{eq} are respectively the Poisson's coefficients, the volumes and equivalent volume of the parts included in computation.

The lead sheathing (C) was modelled using the strain hardening power law creep behaviour available in Abaqus. The properties were calibrated by tensile testing at different strain rates by Viespoli et al. [7]. The material is a lead alloy commercially known as E-Alloy, with the following chemical composition: Pb 99,3 wt%, Sb 0,2 wt%, Sn 0,5 wt%. The formulation of the model is reported for completeness:

$$\dot{\varepsilon}_{eq,cr} = \left\{A\ {\sigma_{eq,d}}^{n}\left[(m+1)\ \varepsilon_{eq,cr}\right]^{m}\right\}^{\frac{1}{m+1}} \qquad (5.1.8)$$

Where $\sigma_{eq,d}$ and $\varepsilon_{eq,cr}$ are the equivalent Von Mises stress and the equivalent creep strain respectively and A, m, n are material constants.

The polyethylene layer (D) is approximated by a simple elastic-plastic material model. The material properties implemented are provided by Nexans Norway and all effects of strain rate on the polymer's response are neglected.

The reinforcement (E) is constituted by galvanized steel tape winded over the component D and its influence is the fundamental object of study in this work. For optimizing the pre-processing and the computational time, the tape was modelled as a continuous body with orthotropic elastic properties, having the maximum stiffness, that is the stiffness of steel, along the winding direction and a stiffness several orders of magnitude lower in the other directions. The orthotropic elastic behaviour with transversely isotropic elasticity was chosen from the Abaqus library and, for its implementation, a cylindrical reference system was created for each orthotropic properties component and rotated accordingly to the winding direction.

Two layers of armour are introduced in these cables with the main purpose of providing axial strength for the cable to sustain its own weight during installation. The armour is made of galvanized steel wires with a thickness of 3 mm and was modelled as an orthotropic material in the same way adopted for the steel tapes. The maximum resistance direction corresponds to the wire axis and that is at an angle from the cable's longitudinal direction of 12.7º for the inner armour (F) and -10.5º for the outer armour (G).

The high-density polyethylene outer sheathing (H) is model, as for the component D, as an elastic-plastic isotropic continuum, neglecting the rate dependent effects, according to the data provided by the producer.

COMPONENT	INPUT DATA
Conductor	Type of material: Copper
	Elastic behaviour: E = 120000 MPa, ν=0.34
Insulation system	Type of material: Kraft paper, oil, copper tapes
	Elastic behaviour: E = 19340 MPa, ν=0.44
Lead sheath	Type of material: E-Alloy
	Elastic behaviour: E = 12000 MPa, ν = 0.431
	Plastic behaviour: see relative table
	Creep behaviour: A = 5.278e-10, m = -0.47, n = 5.22
PE sheath	Type of material: PE
	Elastic behaviour: E = 600 MPa, ν = 0.46
	Plastic behaviour: see relative table
Reinforcement	Type of material: galvanized steel tapes
	Winding angle: 70 degrees from the cable axis
	Orthotropic elastic behaviour: see relative table
Armour 1	Type of material: galvanized steel wires
	Winding angle: 12.7 degrees from the cable axis
	Orthotropic elastic behaviour: see relative table
Armour 2	Geometry, type of material: galvanized steel wires
	Winding angle: -10.5 degrees from the cable axis
	Orthotropic elastic behaviour: see relative table
Outer sheath	Type of material: HDPE
	Elastic behaviour: E = 780 MPa, ν = 0.46
	Plastic behaviour: see relative table

Table 5.1.2. Synthesis of the material properties implemented.

a)		b)		c)	
E (MPa)	12000	**E (MPa)**	600	**E (MPa)**	780
ν	0.431	**ν**	0.46	**ν**	0.46
ε_pl	**σ (MPa)**	**ε_pl**	**σ (MPa)**	**ε_pl**	**σ (MPa)**
0	7.4	0	2	0	10
0.000006	7.9	0.015	3	0.2	10
0.00013	8.45	0.023	4	0.5	10
0.00044	10.5	0.04	6	0.8	10
0.0008	11.6	0.09	7.5	1	10
0.00129	12.26	0.19	9	1.5	10
0.0024	13.15	0.29	9.5	1.7	10.5
0.0052	14.3	0.39	10	2	11.75
0.0088	15.25	0.49	10.5	3	14
0.0248	17.3	0.59	11	4	17
		0.69	11.5	5	20
		0.79	12.5		
		0.89	13		
		0.99	13.5		

Table 5.1.3. Elastic-plastic properties of: C component (a), D component (b), H component (c).

Orthotropic elastic behavior with transversely isotropic elasticity		
E1	2000	MPa
E2	2000	MPa
E3	200000	MPa
Nu12	0,3	
Nu13	0,003	
Nu23	0,003	
G12	769	MPa
G13	770	MPa
G23	770	MPa

Table 5.1.4. Elastic table for the armoring components (E, F, G). They are defined in their own reference system.

5.1.4.2 Meshing

Each component of the cable assembly was discretized using three-dimensional quadratic elements. After an initial phase of mesh size optimization, the following element dimensions were used for the analysis. In the longitudinal direction a characteristic element size of 20 mm was used, while in the tangential direction 24 elements around the circumference were used for components A and B, while 48 were used for components C to H to have a finer mesh for the thinner components. The radial discretization of A and B parts has 5 elements along the thickness, while all the other components have 2 elements along the thickness. These values have been verified to provide reliable results with respect to the required accuracy. A total of 78000 elements and 412389 nodes was generated, see figure 2.

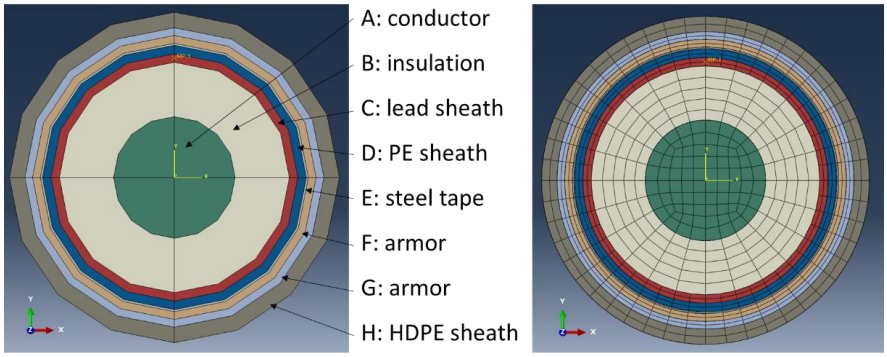

Figure 5.1.2. Abaqus assembly of parts A to H (Left). Cross section of FEM discretization with reference point RP-1 of extraction of the stress output for the lead sheathing (Right).

5.1.4.3 Boundary Conditions

Surface Interactions: Surface-based tie constraints were implemented as interactions between the various parts of the model. This kind of interaction constraints the surfaces linked to have the same displacement, thus separations and sliding are not allowed between the layers, hypothesis valid for most operational conditions when the static slipping resistance of the bedding layers is not exceeded. A manual attribution of the master and slave surface makes for a more efficient model solution. The nodes on the slave surface must have the same motion of the master surface nodes and the master surface should be stiffer than the slave master, thus, a stiffer material and coarser mesh are conditions for the choice of the master surface. Two tie formulations are available in Abaqus: the surface-to-surface formulation and the node-to-surface formulation. The surface-to-surface formulation generally avoids stress noise at tied interfaces. Moreover, with a surface-to-surface approach, there is less sensitivity to the choice of master and

slave surfaces. On the base of these considerations, such formulation was selected and the master/slave surfaces attributed as reported in table 5.

Interaction	**AB**	**BC**	**CD**	**DE**	**EF**	**FG**	**GH**
Master	A_ext	B_ext	C_ext	E_int	F_int	G_int	G_ext
Slave	B_int	C_int	D_int	D_ext	E_ext	F_Ext	H_int

Table 5.1.5. Master/slave surface attribution.

External Constraints: The cable was constrained at the two extremes. Depending on the scenario simulated these sections were either one fully constrained and the other allowed to translate longitudinally or longitudinal translation and rotation in a longitudinal cutting plane were allowed. Further details are provided in the load-cases paragraph.
Load cases: In the present study a series of different load cases and cable designs were implemented to evaluate the influence of the different parameters on the stress state of the lead sheathing. The load cases implemented are described in the following passages.

- *Pre-tensioning of the tape*

The application of the steel tapes on the underlying lead sheath with a certain pre-tensioning was simulated as a cooling of the E component. A typical thermal expansion coefficient of 3,5e-5 (1/K) for the steel was assumed, and a negative thermal excursion was simulated in order to obtain a pre-stress of about 200 MPa along the winding direction of the tape.

- *Sea water pressure*

A representative sea depth of 100 m, corresponding to and external pressure of 1 MPa, was chosen. This value causes a slight increase in the compressive state of the underlying layers, but no deviatoric stress.

- *Thermal expansion of the insulation system*

The insulation layer's thermal expansion due to Joule heating was modelled considering assumptions similar to previous works on the topic of subsea power cables. The initial temperature of submarine ambient is about 4 °C and, at regime conditions, the temperature at the interface between insulation system and lead sheath is around 50°C [13]. Only the heating of the B component was modelled because the thermal expansion coefficient of oil is considerably higher than that of the other components [*13*]. A typical value for the thermal expansion coefficient of the oil is 6.3E-4 1/K [16]. The oil occupies only a certain fraction of the insulation system. This fraction depends on the impregnation level and is defined as the ratio between the oil volume and the total insulation volume. This value is useful in order to compute a reasonable approximation of the thermal expansion coefficient of the assembly. Typical values are comprised by 0.3 to 0.7, but often is used 0.4 [16]. This value is multiplied by the thermal expansion coefficient of the oil to approximate the thermal expansion coefficient of the B component. The oil impregnated paper insulation is affected by the presence of cavities. While the layer heats up these cavities are filled by the oil until a threshold temperature, the cavity free

temperature, above which the insulation starts expanding and pressure builds up as a consequence of the presence of the layers above. A typical value of cavity free temperature is about 30°C [16]. Therefore, a reasonable thermal excursion to attribute for the thermal load modelling is about 20°C.

- *Cyclic bending*

Pure bending condition was assumed in order to analyze the bending behavior of the cable in the full-scale testing and due to the wave motion in the hypothesis of use as dynamic cable. The two extremes of the cable were rigidly rotated over time, keeping the cable at a constant curvature over its length. The amplitude of the rotations was defined as a sinusoidal wave with zero mean with 12 h period. Since the simulations were run both with and without the presence of creep deformation, this long period was chosen to obtain the sheathing's behavior for a high strain rate (corresponding to absence of creep deformation) and for a very low one (creep deformation included and 12 h period). The real response of the material to both the full-scale testing and to tidal motion will be in the middle of these extremes. A simulation time of 15 h was used, corresponding to 1.25 periods, starting from the undeformed position. The strain amplitude imposed at the level of the C component, of 0.001, was selected in order to be of the same order of magnitude of that full-scale testing. The maximum curvature Γ to impose to the cable to reach this value of deformation was computed following the theory of beams:

$$\Gamma = \frac{\varepsilon_{long}}{r_{ext}} = 1{,}25\ °/m$$

Where ε_{long} and r_{ext} are the maximum longitudinal total strains of the lead sheath.

5.1.4.4 FEM Cable designs

Three different winding angles, measured from the longitudinal direction, of the steel tapes were considered in order to verify the effect of this parameter on the stress state of the lead sheath. The winding angle was in practice modelled as a rotation of the coordinate system in which the orthotropic layer's properties are defined. A fourth design, that is a cable in which the tape is replaced by a PE sheathing, was also modelled. In summary, the four models are characterized as follows: 60º, 70º, 80º for the winding angle of the reinforcement and absence of the steel tapes.

5.1.5 Numerical results

The numerical modelling previously described was used to simulate two different scenarios:

- Pre-tensioning of the steel tapes and subsequent cyclic bending, condition equivalent to the testing procedure, in which the cable is not subjected to the internal heating and consequent expansion.

- Sea water pressure, thermal expansion of the insulation system and subsequent cyclic bending in order to evaluate the response of the lead sheathing also with the internal pressure due to the operational conditions in the hypothesis of use in a dynamic application. These simulations where run modelling the lead sheathing both with the strain hardening power law creep model described in the previous section and by attributing to this layer only the elastic plastic properties, but not the time dependent behaviour. This is done to investigate the influence of the creep behaviour on the relaxation of deviatoric stress, but not of the hydrostatic stress, thus increasing the negative magnitude of the stress triaxiality factor, factor positively related to fatigue life. Consequently, the results of a total of 14 simulations are reported in figure 4 to 7. For every simulation, as shown in the following representative figures, there isn't a significative gradient in the stress-strain field along the longitudinal direction, thus, the results were extracted in the lead sheathing's mid-thickness point of the middle section of the cable, see figure 2. From the two most significative diagrams of both kinds of simulation, can arise the following considerations:
- The winding angle of the steel tapes does not influence the Von Mises equivalent stress.
- The winding angle of the steel tapes affects the equivalent pressure. An increase of the winding angle is followed by an increase of the equivalent pressure.
- Considering the average value of the stress triaxiality factor on a cycle (calculated in the span 3-15 hours), it's possible to compute the cyclic average TF for the different cases modelled. The results are shown in the following tables and figures.

The results in table 6 summarize the average triaxiality factor over a bending cycle, that is modelling the full-scale testing conditions. In absence of steel tape the triaxiality factor results virtually zero, while it becomes a negative value comprised between -0.74 and -1.10 considering the presence of the steel tape and its winding angle from the longitudinal direction. Analysing these results in light of the theory on the effect of the triaxiality factor on fatigue life it is predictable that the presence of the tapes, with their pre-tensioning, introduces a beneficial compressive stress which will improve the fatigue life. This is in agreement with the experimental results in figure 1, where is clearly seen how lead sheathing of the MI HVDC cables, which have the steel tapes in their design, has better fatigue performance than that of the XLPE ones, in which the tapes are absent.

Full scale testing modelling	STATIONARY SIMULATION	VISCOUS SIMULATION
Winding angle of tape	**Cyclic mean TF (3-15) h**	**Cyclic mean TF (3-15) h**
Absence of tape	-0.01	-0.03
60 degrees	-0.76	-0.74
70 degrees	-0.90	-0.81
80 degrees	-1.02	-1.10

Table 5.1.6. Average triaxiality factor in the lead sheathing modelling a full-scale testing like situation.

Dynamic cable modelling	STATIONARY SIMULATION	VISCOUS SIMULATION
Winding angle of tape	**Cyclic mean TF (3-15) h**	**Cyclic mean TF (3-15) h**
60 degrees	-0.37	-2.11
70 degrees	-0.54	-2.52
80 degrees	-0.66	-2.89

Table 5.1.7. Average triaxiality factor in the lead sheathing modelling a dynamic cable in an operation like situation.

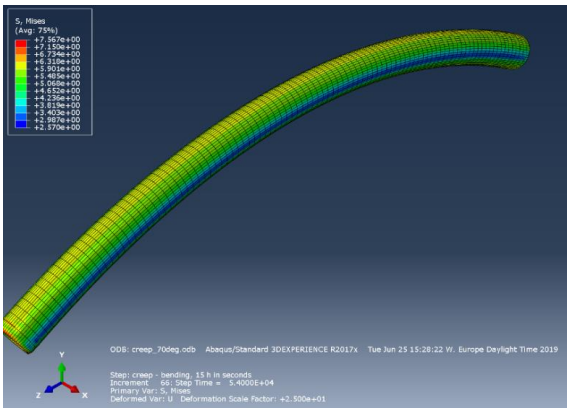

Figure 5.1.3. Deformed lead sheathing layer.

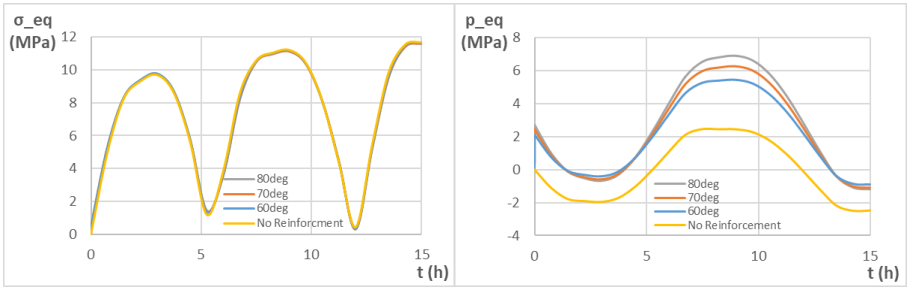

Figure 5.1.4. Non time-dependent modelling of test like situation.

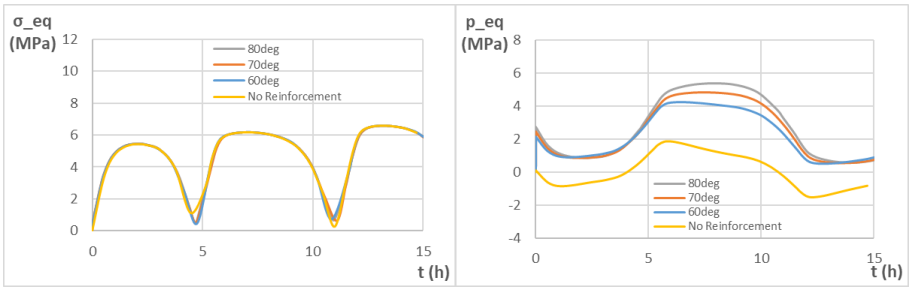

Figure 5.1.5. Time-dependent modelling of test like situation.

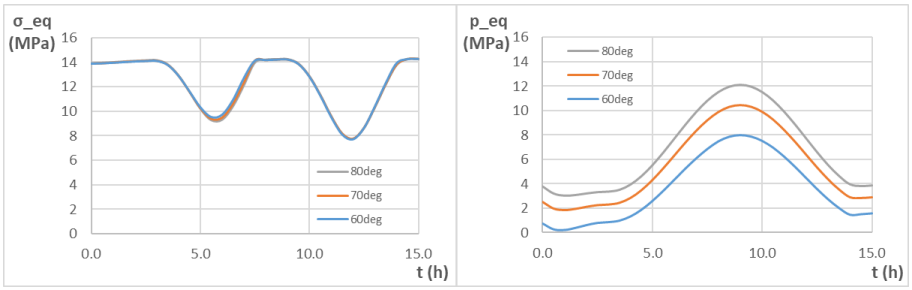

Figure 5.1.6. Non time-dependent modelling of dynamic cable operation like situation.

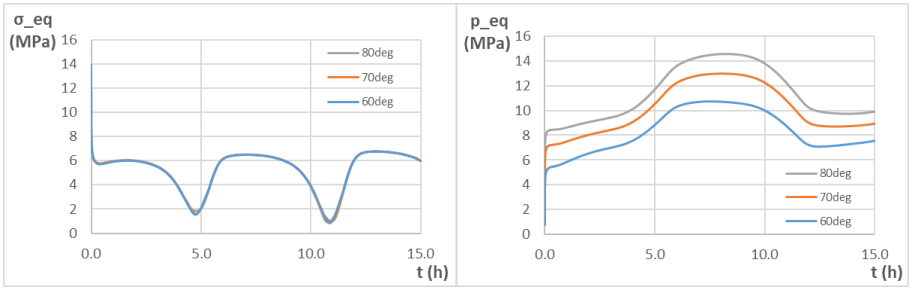

Figure 5.1.7. Time-dependent modelling of dynamic cable operation like situation.

5.1.6 Conclusions

In this work the results of a qualitative numerical investigation on the influence of design parameters on the fatigue performance of the lead sheathing layer of subsea high voltage cables is presented. Some cables have galvanized steel tapes winded over the lead sheathing layer to limit tangential deformations due to thermal expansion. Full scale fatigue testing results in presence and absence of such tapes are available in the literature and show a better performance for cable designs which include the tapes. It is known that a prevalence of hydrostatic compression, quantified with the triaxiality factor, has a positive effect on the fatigue life of metals. In this work the cable was modelled in a series of designs and boundary conditions, that is: without tapes and with tapes winded at

different angles in a full-scale test like situation and in a dynamic operation like situation and including or excluding the effect of creep deformation. The stress state detected in the lead sheathing indicates an increase of hydrostatic compression induced by the steel tapes. This is in agreement with the experimental results, explaining the better fatigue performance of the lead sheathing layer for cable designs including the steel tapes as a consequence of the modification of the stress triaxiality. This effect is enhanced by the presence of creep deformation, which contributes to reduce the deviatoric stress in the sheathing for low strain rate deformations.

Acknowledgements

This work has been financed by Nexans Norway and the Research Council of Norway through ENERGIX Programme, Contract No. 256367/E20.

References

[1] Moore, Herbert Fisher; Alleman, Norville James. The creep of lead and lead alloys used for cable sheathing, a report of an investigation conducted by the Engineering Experiment Station. University of Illinois, Engineering Experiment Station, Bulletin no. 243. 1932.
[2] Dollins, Curtis Walter; Betzer, Cecil E. Creep, fracture, and bending of lead and lead alloy cable sheathing. University of Illinois, Engineering Experiment Station, Bulletin no. 440. 1956.
[3] P. Feltham. On the Mechanism of High-Temperature Creep in Metals with Special Reference to Polycrystalline Lead. Proceedings of the Physical Society. Section B vol. 69 issue 12 pp: 1173-1188. 1956.
[4] David Glyn Havard. Fatigue of lead cable-sheathing alloys. Ontario hydro research quarterly. 1972.
[5] P. Anelli, F. Donazzi, W.G. Lawson. The fatigue life of lead alloy E as a sheathing material for submarine power cables. IEEE Transactions on Power Delivery. Volume: 3, Issue: 1. 1988.
[6] M.K. Sahota, J.R. Riddington. Compressive creep properties of lead alloys. Materials and Design 21, p. 159-167. 2000.
[7] Viespoli, Luigi Mario; Johanson, Audun; Alvaro, Antonio; Nyhus, Bård; Sommacal, Alberto; Berto, Filippo. (2018) Tensile characterization of a lead alloy: creep induced strain rate sensitivity. Materials Science & Engineering: A. vol. 744.
[8] Viespoli, Luigi Mario; Johanson, Audun; Alvaro, Antonio; Nyhus, Bård; Berto, Filippo. (2019) Strain controlled medium cycle fatigue of a notched Pb-Sn-Cd lead alloy. Engineering Failure Analysis. vol. 104.

[9] Johanson, Audun; Viespoli, Luigi Mario; Nyhus, Bård; Alvaro, Antonio; Berto, Filippo. (2018) Experimental and numerical investigation of strain distribution of notched lead fatigue test specimen. MATEC Web of Conferences. vol. 165:05003.
[10] Viespoli, Luigi Mario; Johanson, Audun; Alvaro, Antonio; Nyhus, Bård; Berto, Filippo. (2019) Room temperature creep mechanism of a Pb-Sn-Sb lead alloy. Procedia Structural Integrity. vol. 18.
[11] Johanson, Audun; Viespoli, Luigi Mario; Alvaro, Antonio; Berto, Filippo. (2019) Small and Full-Scale Fatigue Testing of Lead Cable Sheathing. ISOPE - International Offshore and Polar Engineering Conference. Proceedings.
[12] Z. Y. Huang, J. A. Pilgrim, P. L. Lewin, S. G. Swingler, and D. Payne, 'Current rating methodology for mass impregnated HVDC cables', Electrical Insulation Conference (EIC), 2013
[13] Z. Y. Huang, J. A. Pilgrim, P. L. Lewin, S. G. Swingler, and G. Tzemis, 'Numerical thermo-mechanical stress analysis for HVDC Cables', Electrical Insulation Conference, 2014
[14] S.S. Manson, G.R. Halford, 'Fatigue and Durability of Metals at High Temperatures', ASM International, 2009
[15] Peter Bonacuse, 'Elevated Temperature Axial and Torsional Fatigue Behavior of Haynes 188', Journal of Engineering Materials and Technology, 1995
[16] E. Ildstad, Rolf Hegerberg 'Cavity Formation in Mass-Impregnated HVDC Subsea Cables-Mechanisms and Critical Parameters', IEEE Electrical Insulation Magazine, 2014

Chapter 6: Conclusions

This chapter summarizes the main conclusions of the thesis.

Conclusions

This thesis summarizes the work of years of industry driven research on the mechanical properties of lead alloys employed for the manufacturing of submarine cable sheathing. The core goal of the studies performed is to provide the industry with the necessary knowledge on the mechanical behaviour of these alloys in order to improve the current design methodologies, often relying on experience and outdated results, with consequent economic and environmental advantages. The main contributions provided, the conclusions of which are reported in the following paragraphs, regard the following subjects:

- Tensile behaviour: strain rate sensitivity, secondary creep regimes and microstructure;
- Fatigue performance at different strain rate, including full scale component testing and in-situ observation of deformation and damage;
- Influence of geometrical discontinuities on structural integrity under fatigue load;
- Influence of design parameters of the stress state and consequent fatigue life of the component.

Chapter 2 (Papers I and II)

This chapter contain the results of the testing focused on the characterization of the tensile behaviour of the material, its secondary creep properties and microstructure investigation. In the first paper, the behaviour of the alloy at three different strain rate values was analysed. Tensile tests were conducted on three different geometries, finding a relation between thickness and steady state stress. Based on the test results, two different calibrations were performed, one for the 3.3 mm thick specimen and one suited for the 1.8mm and 1.1mm thick specimens. The derived constitutive laws were implemented in the commercial FEM code Abaqus. Two different models are adopted in this paper. The power law model, most suited for describing the primary creep region, which is attractive for its simplicity. The Anand model, on the other hand, is defined by fifteen parameters and is able to correctly represent also the secondary creep region and the temperature dependent response. Since no temperature dependent test were conducted only the strain rate behavior was calibrated. Isight was used in conjunction with Abaqus for optimizing the model. Due to the highly viscous and non-linear behaviour of the material, DIC has been necessary for computing the actual strain values on the specimen's surfaces. In particular, during the relaxation test made on the 3.3 mm thick specimens, a reduction of the longitudinal strain is observed. Considering this trend, the result is in agreement with numerical simulations. For explaining the thickness-effect a metallographic investigation has been done, finding bigger average grain size in the 3.3mm specimen. This result explains the different value of steady state stress reached in the experimental test, due to

the higher creep resistance for the thicker extrusion. The second paper focuses on the secondary creep stress strain exponent and the information it provides on the deformation mechanism. From the results of a tensile test composed of several steps at different stress levels, each of which reached the secondary creep stage, the exponent correlating stress and strain rate for steady state creep was obtained between 3 and 12 MPa. To summarize the main conclusions of the chapter are:

- The power law creep model is desirable for its simplicity and well performed at the higher strain rates.
- The Anand creep model performed better for the lower strain rates.
- The Anand creep model is indicated also for the time stress response at constant deformation.
- The extrusion thickness resulted proportional to the average grain size, giving an improved resistance for a higher thickness.
- The digital image correlation is an irreplaceable technique when dealing with very ductile alloys.
- The values assumed by the steady strain rate stress exponent in the range of interest indicate that mechanisms of diffusional creep are active in the low stress range of 3 to 5 MPa, with a value of the exponent close to 1, while dislocation creep is the dominating mechanism for higher stresses, with values ranging from 5.5 to 8.4.
- Further testing for different average grain size would then be necessary in the low stress range to determine whether vacancy diffusion through the crystal lattice or vacancy diffusion along the grain boundaries is predominant.

Chapter 3 (Papers III, IV and V)

The third chapter is focused on the analysis of the fatigue properties of the alloy of interest observed in different conditions: small scale specimens, microscale with in-situ observation and full scale. The purpose is to quantify the fatigue resistance in function of the strain rate, observe the dominant deformation mechanisms and investigate the performance of the full-scale component. The main conclusions of the chapter are:

- The fatigue performance of the alloy is influenced by creep deformation. A shift of the strain rate causes an important shift in fatigue life in terms of number of cycles, with slower deformation causing cracking after fewer cycles.
- The crack propagation in lead is typically both intergranular and transgranular, with a lower strain rate increasing the formation of secondary cracks and having a detrimental impact on the grain boundaries.
- The development of a fatigue-creep interaction model based on the deformation and damage mechanisms active in the class of alloys of interest is a complex task,

but necessary for a safe and knowledge-based prediction of the operational life of the components, whose real operating conditions are in fact dominated by low strain rates and elevated duration in terms of time.

- The fatigue life of lead strongly depends on loading mode. Reverse bending of small-scale test specimen results in significantly improved fatigue life compared to tension- compression. Power cable subjected to bending introduce mostly tension-compression type of load on its lead sheath. Based on this it is not advisable to base fatigue calculation of tubular sheathing from reverse bending of small-scale specimens.
- The fatigue life of lead is greatly enhanced when tested in a MI Power cable design compared to small- scale. The tested MI power cable designs used axial and transversal armouring which would introduce hoop stress and potentially prevent local ratcheting. The latter is supported by the post- test dissections where the ridges observed on the XLPE power phases are absent. The extension of full- scale fatigue life can also be related to modification of the hysteresis under bending where compression from the armouring elements shift the hysteresis towards compression which could modify both crack- opening, closing and potentially arrest.
- The enhanced fatigue life of observed for MI power cables compared to small-scale results appears to be significantly reduced or absent for XLPE power phases.
- The majority of the fractures on full scale tests appear to initiate in surface discontinuities. It is evident that the identified discontinuities do affect the fatigue life.

Chapter 4 (Papers VI and VII)

The papers composing chapter 4 summarize the results of static and fatigue testing performed on a set of Pb-Sn-Cd lead alloy specimen, material used in the production of sub-sea power-cable sheathing, with particular focus on the influence of notches. The testing was performed in displacement control at two strain ranges and two frequencies. To simulate the presence of defects in the components after the extrusion process, a blind notch was machined in part of the specimens. Some of the tests have been recorded by a digital camera for obtaining an approximation of the real strain field with DIC post-processing. The fractures of these samples were then investigated in SEM. An approximation of the strain field originated by the notch has been obtained in FEM. The main conclusions on the influence of notches on the fatigue performance of the lead alloy investigated are the following:

- Numerical calculations show that the notched detail is associated with the highest strain concentration which justifies both the reduction in fatigue life and change

in failure location. However, as the final crack do not tend to initiate at notch and the test results appear inconsistent with the analysis.

- The results obtained demonstrate how the highly plastic behaviour of the alloy tested yields to a minimal notch sensitivity, with fatigue cracks starting from other location at a much inferior geometrical stress concentration factor. That is, the presence of small defects in the cable sheathing, although to be avoided, does not constitute a high threat to the structural integrity of the same.
- The propagation of the fatigue cracks at an angle of 45º from the loading direction, that is along the maximum shear plane, means that the propagation of a fatigue crack in a plastic material in fully reversed load is strongly influenced by mode II fracture propagation.

Chapter 5 (Paper VIII)

In this chapter the results of a qualitative numerical investigation on the influence of design parameters on the fatigue performance of the lead sheathing layer of subsea high voltage cables is presented. Some cables have galvanized steel tapes winded over the lead sheathing layer to limit tangential deformations due to thermal expansion. Full scale fatigue testing results in presence and absence of such tapes are available in the literature and show a better performance for cable designs which include the tapes. It is known that a prevalence of hydrostatic compression, quantified with the triaxiality factor, has a positive effect on the fatigue life of metals. The cable was modelled in a series of designs and boundary conditions, that is: without tapes and with tapes winded at different angles in a full-scale test like situation and in a dynamic operation like situation and including or excluding the effect of creep deformation.

- The stress state detected in the lead sheathing indicates an increase of hydrostatic compression induced by the steel tapes. This is in agreement with the experimental results, explaining the better fatigue performance of the lead sheathing layer for cable designs including the steel tapes as a consequence of the modification of the stress triaxiality.
- This effect induced by the steel tapes is enhanced by the presence of creep deformation, which contributes to reduce the deviatoric stress in the sheathing for low strain rate deformations, thus increasing the relative importance of the hydrostatic stress component.

Appendix: Additional works

The appendix contains two additional works by the author on the topic of high temperature fatigue and creep of two different kind of metallic alloys.

Rapid extrapolation of high temperature low-cycle fatigue curves for a nickel superalloy

Luigi Mario Viespoli, Filippo Berto

Department of Mechanical and Industrial Engineering, Norwegian University of Science and Technology (NTNU), Norway
Luigi.m.viespoli@ntnu.no

Abstract: In many industrial applications, ranging from the energy, the aviation to the microelectronics field, metallic alloys are subjected to fatigue load at elevated temperatures. The detrimental influence of temperature and creep deformation damage on the structural performance of such components has for several decades posed a serious challenge to the work of scientists and engineers and the methods developed to account for creep fatigue interaction require extensive testing and work for being calibrated and implemented. In the present letter the authors propose a quick iterative procedure to translate the fatigue curve of an alloy in order to consider the reduction of resistance caused by creep damage. The method is validated against high temperature fatigue results for the Haynes 230 commercial nickel superalloy showing promising results.

Keywords: Low-cycle fatigue, creep-fatigue interaction, time ductility exhaustion, nickel superalloy.

Time fraction creep damage integration

Taken a specimen undergoing a variety of loads which generate creep deformation, this specimen has a limiting failure time t_R dependent on the applied load σ_i. If the damage generated by each loading condition, lasting a time t_i, is independent of the order, linear damage summation can be applied to determine the total damage of the sequence[1].

$$D_c = \sum_i \frac{t_i}{t_R(\sigma_i)} \quad (1)$$

The results of creep testing in terms of time to failure t_R at different temperatures T and applied nominal stresses σ can be reassumed in a two-dimensional space recurring to the Larson Miller parameter (LMP)[2]. The constant C is equal to 20 for most metals if time is expressed in hours.

$$LMP = T(\log t_R - C) \quad (2)$$

Plotting the nominal applied stress versus the LMP value for the creep tests the results, typical of the alloy, which can be expressed in the form:

$$\sigma = A \cdot LMP^{a} \tag{3}$$

Combining the equations 2 and 3 is possible to obtain the stress causing failure at a given time and temperature:

$$\sigma = A \cdot T^{a}(\log t_R - C)^{a} \tag{4}$$

Dealing with high temperature low cycle fatigue problems, it is necessary to fully characterize the cyclic stress-strain response of the alloy. The correlation between deformation range, temperature, frequency or strain range and stress can be obtained by testing and modeled by the means of an opportune constitutive law.

$$\sigma = \sigma(T, f, \varepsilon) \tag{5}$$

In the hypothesis of high temperature cyclic loading imposed by a triangular deformation wave of frequency f, amplitude ε_a and loading ratio $R = \varepsilon_{max}/\varepsilon_{min} = -1$, combining equation 4 with a constitutive law in the form of equation 5 and with the concept of time fraction damage summation introduced by equation 1, it is possible to obtain the quota of ideal damage introduced in the material by a single loading starting from the undeformed configuration and reaching ε_a linearly in a time corresponding to $t = 1/4f$, by integrating in the form:

$$d_{ci} = \int_0^{t=1/4f} \frac{dt}{10^{\left[(\sigma(T,f,\varepsilon(\varepsilon_a,f,t))/A)^{1/a}/T-C\right]}} \tag{6}$$

The integral corresponds to the addition of the damage caused by the infinitesimal load application time dt divided by the instantaneous time to failure, from equation 4, in which the instantaneous load is given by the stress-strain relationship calibrated on cyclic testing, thus dependent on temperature, strain rate and strain range. It is necessary to experimentally determine the material response to a fatigue load at a reference temperature and frequency, which can be described by the known Smith Watson Topper (SWT) equation[3].

$$\varepsilon_a\left(T_{ref}, f_{ref}, N\right) = \frac{\sigma_f'}{E}(N)^{b} + \varepsilon_f'(N)^{c} \tag{7}$$

The low cycle fatigue response of the material for temperatures different from the reference temperature can be obtained by translating the reference curve proportionally

to the logarithm of the creep damage introduced at the new temperature, divided by the logarithm of the ideal damage at refence temperature since the reference curve must be computed equal to itself:

$$\varepsilon_a(T,f,N) = \varepsilon_a\left(T_{ref},f_{ref},N\right)\frac{\log d_{ci}(T,f,N)}{\log d_{ci}\left(T_{ref},f_{ref},N\right)} \qquad (8)$$

The creep damage computed by equation 6 is dependent on the deformation amplitude to which the material is subjected for a given number of cycles. An iterative is then necessary. The application of the here presented approximation is summarized as follows:
1) Perform creep testing to failure in the range of temperatures of interest to obtain the constants A and a.
2) Characterize the cyclic response of the alloy for the necessary range of temperatures and frequencies to calibrate a correlation in the form of equation 5.
3) Perform fatigue testing at a certain reference temperature and strain rate to calibrate the SWM model.
4) Generate an array of number of cycles on which to compute the relative deformation amplitude for the temperature of choice.
5) Assume and initial strain amplitude equal to the strain amplitude of the reference fatigue curve and compute the integrated creep damage component both at the desired temperature and at the reference temperature.
6) Apply equation 8 and repeat the computation of the integrated creep damage at the new temperature until convergence is reached.

High temperature fatigue curve extrapolation for a nickel superalloy

The procedure introduced in the previous paragraph was applied to compute the low cycle fatigue curves at various temperatures for the commercial nickel superalloy Haynes 230. The experimental results chosen as framework for the verification of the model were not performed by the authors but are of public dominion. Barrett et al.[4] and Ahmed et al.[5] performed cyclic testing at the temperatures and frequencies required to obtain the stabilized hysteresis cycle in the same conditions of the fatigue data. Fatigue and creep testing results are instead reported by the manufacturer[6]. The creep results for samples realized from plates and tested at temperatures ranging from 649 to 1149 ºC are reported in figure 1a. The constants of equation 3 are calibrated on the results of the tests performed up to 982 ºC, which corresponds to the highest fatigue testing temperature, obtaining $A = 7.94855E-33$ and $a = -7.26155$. The fatigue tests as well were performed on specimens manufactured from plates, at a frequency $f = 0.33\,Hz$ and temperatures ranging from 427 to 982 ºC. The fatigue results at the lowest temperature, 427 ºC, were chosen as reference, calibrating the SWT parameters as: $E = 190000\,MPa, \sigma_f' = 1400\,MPa, b = -0.1, \varepsilon_f' = 0.4, c = -0.58$, see figure 1b. All the fatigue results are

plotted in figure 2a, where the solid lines represent the result of the extrapolation according to equation 8. Figure 2b shows how the deformation amplitude imposed in the test versus the extrapolated amplitude for the corresponding number of cycles is included in a scatter band of ±20%, indicating a good accuracy. The validity of the proposed method, verified for this specific case, remains to be tested against a series of different conditions. In particular: strong frequency variation in high temperature fatigue and extrapolating from a reference curve obtained at a temperature under the minimum value for the onset of creep deformation phenomena.

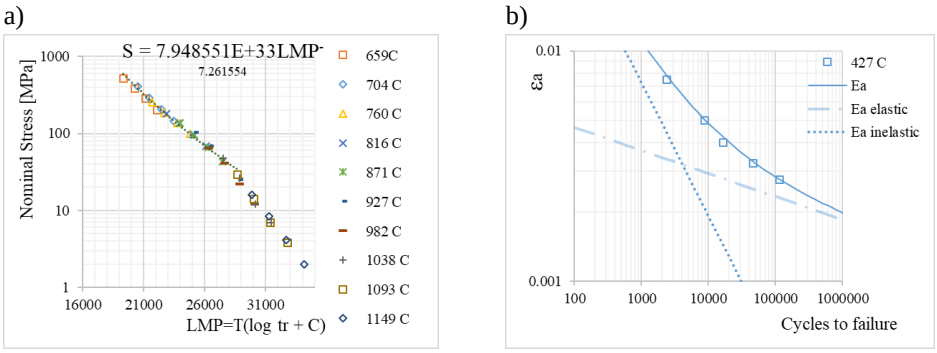

Figure 1. Creep failure results and trendline for the range of temperatures of interest for the fatigue testing (a). Reference fatigue curve at 427 ºC (b).

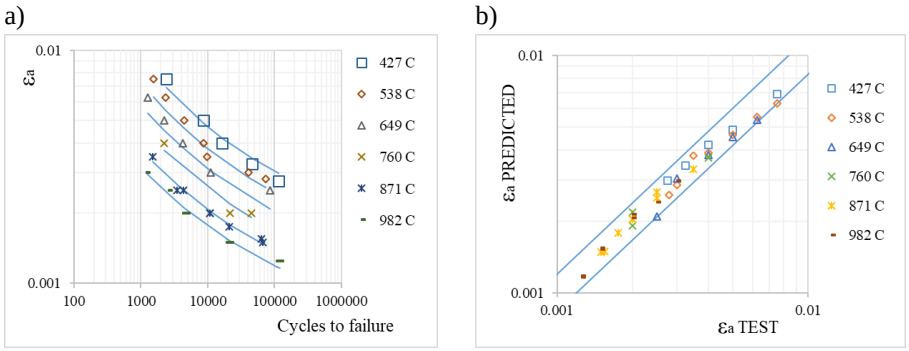

Figure 2. Fatigue testing results from 427 to 982 ºC. The lines indicate the extrapolated fatigue curves (a). Predicted versus experimental fatigue strain amplitude, scatter ±20% (b).

Conclusions

A method for computing the influence of temperature on fatigue life through the basic concepts of creep damage is presented. Obtained a full characterization of the mechanical

response under cyclic loading, of the creep life time versus load and temperature and a fatigue curve obtained at a reference temperature and testing frequency, it has been possible to extrapolate the fatigue response for higher temperatures obtaining results in good agreement with the experimental data available at these temperatures. The method accounts for the influence of frequency on the creep damage, introduced indirectly trough the material cyclic response and directly through the integration time for the integrated creep damage. The accuracy of the method to predict the fatigue response to different frequencies than the reference one has not been validated by experimental results. Should this ability be positively verified, the method would be a powerful tool for the extrapolation of high temperature fatigue curves at low strain range, condition for which experimental testing could require unfeasible time.

References

[1] E.L. Robinson. Effect of temperature variation on the long-time strength of steels. Trans ASME 74 (5) 1952; 777-780.
[2] Larson, F.R. and Miller, J. (1952) Time-Temperature Relationship for Rupture and Creep Stresses. Transactions of ASME, 74, 765-771.
[3] Smith, K. N., Watson, P. and Topper, T. H. (1970) A stress strain function for the fatigue of metals. J. Mater. JMLSA 5, 767– 778.
[4] Paul R. Barrett, Raasheduddin Ahmed, Mamballykalathil Menon, Tasnim Hassan, Isothermal low-cycle fatigue and fatigue-creep of Haynes 230, International Journal of Solids and Structures, Volumes 88–89, 2016, Pages 146-164.
[5] Raasheduddin Ahmed, Paul R. Barrett, Tasnim Hassan, Unified viscoplasticity modeling for isothermal low-cycle fatigue and fatigue-creep stress–strain responses of Haynes 230, International Journal of Solids and Structures, Volumes 88–89, 2016, Pages 131-145.
[6] https://www.haynesintl.com/docs/default-source/pdfs/new-alloy-brochures/high-temperature-alloys/brochures/230-brochure.pdf.

Creep and high temperature fatigue performance of as build selective laser melted Ti-based 6Al-4V titanium alloy

Luigi Mario Viespoli[1,2], Stefano Bressan[2], Takamoto Itoh[2], Noritake Hiyoshi[3], Konda Gokuldoss Prashanth[4,5,6], Filippo Berto[1]

[1] *Department of Mechanical and Industrial Engineering, Norwegian University of Science and Technology (NTNU), Norway*
[2] *Department of Mechanical Engineering, Ritsumeikan University, 1-1-1, Nojihigashi, Kusatsu, Shiga 525-8577, Japan*
[3] *Division of Engineering, Faculty of Engineering, University of Fukui, 3-9-1 Bunkyo, Fukui-shi, Fukui 910-8507, Japan*
[4] *Department of Mechanical and Industrial Engineering, Tallinn University of Technology, Ehitajate Tee 5, 19086 Tallinn, Estonia*
[5] *Erich Schmid Institute of Materials Science, Austrian Academy of Sciences, Jahnstraße 12, 8700 Leoben, Austria*
[6] *CBCMT, School of Mechanical Engineering, VIT University, Vellore - 632014, Tamil Nadu, India*

Abstract: The present work focuses on the room and high temperature low-cycle fatigue and creep testing of Ti-6Al-4V manufactured by selective laser melting (SLM) or laser-based powder bed fusion process (LBPF). The fatigue specimens were tested in a strain control mode with the as-built and machined surfaces, evaluating the influence of the surface roughness on the fatigue performance. This helps in understanding the potential negative influence of a surface defect/roughness on the fatigue performance of the complex components produced by SLM (in as-built state), where surface machining may not be possible due to geometrical constraints. The fatigue fractures at room and high temperature were investigated with the help of a scanning electron microscope. The creep tests were performed at three different temperatures with as-built SLM samples, demonstrating an equivalent or better performance when compared to their counterparts produced by hot-forging.

Keywords: Additive manufacturing, titanium alloy, creep, high temperature fatigue, surface defect.

Introduction

The extreme design flexibility offered by additive manufacturing (AM) technologies has drawn great interest both from the industry and academia. On one side, the industry aims

to improve the efficiency of production by reducing the processing steps and on the amount of components to be assembled to create a complex geometry. In addition, the feasibility of producing complicated nature-inspired and topologically optimized geometries that would be expensive or impossible to be manufactured with the traditional technologies like casting, forging and material removing was explored [1]. On the other side, scientific research is focused on understanding the microstructure and performance of the components produced SLM, as compared to their cast counterparts [2,3]. The process specific conditions may create variations in the microstructure and in turn their mechanical properties [4]. The present day research is focused on the below mentioned aspects: develop rapid production and energy-effective technologies, optimize the processes to reduce the amount of defects present in the AM components and develop had-hoc criteria that may accurately predict the fatigue and fracture behavior of such materials, ideally including the effects of anisotropy, residual stresses, surface finish and internal defects generated by different combinations of the production parameters [5-8].

Ti-6Al-4V titanium alloy, one of the widely fabricated alloys by SLM, with variety of applications, ranging from the aerospace industry to biomedical applications, in virtue of its excellent mechanical properties and chemical resistance is chosen for the present study. Due to the ease of manufacturing and the importance of this alloy itself, several studies have been carried out, especially on the mechanical properties, since the early days, produced by conventional techniques like casting. The introduction of these novel production techniques and the specific properties of components produced by the means of them have attracted great interest in studying the alloy manufactured by these new AM methods. Tokaji [9] studied the fatigue behavior at elevated temperatures focusing on the propagation of small cracks at the different regimes. In terms of stress amplitude, a reduction of fatigue resistance is observed increasing with the temperature from 623 K to 723 K at low cycle regime, but not in the high cycle regime. The high temperature crack propagation is more brittle than at room temperature. Severino et. al. [10] studied the oxidation resistance of the alloy at 1073 K for different times and the influence of the oxide layer on the tensile behavior at 873 K. The ultimate strength was very slightly influenced compared to the un-oxidized, but a reduction of elongation at break was detected.

Richie et. al. [11] investigated the fatigue behavior of a Ti-6Al-4V alloy employed for the production of axial compressor blades. The study was performed on large-cracks and small-cracks at frequencies ranging from 20 Hz to 1500 Hz and load ratios R ranging from 0.1 to 0.95 in air and vacuum. No influence of the frequency was detected, while the presence of air increased of three orders of magnitude the crack propagation rate and the worst-case fatigue threshold was measured to be 1.9 MPa$\sqrt{m}$. Li et. al. [12] provided a comprehensive overview on several results obtained on traditionally and AM manufactured Ti-6Al-4V in different conditions of surface finish and thermal treatment. Molaei and Fatemi [13] studied the influence of typical defects such as entrapped gas pores or lack of fusion, correlated to the technological parameters, on the fatigue

performance. Shunmugavel et. al. [14] compared the microstructure and the tensile properties of wrought and AM manufactured Ti-6Al-4V alloy, where a higher tensile strength, but decreased ductility was observed for AM processed material. Tong et. al. [15] compared the influence of different combinations of building direction and thermal treatment on hardness and static and fatigue behavior of the alloy manufactured by powder bed selective laser melting (SLM) and by electron beam melting (EBM). Wu et. al. [16] applied several failure criteria to AM processed Ti-6Al-4V and tested in proportional and non-proportional multi-axial strain controlled low-cycle fatigue, where good data correlations with the Fatemi-Socie [17] and the non-proportional strain range criteria were observed [18]. No additional hardening, but a severe reduction of the fatigue life due to the non-proportionality of the load, was detected. Zhai et al. [19] investigated the static and fatigue crack growth properties of Ti-6Al-4V manufactured with the additive techniques of Laser Engineered Net Shaping (LENS) and Electron Beam Melting (EBM), with attention to the difference in performance to wrought alloys.
The present work aims to integrate the number of results available focusing on the influence of surface defects and temperature on fatigue performance and creep resistance of SLM processed Ti-6Al-4V.

Material production and microstructure

The specimens used for the present study were manufactured by selective laser melting using a SLM Solutions (SLM 280) device. The build direction coincides with the longitudinal axis and the process details are indicated in table 1. The two geometries produced, for fatigue and creep testing, are reported in Fig. 1 (A and B) respectively. During SLM fabrication a defect was introduced in the form of a slight misalignment of the build axis in correspondence of the minimum cross section trait, as indicated in Fig. 1C. The fatigue specimens were produced to a minimum diameter of 6 mm. Four of them were being tested at room temperature with the as-built surface, while the rest of them had the surface lathe-machined down to a diameter of 5 mm as reported in Fig. 1A. The creep specimens where tested with the as-built surface. All the specimens were tested with the as-built microstructure consisting of acicular α’ martensitic phase in elongated β grains as shown in Fig. 2. A certain degree of porosity can be detected in the longitudinal cut as observed from Fig. 2.

Device	SLM 280HL – SLM Solutions
Laser power [W]	275
Laser scan speed [mm/s]	1100
Hatch style	Strip hatch
Hatch rotation [º]	15
Hatch distance [µm]	120
Hatch length [mm]	10
Atmosphere	Argon
Material	Ti6Al4V

Table 1. Table detailing the SLM process and the fabrication parameters.

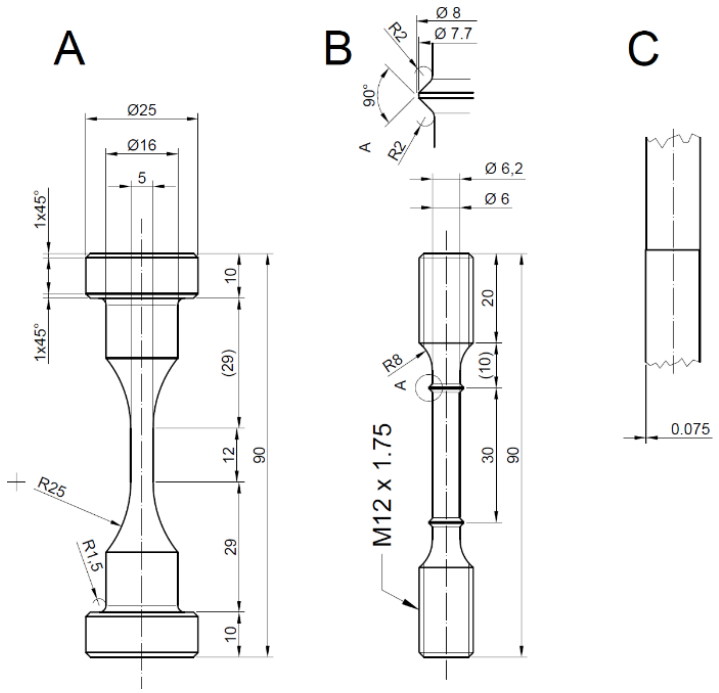

Figure 1. Room and high temperature fatigue specimen (A). Creep specimen (B). Surface defect (C).

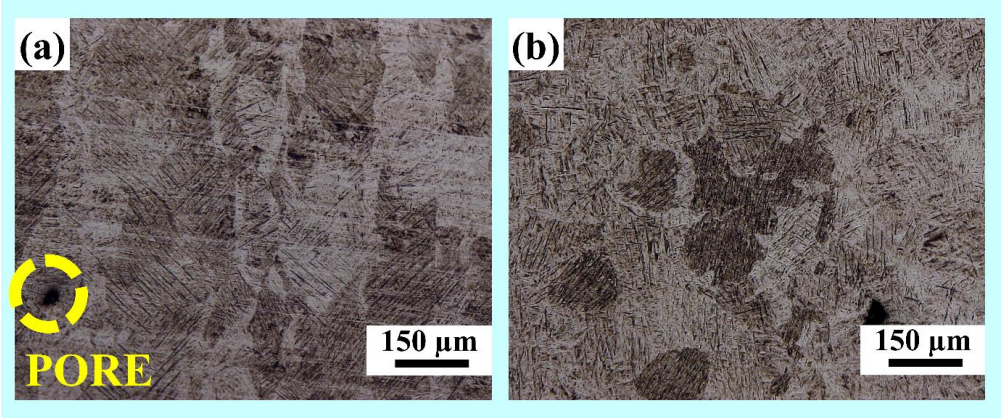

Figure 2. Optical microscopy of the as-built Ti6Al4V SLM microstructure, showing elongated β phase grains containing acicular α' martensitic phase. Along build direction (a) and horizontal direction (b).

Fatigue testing

The fatigue testing was performed, by a hydraulic machine, in strain control applying a fully reversed displacement, that corresponds to a displacement ratio -1, at a strain rate of 0.1 %/s with the feedback provided by an induction axial extensometer. The extensometer, of the kind suited for high temperature testing, had ceramic pins clipped in small pits practiced at a distance of 10 mm in the central section of the specimen. Three series of specimens were fatigue tested: four at room temperature with the as-built surface, six at room temperature with machined surface and four at high temperature and machined surface after having been warmed up to 600 ºC for 30 min by an induction coil. The temperature was detected by a thermocouple welded to the fillet radius area, in order to not weaken the neat cross section by practicing a weld. The temperature in the center area was correctly known by having calibrated the correlation between the temperatures in the two points on a dummy specimen. The fatigue results are reported in Fig. 3.
The tests performed at room temperature on machined surface specimens show a behavior which is in perfect agreement with analogous tests in the literature [16]. Assessed so the reproducibility of the results, the other two series show the strong weakening produced by a surface defect and by an increase of temperature. The specimens tested with an as-built surface in presence of the defect have all experienced failure with cracks starting from the defect, see Fig. 4a, and a fatigue life noticeably inferior to the machined specimens. Considered the entity of the defect, a misalignment of the build axis of 75 µm, it is evident how even a small defect can have huge repercussions on the structural integrity, which is particularly of importance for the production of complicated topology-optimized geometries, the realization of which is allowed by the great flexibility of the AM technologies, where postproduction surface machining can be non-cost effective or

impossible. A similar reduction of strain-controlled fatigue life is originated by an increase of ambient temperature to 600 ºC. The fatigue failure at high temperature is characterized by a diffused secondary cracking originated by weakening of the grain boundary regions, as seen in Fig. 4b.

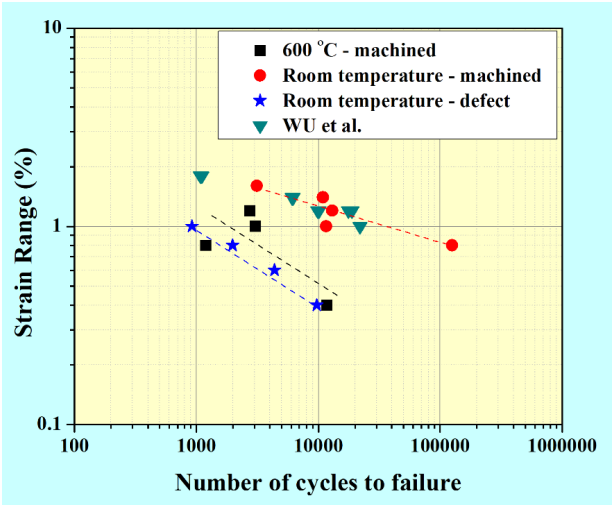

Figure 3. Fatigue results summary [16].

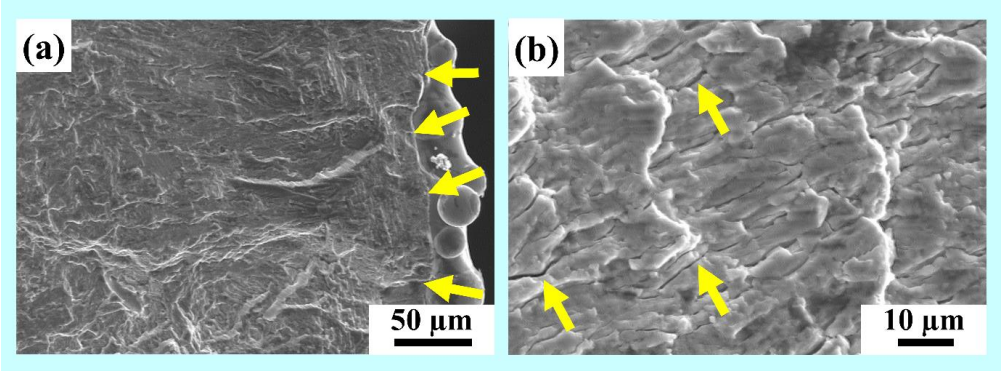

Figure 4. Fatigue crack initiation at a surface defect and partially melted particles (a). Secondary cracking in high temperature fatigue fracture (b).

Creep testing

The creep testing was performed on a series of 8 specimens of the geometry specified in Fig. 1b. The samples where tested applying a constant nominal stress with a drop weight machine with induction heating at temperatures of 450, 550 and 650 ºC, respectively. The results are reported in Fig. 5 in terms of nominal stress vs time to failure, showing a consistent behavior for the whole range of time to failure, from 120 s to 655 h. The consistency of the behavior is evident in the summary of the results in terms of nominal stress versus Larson Miller parameter, in Fig. 6, in which all the results can be

approximately described by a single power function. Observing the steady state creep behavior reported in Fig. 7 as applied stress versus strain rate, the stress exponent shows a reduction with increased temperature and lower applied stress, thus indicating an increased importance of the diffusive creep deformation versus the dislocation dominated creep, which is predominant for lower temperatures and higher stress levels. Comparing the results obtained to creep testing results available in the literature in hot forged and forged and annealed Ti6Al4V alloy, the as built SLM material has an analogous performance in terms of Larson Miller parameter vs applied stress [20,21].

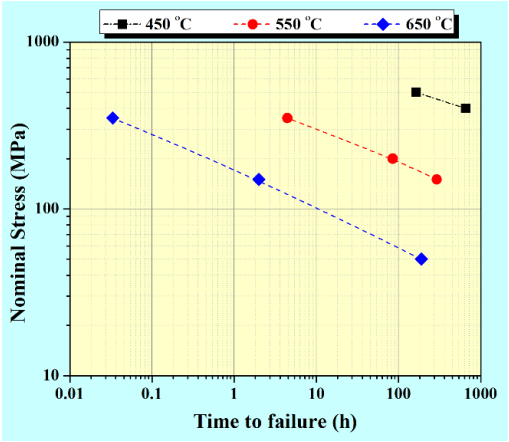

Figure 5. Creep testing results: nominal stress vs time to failure.

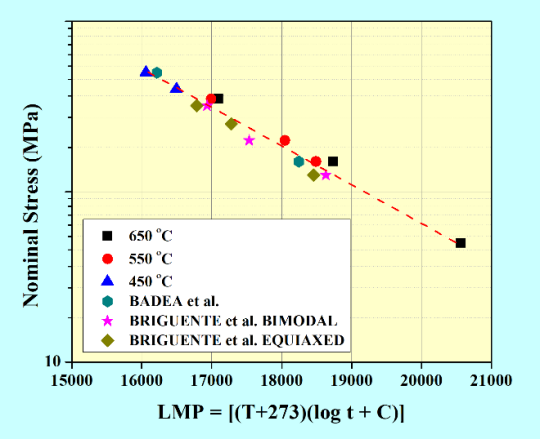

Figure 6. Creep testing results: nominal stress vs Larson Miller parameter [19,20].

Fig. 8 reports the correlation between the applied stress and the ductility for the three test temperatures. The nominal strain was measured during the creep tests by the means of an extensometer attached to the two rings, which delimitate the uniform diameter section of

the creep specimens. Despite the important scatter of the results, it is evident that the applied stress has a determinant influence on the elongation to failure, with values ranging from 75 % at a nominal stress of 50 MPa at 650 ºC down to 20 % for 500 MPa applied at a temperature of 450 ºC. Fig. 9 presents the SEM magnification of the fracture surfaces of two creep specimens, tested at 650 ºC, 50 MPa and 450 ºC, 500 MPa. The failures are characterized by pore nucleation and growth, but they present a different aspect according to the test duration, with a much rougher surface in case of higher T and lower stress. This is possibly due to material oxidation.

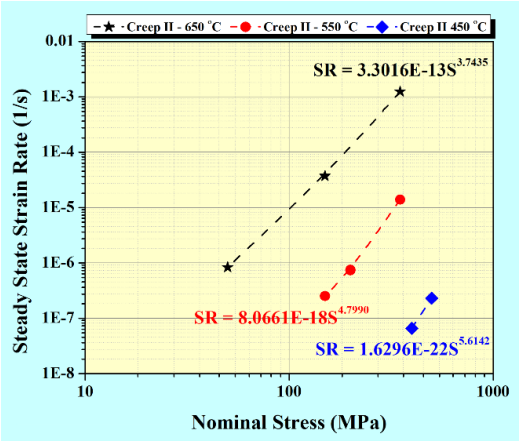

Figure 7. Creep testing results: secondary creep (steady state) strain rate vs nominal stress.

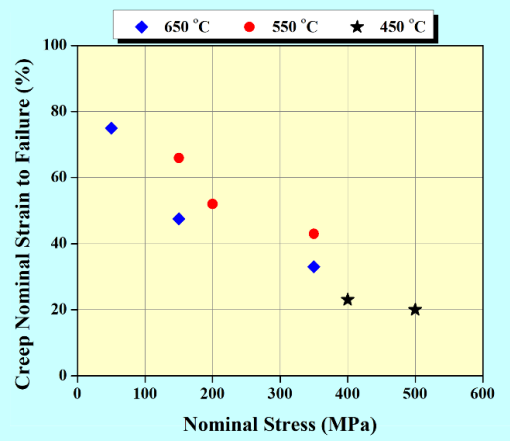

Figure 8. Creep testing results: Influence of stress on ductility for different temperatures.

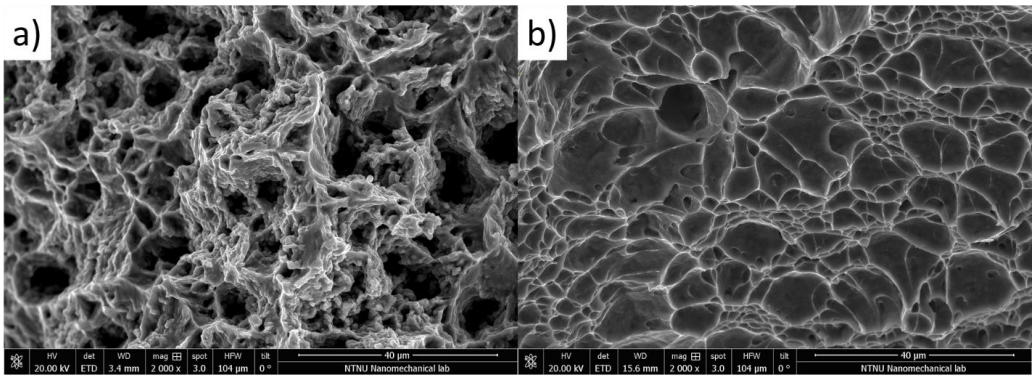

Figure 9. Fracture surface of specimen creep tested at: 650 ºC, 50 MPa (a) and 450 ºC, 500 MPa.

Conclusions

A series of fatigue and creep tests has been performed on Ti-6Al-4V alloy processed by SLM without post-processing thermal treatment. The fatigue tests were executed in strain control mode with the as-built surface at room temperature and with machined surface at room temperature and 600 ºC. The creep tests were carried out on as-built specimens using a drop weight machine with the following temperatures: 450, 550 and 650 ºC. The high temperature fatigue tests show a strong influence of ambient temperature at 600 ºC. Most importantly, it is evidenced the high decrement of fatigue resistance caused by a poor as-built surface. This is particularly relevant for the case of intricated geometries, the surface of which might result unfeasible to machine after the additive production process. The creep tests show a performance analogous to the same alloy produced in the form of forged billets and bars in terms of Larson Miller parameter vs nominal stress. The steady state creep rate exponents, ranging from 3.7 to 5.6 and with inverse proportionality to temperature, indicate the dominant presence of dislocation driven creep with an increased influence of diffusion at higher temperatures. The creep ductility at failure presents a reversed proportionality to the applied load. The surface defect had no influence on the creep failure.

Acknowledgements

Estonian Research Council’s grant MOBERC15 is acknowledged.

References

[1] Orme, M.; Madera, I.; Gschweitl, M.; Ferrari, M. Topology Optimization for Additive Manufacturing as an Enabler for Light Weight Flight Hardware, Designs 2 (2018) 51.

[2] K.G. Prashanth, S. Scudino, H. J. Klauss, K. B. Surreddi, L. Löber, Z. Wang, A.K. Chaubey, U. Kühn, J. Eckert, Microstructure and mechanical properties of Al-12Si produced by selective laser melting: Effect of heat treatment, Mater. Sci. Eng. A 590 (2014) 153-160.

[3] S. Scudino, C. Unterdoerfer, K.G. Prashanth, H. Attar, N. Ellendt, V. Uhlenwinkel, J. Eckert, Additive manufacturing of Cu-10Sn bronze, Mater. Lett. 156 (2015) 202-204.

[4] K.G. Prashanth, S. Scudino, J. Eckert, Defining the tensile properties of Al-12Si parts produced by selective laser melting, Acta Mater. 126 (2017) 25-35.

[5] J. Suryawanshi, K.G. Prashanth, S. Scudino, J. Eckert, O. Prakash, U. Ramamurty, Simultaneous enhancements of strength and toughness in an Al-12Si alloy synthesized using selective laser melting, Acta Mater. 115 (2016) 285-294.

[6] P. Kumar, U. Ramamurty, Microstructural optimization through heat treatment for enhancing the fracture toughness and fatigue crack growth resistance of selective laser melted Ti6Al4V alloy, Acta Mater. 169 (2019) 45-59.

[7] J. Suryawanshi, K.G. Prashanth, U. Ramamurty, Tensile, fracture, and fatigue crack growth of a 3D printed maraging steel through selective laser melting, J Alloys Compd. 725 (2017) 355-364.

[8] J. Suryawanshi, K.G. Prashanth, U. Ramamurty, Mechanical behavior of selective laser melted 316L stainless steel, Mater. Sci. Eng. A, 696 (2017) 113-121.

[9] K. Tokaji, High cycle fatigue behaviour of Ti–6Al–4V alloy at elevated temperatures, Scripta Mater. 54 (2006) 2143-2148.

[10] (2014), Study of high temperature mechanical behavior. Mat.-wiss. u. Werkstofftech, 45: 269-280. doi:10.1002/mawe.201400226.

[11] R.O. Ritchie, D.L. Davidson, B.L. Boyce, J.P. Campbell, O. Roder. High-cycle fatigue of Ti–6Al–4V. Fatigue & Fracture of Engineering Materials & Structures. VL - 22 IS - 7 SN - 8756-758X (1999), pp. 621-631.

[12] P. Li, D.H. Warner, A. Fatemi, N. Phan, Critical assessment of the fatigue performance of additively manufactured Ti–6Al–4V and perspective for future research, Int. J Fatigue, 85 (2016) 130-143.

[13] R. Molaei, A. Fatemi, Fatigue Design with Additive Manufactured Metals: Issues to Consider and Perspective for Future Research, Procedia Eng. 213 (2018) 5-16 .

[14] M. Shunmugavel, A. Polishetty, G. Littlefair, Microstructure and Mechanical Properties of Wrought and Additive Manufactured Ti-6Al-4V Cylindrical Bars, Procedia Technol. 20 (2015) 231-236.

[15] J. Tong, C. R. Bowen, J. Persson, A. Plummer, Mechanical properties of titanium-based Ti–6Al–4V alloys manufactured by powder bed additive manufacture, Mater. Sci. Technol. 33 (2017) 138-148.
[16] M. Wu, T. Itoh, Y. Shimizu, H. Nakamura, M. Takanashi, Low cycle fatigue life of Ti–6Al–4V alloy under non-proportional loading, Int. J Fatigue, 44 (2012) 14-20.
[17] A. Fatemi, D.F. Socie, A critical plane approach tomultiaxial fatigue damage including out-of-phase loading, Fatigue Fract. Eng. Mater. Struct. 11 (1988) 149-165.
[18] T. Itoh, M. Sakane, M. Ohnami, D.F. Socie, Nonproportional Low Cycle Fatigue Criterion for Type 304 Stainless Steel, ASME. J. Eng. Mater. Technol. 117 (1995) 285-292.
[19] Yuwei Zhai, Haize Galarraga, Diana A. Lados, Microstructure, static properties, and fatigue crack growth mechanisms in Ti-6Al-4V fabricated by additive manufacturing: LENS and EBM, Engineering Failure Analysis, Volume 69, 2016, Pages 3-14
[20] L. Badea, M. Surand, J. Ruau, B. Viguier, Creep behavior of Ti-6Al-4V from 450°C to 600°C, University Polytechnica of Bucharest Scientific Bulletin, Series B, 76 (2014) 185-196.
[21] L.A.N.S. Briguente, A.A. Couto, N.M. Guimaraes, D.A.P. Reis, C. Moura Neto, M.J.R. Barboza, Determination of Creep Parameters of Ti-6Al-4V with Bimodal and Equiaxed Microstructure, Defect Diff. Forum, 326-328 (2012) 520-524.